OCS Study
BOEM 2021-83

Electromagnetic Field Impacts on American Eel Movement and Migration from Direct Current Cables

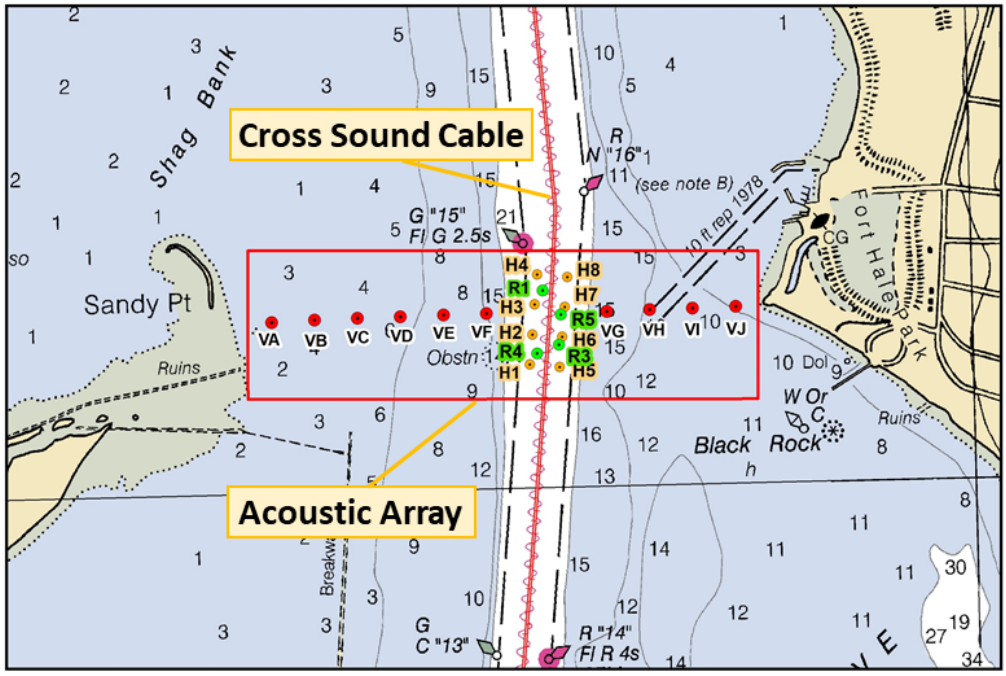

U.S. Department of the Interior
Bureau of Ocean Energy Management
Office of Renewable Energy Programs

BOEM
Bureau of Ocean Energy Management

OCS Study
BOEM 2021-83

Electromagnetic Field Impacts on American Eel Movement and Migration from Direct Current Cables

December 2021

Authors:

Zoë L. Hutchison, University of St Andrews, UK
Peter Sigray, KTH, Royal Institute of Technology, Sweden
Andrew B. Gill, Cefas, Centre for Environment, Fisheries and Aquaculture Science (Cefas), UK
Théo Michelot, University of St Andrews, UK
John King, Graduate School of Oceanography, University of Rhode Island, USA

Prepared under BOEM Contract 140M0118C0001
by

The Coastal Mapping Laboratory
Graduate School of Oceanography
University of Rhode Island
215 South Ferry Road
Narragansett, RI 02882

Published by

U.S. Department of the Interior
Bureau of Ocean Energy Management
Office of Renewable Energy Programs

BOEM
Bureau of Ocean Energy Management

DISCLAIMER

Study concept, oversight, and funding were provided by the US Department of the Interior, Bureau of Ocean Energy Management (BOEM), Environmental Studies Program, Washington, DC, under Contract Number 140MO118C0001. This report has been technically reviewed by BOEM, and it has been approved for publication. The views and conclusions contained in this document are those of the authors and should not be interpreted as representing the opinions or policies of the US Government, nor does mention of trade names or commercial products constitute endorsement or recommendation for use.

REPORT AVAILABILITY

To download a PDF file of this report, go to the US Department of the Interior, Bureau of Ocean Energy Management website at www.boem.gov/Environmental-Studies-EnvData/, click on the link for the Environmental Studies Program Information System (ESPIS), and search on 2021-83.

CITATION

Hutchison, Z. L., P. Sigray, A. B. Gill, T. Michelot, and J. King, 2021. "Electromagnetic Field Impacts on American Eel Movement and Migration from Direct Current Cables." Sterling (VA): U.S. Department of the Interior, Bureau of Ocean Energy Management. OCS Study BOEM 2021-83.

ABOUT THE COVER

Cover images:

Top left: American eels (*Anguilla rostrata*) collected for the free-ranging tracking study. *Photo credit: Zoë L. Hutchison, used with permission.*

Bottom: Cross Sound Cable eel study area, within New Haven Harbor, CT, superimposed on a NOAA chart. *Map credit: Carol Gibson, used with permission.*

ACKNOWLEDGMENTS

The project required a diverse research team with a wide variety of expertise and technical skills. Special thanks to:

Bureau of Ocean Energy Management (BOEM), Office of Renewable Energy Programs: Mary Boatman and Brian Hooker.

Coastal Mapping Laboratory Research Staff (Graduate School of Oceanography, University of Rhode Island): Brian Caccioppoli, Danielle Cares, Catherine Cipolla, Evan Ernst, Carol Gibson, Roger Kelly, Monique LaFrance Bartley and Gary Savoie.

Marine Research Facility (Graduate School of Oceanography, University of Rhode Island): Ed Baker, Katie Nickles, Kelly Dubreuil, and Brielle Michener.

Research Divers (Graduate School of Oceanography, University of Rhode Island): Anya Hanson, Alexandra Moen, Ryan Patrylak, Katie Nickles, Mark Wegiel, Kiel Quinn, Olivia Ayers and Matt Palasciano.

Eel Access: Timothy Wildman (Connecticut Department of Energy and Environmental Protection), and Paul Hyatt and colleagues (Groton Utilities).

Cross Sound Cable Company, LLC: Brian Reinhart.

United States Coast Guard: New Haven, CT station.

New Haven Shipping Companies.

Vemco USA: Dana Allen, Chris Fougere and colleagues.

University of St Andrews: Dr Mark James.

Contents

List of Figures

and the red box indicates the eel study area where a high density of transects were undertaken. The labels numerate the surveys in north to south order (track 1-22). Right panel: the eighteen surveys conducted in the eel study area (track 2-19).

Figure 2.2. Swedish Electromagnetic Field Low-Noise Apparatus. *E's* mark the location of the six electrodes, *F* indicates the location of the fluxgate sensor, *C* is the cylindrical casing where the subsea electronics were stored and *U* the cable that connected the SEMLA with the boat unit. Image from Hutchison et al., (2018).

Figure 2.3. An example of the AC and DC fields measured within the eel study area. a) The observed DC magnetic field obtained at transect 12. b) The observed AC magnetic field obtained at transect 12. c) The observed AC electric field obtained at transect 12.

Figure 2.4. Correlation between cable depts and magnetic fields. a) The DC magnetic field dependence on the estimated burial depth using the DC EMF model. The correlation, R^2, was 0.88. b) The AC magnetic field dependence on the estimated burial depth applying the AC EMF model. The correlation, R^2, was 0.94. Unreasonable burial depths (i.e., those greater than 4.0 m) were excluded from the graph.

Figure 3.1. A schematic diagram of the life cycle of anguillid eels and pertinent threats. An illustration of how the different life stages are potentially impacted by a variety of threats according to the advisory IUCN categories. The darker blue arrows of the life cycle represent the oceanic phases and the lighter blue, the continental phases. From Jacoby et al., (2015), used under the Creative Commons license.

Figure 3.2. Efforts to establish the response of the European eel to cable type EMFs. (a) Four transects of acoustic hydrophones enabled the swimming speed of the *A. anguilla* to be compared in the vicinity of the three-phase AC Kalmar Strait Cable in the Baltic Sea (operating with 140-300 A) with swimming speeds north and south of the cable (Westerberg and Lagenfelt, 2008). (b) A laboratory experiment determining the response of *A. anguilla* to AC magnetic fields using Helmholtz coils (Orpwood et al., 2015). Images (a) reproduced with permission (Westerberg and Lagenfelt, 2008) and (b) reproduced under creative commons license.

Figure 3.3. Exposure of a receptive species to cable EMF is dependent on the distance from the cable. (a) The animal's position in the water column influences the distance from the cable (EMF source). (b) The cable burial depth may vary along a cable route. For a species moving along the seabed, the variable burial depth of the cable, changes the distance from source and exposes the animal to variable EMF intensities. Burial depths depicted are approximations and not to scale; (a) 2.0 m, (b) 3.0 m, (c) 2.5 m, (d) 1.5 m. Image (b) reproduced from Hutchison et al., (2021).

Figure 3.4. An overview of the eel study area. The eel collection point from Groton Utilities and release point in the upper stretch of West River are indicated in the upper panel. The release point was 6.2 km (3.9 miles) from the acoustic array between Sandy Point and Fort Nathan Hale in New Haven Harbor, CT, where a high-definition array (small purple box, lower panel) around the HVDC Cross Sound Cable was accompanied by a presence-absence array east and west of the cable (large red box, lower panel). Map created with ESRI ArcMap (version 10.8.1) using basemap 'US States' and 'NOAA Raster Nautical Charts'.

Figure 3.5. The acoustic array range test. Due to restrictions of working in the shipping channel, the range test was completed on flat seabed east of the channel (red box). Being close to the channel ensured relatively similar environmental conditions in shallower depths (15 ft MLLW) (NOAA, 2012). Four VR2W and four HR receivers were deployed with three reference tags to obtain a range of distances.

Figure 3.6. Ensuring appropriate acoustic receiver position to obtain full coverage across the harbor transect. (a) Having the receivers too close together would provide unnecessary overlap in detection. (b) Having the receivers too far apart would reduce the coverage such that eels may pass through the transect without being detected. (c) The ideal scenario provided sufficient overlap in detection to ensure full coverage of the transect area. The ideal

coverage for the HR receivers (circles) in the central array provided overlap between three receivers enabling 2D and 3D triangulation of the eel tag position.

Figure 3.7. Full Vemco acoustic array deployment. Eight HR receivers were deployed within the shipping channel (H1-H8) creating a high-resolution detection area around the buried HVDC cable. Ten VR2W receivers (VA-VJ) were deployed outside of the channel, six on the west side of the channel and four on the east side of the channel. Two reference tags (R1, R3) and four reference tags (R1, R3, R4, R5) were deployed in year 1 (2018) and year 2 (2019) respectively. The basemap used is the 'NOAA Nautical Chart 12371'.

Figure 3.8. The eel telemetry data were analyzed qualitatively and quantitatively. Year 1 and Year 2 data were qualitatively analyzed (see Section 3.4.2.1) and the Year 2 data were quantitatively analyzed (see **Section 3.4.2.2** and **Figure 3.9** for an overview).

Figure 3.9. An overview of how data were combined for the quantitative assessment. The measurement and subsequent modeling of EMF is described in **Section 2**. The collection of 3D telemetry data as an eel passed over the HVDC cable is described in **Section 3.2**. The combination of these datasets with the specific operational characteristics of the cable at the time of the eel passing through the array, allowed the DC and AC EMF for each eel position to be determined. Subsequent statistical analyses allowed the behavioral response to the EMF to be determined. The image of the SEMLA is used with permissions from Hutchison et al., (2018) and the VPS image from Innovasea (2020) is used under the creative commons license.

Figure 3.10. Regularized step intervals were used in the Hidden Markov Model. The telemetry data collected provided positions on an irregular step interval, i.e., positions which varied in distance (cm) and time (seconds). For the analysis, the positions and DC magnetic field encountered were regularized, providing positions every 5 seconds with step lengths which varied in distance. The step length (i.e., distance moved) was the metric analysed and was considered an indicator of speed. Note, that where tracks had intervals greater than 60s, sub-tracks were created to avoid bias in the analysis.

Figure 3.11. A summary of the Hidden Markov Model applied to the three-dimensional eel position data and encountered DC magnetic field. (a) The observed data were regularized to 5 second intervals allowing the step length (i.e., distance moved) to be used in the model (see **Figure 3.9** for an overview of regularization). The HMM was applied to the regularized observed data to determine the behavioral states and dynamics based on transition probabilities. Based on the transition probabilities, the behaviors of the eels were described facilitating the assignment of eels tracks to groups. (b) The behavioral states were based on the step length (i.e., distance moved in 5 s intervals). The HMM characterizes the behavioral states based on the regularized observed step length data (mean, sd, confidence intervals) and can be considered descriptors of low or no activity (small steps), medium speed (medium steps) and high speed of movement (larger steps). (c) The transition probabilities are also derived from the regularized observed data and are indicative of the behavioral dynamics within a track (i.e., probability of changing between states). For example, an eel may move from states 1 to 2 to 1 to 2 to 3 indicating low – medium – low – medium – high activity. The reverse pattern can also occur. A combination of patterns is possible, but eels cannot jump from state 1 to 3 and vice versa they must move through state 2. The change between states is characterized for the observed data in terms of probability of state changes for each eel track and based on the probabilities they can be grouped for their characteristic behaviors (a). (d) While the HMM describes the eel behavior in terms of the behavioral state, transition probabilities and groups the eel tracks accordingly, the question of if the eels respond to the DC magnetic field is assessed at the level of the behavioral state.

Figure 3.12. Cross Sound Cable power activity during the eel migration period in 2015-2019. The hourly power level (ISO New England) is shown as the mean daily power during the months of September through to the end of December between 2015 and 2019.

Figure 3.13. The number of individual eels and number of detections by the VR2W array. The VR2W receivers were positioned at stations (VA-VJ), west to east (W-E) either side of the channel and provided an indication of

presence only. The number of individual eels (left) and number of detections (right) are shown for 2018 (upper panel) and 2019 (lower panel). For reference the VPS array was positioned in the channel between stations VF and VG.

Figure 3.14. The number of detections per eel for each VR2W station in 2018 and 2019. The VR2W receivers were positioned at stations (VA-VJ), west to east (W-E) either side of the channel and provided an indication of presence only. For reference the VPS array was positioned in the channel between stations 'VF' and 'VG'. The number of detections for each eel (represented by black circles), and each station provides an indication of spatial use by individual eels within the array area. A larger number of detections is indicative that the eel spent more time near a station, within each year.

Figure 3.15. Eel movement inferred from the VR2W array. While data from the VR2W receivers only provides an indication of presence in the area, serial data from multiple receivers in a west to east array can provide an indication of movement across the harbor area and also relative speed of movement.

3.16. An overview of the eel tracks from the VPS array in 2018 and 2019. The Cross Sound Cable is indicated as a back line as a visual reference but was buried in the seabed. The VPS High Residency (HR) receivers are indicated as black dots. In 2018 (left) a greater number of eels were detected (n = 21) providing 28 tracks. In 2019 (right) fewer eels were detected (n=12), providing 13 tracks. The eel tracks are color coded by individual eel per year.

Figure 3.17. The eel release and detection dates relative to the daily mean power in the HVDC Cross Sound Cable. The hourly power level (ISO New England) is shown as the mean daily power during the months of September through to the end of December between 2015 and 2019. Eels were released on 5 and 6 dates in 2018 and 2019, respectively, indicated by the red vertical lines (**Table 3.2**) and the date of VPS detections are shown in blue (**Table 3.3. and 3.4**).

Figure 3.18. The DC magnetic field encountered by American eels in 2019. For each 3D eel position, the emitted DC magnetic field and its interaction with the geomagnetic field was modeled. The encountered DC magnetic field is shown with the geomagnetic field (blue, 54.44 μT) as a reference so that the anomaly is clear.

Figure 3.19. The AC magnetic field encountered by American eels in 2019. For each 3D eel position, the emitted AC magnetic field was modeled. The encountered absolute AC magnetic field anomaly is shown.

Figure 3.20. The 3D Hidden Markov Models (HMM) identified three behavioral states. The HMM (shows three behavioral states identified from 12 eels, 13 tracks and 19 sub-tracks from 2019.

Figure 3.21. The horizontal movements of 2019 group 1 eel tracks and behavioral states as determined by the 3D Hidden Markov Model. The eel tracks shown were categorized as group 1 according to the transition probabilities (**Table 3.7, 3.8**). The high residency receivers (HR) are indicated as a spatial reference.

Figure 3.22. The horizontal movements of the 2019 group 2 or mixed group eel tracks and behavioral states as determined by the 3D Hidden Markov Model. The eel tracks shown were categorized predominantly as group 2 according to the transition probabilities (**Table 3.7, 3.8**). The first sub-track of Track 181a was uncertain (either group 1 or 2), followed by 2, 1, 3 and 3. The sub-tracks of Track 181b were both group 2 and the sub-tracks of Track 186 was categorized as group 2, but the second sub-track was uncertain (1 or 2). The high residency receivers (HR) are indicated as a spatial reference.

Figure 3.23. The dive profiles of the 2019 eel tracks and behavioral states as determined by the 3D Hidden Markov Model. The eel tracks shown were categorized as group 1 according to the transition probabilities (**Table 3.6, 3.7**). The dive profile is shown on a standardized scale allowing comparability irrespective of the tidal state, to a reference depth (12.9 m) in the shipping channel.

Figure 3.24. The dive profiles of the 2019 eel tracks and behavioral states as determined by the 3D Hidden Markov Model. The eel tracks shown were categorized predominantly as group 2 according to the transition probabilities (**Table 3.6, 3.7**). The first sub-track of Track 181a was uncertain (either Group 1 or 2), followed by 2, 1, 3 and 3. The sub-tracks of Track 181b were both group 2 and the sub-tracks of Track 186 was categorized as group 2, but the second sub-track was uncertain (1 or 2). The dive profile is shown on a standardized scale allowing comparability irrespective of the tidal state, to a reference depth (12.9 m) in the shipping channel.

Figure 3.25. The effect of the DC magnetic field anomaly encountered on the step mean parameter within behavioral states in American eels. The 3D HMM based on 2019 eel data, identifies the effect of the DC magnetic field anomaly encountered within behavioral state 2 (left) and state 3 (right). An increase in the mean step parameter is observed for both state 2 and state 3 (with confidence intervals). This analysis is based on the movement and encountered DC magnetic field of 12 eels (captured in 13 tracks and 19 sub-tracks).

Figure 3.26. The effect of the DC magnetic field anomaly encountered on the step standard deviation parameter within behavioral states in American eels. The 3D HMM based on 2019 eel data, identifies the effect of the DC magnetic field anomaly encountered within behavioral states. A decrease in the step standard deviation (SD) parameter was observed for state 3 (with confidence intervals). This analysis is based on the movement and encountered DC magnetic field of 12 eels (captured in 13 tracks and 19 sub-tracks).

Figure 3.27. The step length and encountered DC magnetic field for the 2019 eel tracks, and behavioral states as determined by the 3D Hidden Markov Model. The eel tracks shown were categorized as group 1 according to the transition probabilities (**Table 3.6, 3.7**). Step length is the distance moved between two positions at a regularized 5 s interval. The encountered DC magnetic field anomaly was calculated based on the 3D proximity to the HVDC cable, the power level at the specific time and the cable properties at that location. The data were also regularized to the 5 s time interval.

Figure 3.28. The step length and encountered DC magnetic field for the 2019 eel tracks, and behavioral states as determined by the 3D Hidden Markov Model. The eel tracks shown were categorized predominantly as group 2 according to the transition probabilities (**Table 3.6, 3.7**). The first sub-track of Track 181a was uncertain (either group 1 or 2), followed by 2, 1, 3 and 3. The sub-tracks of Track 181b were both group 2 and the sub-tracks of Track 186 was categorized as group 2, but the second sub-track was uncertain (1 or 2). Step length is the distance moved between two positions at a regularized 5 s interval. The encountered DC magnetic field anomaly was calculated based on the 3D proximity to the HVDC cable, the power level at the specific time and the cable properties at that location. The data were also regularized to the 5 s time interval.

Figure 3.29. The importance of combining the operational characteristics of the cable and animal movement ecology. The three scenarios depict a fish taking the same movement path under three different operational power levels. In Scenario 1, the cable operates at 0 MW with only the maintenance current of 16 A and the fish encounters a DC magnetic field of 3 nT at 10 m distance from the cable and 44 nT at 2.7 m from the cable. In Scenario 2, the cable operates at 330 MW (1175A) and the fish encounters a DC magnetic field of 230 nT at 10 m from the buried cable and 3200 nT at 2.7 m from the cable. In scenario 3, the fish encounters the cable operating at 330 MW and therefore encounters 230 nT at 10 m distance from the cable and as the fish moves closer the operational power level changes to 0 MW (16 A) and the fish encounters a lower DC magnetic field of 44 nT despite being closer to the buried cable (2.7 m). Note that the DC magnetic field is modeled using a mean cable burial depth (2.7 m) and twist (0.8 radians) based on the eel study area and specific HVDC Cross Sound Cable characteristics (the AC EMF is not shown). The image is a hypothetical representation of 3D movements in a 2D vertical plane based on what was found in this study and is not to scale.

Figure A1.1. The percentage of eel position data and number of eel tracks retained at different HPE filter levels. The full unfiltered eel data set obtained in 2019 contained 8,290 positions and a total of 17 eel tracks in 3D.

Figure A1.2. All reference tag positions for the full and filtered datasets (HPE <5). The full dataset is shown in figure a color coded for the four reference tags (a) and then color coded for HPE level (b) which the hydrophones (HD) indicated as a reference. The filtered dataset at HPE <5 is shown color coded for the four reference tags (c) and for the HPE level (d) indicating the majority of data has an HPE <1. It is not possible to visualize the proportion of data that overlaps with the known position.

Figure A1.3. The reference tag drags indicate good agreement in positions. Reference tag drags were completed in the upper, middle and lower quadrants of the array, with tags attached at four different depths on a line suspended from a drifting vessel. Each reference tag shows good track agreement (a) and demonstrates a low HPE.

Figure A1.4. The control V9p tag drags indicate good agreement in positions and depths. Control V9p tag drags were completed in middle quadrant of the array, with tags attached at four different depths on a line suspended from a drifting vessel. Each reference tag shows good track agreement (a) and good depth profiles (c) with predominant low HPE. The start and end times of the tag drags are marked as blue vertical lines.

Figure A1.5. The unfiltered and filtered V9p data (HPE <5) for the 2019 study period. All V9p tracks and positions are shown in (a) color coded for individual tags (note that tags 4, 5, 6, and 7 were the control tag drags) which HD hydrophone positions indicated as a reference (black). The retained data (red) versus the lost data (grey) is shown in (b) for an HPE <5.

List of Tables

List of Abbreviations and Acronyms

A	Amps
AC	Alternating Current
AD	Analog-to-Digital
BOEM	Bureau of Ocean Energy Management
CSC	Cross Sound Cable
CT	Connecticut, USA
CI	Confidence Interval
dB	decibel
DC	Direct Current
EMF	Electromagnetic Field
GPS	Global Positioning System
GSO	Graduate School of Oceanography (University of Rhode Island)
HVDC	High Voltage Direct Current
Hz	Hertz
IACUC	Institutional Animal Care and Use Committee
kHz	Kilohertz
kV	Kilovolt
MDL	Micro Data Logger
ML	Maximum Likelihood
mT	milliTesla = T x 10^{-3}
MW	Megawatt
mV/m	Millivolt per meter
nT	nanoTesla = T x 10^{-9}
nV	Nanovolt
NY	New York
OWF	Offshore Wind Farm(s)
p	p-value
PSD	Power Spectral Density
pT	picotesla
REML	Restricted Maximum Likelihood
RI	Rhode Island, USA
SE	Standard error
SEMLA	Swedish ElectroMagnetic Low-noise Apparatus
SD	standard deviation
T	Tesla – SI derived unit used to measure magnetic fields
URI	University of Rhode Island
UTC	Coordinated Universal Time
µT	microTesla = T x 10^{-6}
µV/m	microvolt per meter

Executive Summary

The project was commissioned by the Bureau of Ocean Energy Management (USA) and had the overall aim to research the potential for impacts on American eel (*Anguilla rostrata*) migratory movement from electromagnetic fields (EMFs) emitted by high voltage direct current (HVDC) cables.

Over the past few decades concerns have grown for freshwater eels (Anguillidae) owing to a significant global decline in numbers of all 16 species. The international effort to assist eel conservation is limited by a lack of knowledge on how human activities affect eels during their complex lifecycle, particularly the stage where they undertake large-scale migration from rivers, through coastal waters into the ocean to reproduce. These same coastal and marine waters are areas of rapid industrial expansion, with plans to install several thousand offshore wind turbines and associated subsea power cables.

In the USA, there is only one species of Anguillid eel, the American eel (*A. rostrata*), that has a broad geographical range across the northwest and western Atlantic. The USA eel population is presently considered stable, however, their geographical range overlaps with plans for large-scale offshore wind (OSW) energy development along the northeast Atlantic coast. Therefore, the question of whether there will be environmental impacts for migrating eels is an important consideration, for both the management of the American eel population and the development of an environmentally responsible OSW industry in the US coastal and offshore waters.

Eels are an example of magnetoreceptive species which migrate using cues from the earth's magnetic field, and the potential encounter with anthropogenic electromagnetic fields (EMFs) from subsea cables has been raised as a concern in several studies over the last 10-15 years. However, knowledge is limited. Here we report on research directed at understanding the responses of the migratory eel, to changes to their natural EMF environment due to interactions with anthropogenic EMFs from subsea cables. High voltage (HV) cables either transmit alternating current (AC) or direct current (DC). In the US, OSW projects are expected to use primarily HVAC, but as OSW expands farther offshore, HVDC cables may be considered better export cables to transmit high power over greater distances. Therefore, HVDC cable EMFs may become more frequently encountered by migratory species in the future.

The specific goals of this multi-disciplinary project were to (i) characterize the EMF emissions from an existing HVDC cable in US coastal waters, set within the context of the local geomagnetic field and (ii) determine both the potential encounter and responses of migratory American eels to the EMF. Collectively, this information allowed the determination of potential impacts of cable EMF on the eels. As there were no large-scale OSW installations in USA waters at the time of the study, we focused on an HVDC transmission cable called the Cross Sound Cable (CSC), which has similar characteristics to those that are anticipated to be used in future OSW developments.

In situ measurements of EMF emissions from the HVDC CSC were conducted with a bespoke sensor system (the SEMLA) to characterize the EMF environment in a coastal area where local migratory eels would encounter the cable on their outward migration to sea. This cable had been characterized previously and it was known to emit both DC and AC magnetic fields (MFs) and AC electric fields (EFs). To better characterize the emitted EMF along the HVDC cable route, measurements of the EMFs from the upper reach of the cable extending into Long Island Sound were also undertaken. The measured DC MF was used in a previously verified model to determine the burial depth of the HVDC cable at the point

the SEMLA crossed the cable. The amplitude of the DC MF was greater than the AC MF. The spatial extent of the DC MF and the AC MF were similar whilst the induced AC EF had a greater spatial range. Modeling was used to determine both the DC MF and the AC MF encountered by an eel at a specific position in space and time (i.e., based on the 3D proximity to the cable and the power level in the cable at the time). At this stage further work is required on the AC MF model to verify its suitability to a HVDC cable in relation to burial depth, twist of the bundled cable pair, and power level.

Within the eel study area, the burial depth of the cable was determined to be between 1.8 and 3.7 m. DC MF deviations can be positive or negative relative to the geomagnetic field. The maximum DC MF deviation was 7.5 µT (7500 nT) and the maximum AC MF 0.19 µT (190 nT). There was a strong relationship between the modeled burial depth and the amplitude of the DC MF and also between the modeled burial depth and the amplitude of the AC MF. The EMF modeled burial depths were compared to the 'as-laid' burial depths (i.e., the recorded burial depth at the time of cable-laying) and were found to be within reasonable range of these burial depths, however, the as-laid burial depths were not sufficiently accurate to model the encountered EMF for the eel study.

Building on the present knowledge base of potential eel responses to cable EMFs, we developed an *in situ* observational experiment focusing on the outward migration of the silver American eel past the HVDC CSC. The first aspect when assessing if migratory eels (or any EM-sensitive species) respond to EMF is to determine if they are likely to encounter the HVDC cable EMF. However, to determine the EMF encountered, both horizontal (2D) movement data and vertical movement data are important, since, for the receptive species, it is the distance from the cable (the EMF source) that is the most relevant in the potential exposure to the emitted EMF. Both the movement ecology of the receptive species and the burial depth of the cable are therefore significant factors in determining the distance from the cable and these factors may change along the route of a cable. The true proximity to the cable must also be considered with the operational characteristics of the cable at the specific time of encounter. An overview of cable operations showed the power transmitted was variable, particularly from the fall into winter. Furthermore, the power level varied by the hour based on data from the power cable company.

Advancing on previous work we used a fine-scale 2D and a novel 3D telemetry approach (Vemco VPS array with a VR2W array for presence-absence) to explore the interaction of migratory eels with HVDC cable EMFs in 2018 (Year 1) and 2019 (Year 2). Following a systematic method of field testing, the 3D data from the acoustic tags and receiver array system were assessed and put through a series of positional filtering to maximize accuracy and precision. This resulted in a median error sensitivity of 0.09 m in 2D and 0.10 m in the third dimension. This accuracy in the tracking data was important when determining the true position of the eels and the actual EMF intensity that eels encountered.

Wild-caught silver eels were tagged externally, under appropriate scientific permits and ethical approval, with acoustic tags (with pressure sensors for depth data in year 2). The eels were released into the West River, CT upstream of the CSC area designated for the eel study. The eel telemetry data were assessed in two ways. The year 1 and year 2 data were qualitatively assessed, and year 2 data only were quantitatively analyzed. The qualitative analyses provided information on eel movements across the bay and environmental influences. Assessment of the eel movement data provided the likelihood of encountering the HVDC cable EMF based on 2D proximity to the cable.

The quantitative analyses of the year 2 data were used to determine the true 3D distance of the eels from the HVDC cable. Using the 3D data, the DC and AC components of the EMF were modelled to

provide the MFs encountered by the eels at each of the 3D positions in the animal movement track (at sub-second resolution). Combining the modeled EMF with the operational characteristics of the cable provided realistic information on the DC and AC MFs encountered as the eels passed through the study area. This analysis also enabled consideration of any ecologically meaningful change in the eel movement behavior through the application of Hidden Markov Models (HMMs). The HMM facilitated the characterization of the eel behavior focusing on the speed of movement. In doing so, three states were identified based on the step length (i.e., distance moved in a time interval), the transition between states and characterization of the tracks based on behavioral dynamics (groups). The response to the EMF was assessed based on any change in the step length within each behavioral state.

In 2018, 25% of the eels released were detected by the full acoustic array, and 21% were detected by the high-resolution VPS array located in the area of the cable route. In 2019, 15.5% of eels released were detected by the full array and 8.5 % were detected by the VPS array. The VR2W array (presence-absence) detected eels over the full span of the transect across the harbor. Moving eels were detected for variable time periods (2 min to 1 hr 41 min) and some eels made return visits to the array over 1-5 days. Brief residency (12 hr to 3 days) was observed, and directional movements were determined from the acoustic array, however, these data lacked sufficient detail to derive the encountered EMF or determine eel responses. The VPS array (fine-scale) provided high-resolution movement tracks for tagged eels. Eels were predominantly first detected during the night and in an ebbing or slack tide

In 2018, 21 eels detected provided 28 tracks and in 2019, 12 eels detected provided 13 tracks. Unfortunately, in 2018, the HVDC cable was not transferring power when the eels were detected by the VPS array. In 2019, eels were caught and then released earlier and in greater numbers over a longer period. Eels were recorded passing through the VPS array when the HVDC cable was transferring between 0 and 229 MW, therefore these eels encountered a range of DC and AC MF intensities. The change in EMF encountered by the eels as was defined as an 'anomaly' in the EMF environment, calculated as the difference relative to the background geomagnetic field. In this study eels encountered anomalies ranging from -17.9 to 86.9 nT for the DC MF and 0.8 to 147.7 nT for the AC MF. The maximum anomalies for the DC and AC magnetic fields were correlated.

To analyze the data, a Hidden Markov Model (HMM) was applied to the 3D eel data and encountered DC MF to first characterize the behavior and then determine if there was a response to the DC MF. The observed data were regularized to 5 second intervals allowing the step length (i.e., distance moved) to be used in the HMM. The HMM was applied to the regularized data to determine the behavioral states and dynamics based on transition probabilities. The HMM characterized the behavioral states based on the regularized step length data (mean, sd, confidence intervals) and they can be considered descriptors of low or no activity (small steps), medium speed (medium steps) and high speed of movement (larger steps). The HMM also provided transition probabilities which indicated the probability of an eel moving from one behavioral state to another during one step to the next. The change between states was characterized for the observed data in terms of probability of state changes for each eel track and based on the probabilities they were grouped for their characteristic behaviors. Three groups of eels were identified (Group 1 to 3). Group 1 eels exhibited were most likely to stay in state 3 and exhibited movement with the greatest purpose. In general eels were highly likely to stay in the same state. However, Group 1 and 2 eels did transition (<20%) between state 2 and 3 and these were the fastest moving eels. Group 3 eels were most likely to be in State 1 or 3 and were the least active eels. While the HMM describes the eel behavior in terms of the behavioral state, transition probabilities and groups the

eel tracks accordingly, the question of if the eels respond to the DC MF was assessed at the level of the behavioral state.

In terms of a response to the DC MF, a change in the step mean parameter and the step standard deviation parameter were observed in response to the DC MFs encountered by eels. The findings are specific to the range of DC MF encountered by eels (-17.9 to 86.9 nT) in this study. The HMM revealed that eels in this study responded to the DC MF by increasing their mean step length. Step length increased with increasing DC MF (up to 86.9 nT). In state 2 (intermediate steps, medium activity), the mean step length became longer in response to greater DC MF anomalies. In state 3 (large step length, higher activity), the mean step length became longer and less variable (i.e., more similar) in response to the greater DC MF anomalies. The assessment was made in relation to the DC MF, however, owing to the correlation between the DC and AC MFs, it is plausible that eels responded to either DC or AC MFs.

The proximity to the cable and the operational characteristics of the cable determined the exposure to the EMF and therefore the encountered EMF. It is generally assumed that the closer the eel is to the HVDC cable, the stronger the EMF the eel will encounter, however, this assumption is based on a constant operational power level and therefore EMF level. In reality, the proximity of an eel to the cable and the variable operational characteristics of the power transmission must be accounted for, together. This means that, an eel passing the cable in midwater (i.e., further away) while the cable operates at a high power level may encounter a stronger MF anomaly than an eel passing a cable swimming close to the seabed (i.e., closer to the cable) when the power level is low. The DC MF anomalies in this study were both negative and positive deviations from the geomagnetic field. The response observed (change in step length parameters) was observed to be greater with the greater positive anomalies however the negative anomalies were not as strong; it is important that the observed result is interpreted within context of the range of DC MF encountered (-17.9 to 86.9 nT). The assessment of behavioral response was made in relation to the DC MF, however, owing to the correlation between the DC and AC MFs, it is plausible that eels responded to the DC and/or AC MF.

The resolution of the tracking in this study is far greater than previous studies of eels in the context of cables and EMFs. The levels of MF encountered by the eels and the observed response, aligns with the anticipated sensitivity levels based on magnetite-based reception. The major finding of this study is that the eels responded to the HVDC cable DC MF. This did not constitute an absolute barrier to migration however, the importance of the cable EMF in the context of deriving locational cues from the geomagnetic field requires further work. The potential for cumulative effects is also a consideration.

The study reported here highlights that taking the vantage point of an animal in terms of their exposure and response to EMF requires 3D knowledge on both the EMF anomaly and the movements of the animal, on spatio-temporal scales relevant to the species. For the modeling of EMF encountered by the eels it was essential to have information on cable characteristics, the power level in the cable, the interaction of the cable EMF with the geomagnetic field, and the horizontal and vertical proximity of the eel to the buried cable, to determine exposure. These parameters allowed the speed of movement of migratory eels to be assessed in the response to the EMF and indicated that eels were faster and more directed in their movement. Key recommendations to advance the knowledge of organism response to subsea cable EMF and in parallel further the knowledge of subsea power cable EMFs emitted are provided.

1. Introduction

1.1. Project Overview

Over the past few decades concern has been growing for freshwater eels (family Anguillidae) owing to a significant decline in the numbers of all 16 species across the world (IUCN Anguillid Eel Specialist Group (AESG)). The international effort to enable eel conservation is limited to a large degree by a lack of knowledge on how human activities are affecting the eels during their complex lifecycle, which takes them into a range of aquatic environments including rivers, and then large-scale migration from rivers, through coastal waters into the ocean to reproduce. These same coastal and marine waters are presently the subject of rapid industrial expansion, with plans to install several thousand offshore wind turbines and associated subsea power cables (alternating current, AC, and direct current, DC).

In the USA, there is only one species of Anguillid eel, the American eel (*Anguilla rostrata*), that has a broad geographical range across the northwest and western Atlantic (**Figure 1.1**), (Teng et al., 2009; Jacoby et al., 2017). This geographical range overlaps with the anticipated large-scale development of offshore wind energy along the northeast Atlantic coast (**Figure 1.1**). Therefore, the question of whether there will be environmental impacts for migrating eels is an important recent consideration, for both the management of the American eel population and the development of an environmentally responsible offshore wind industry. Eels are an example of magnetoreceptive species which migrate using cues from the earth's magnetic field, and the potential encounter with anthropogenic electromagnetic fields (EMFs) from subsea cables has been raised as a concern for them (Ohman et al., 2007; Westerberg and Lagenfelt, 2008; Wyman et al., 2018; Hutchison et al., 2020a). However, knowledge on the responses of marine species to changes in their natural magnetic cues from the interaction with anthropogenic EMFs from subsea cables is also limited. The knowledge gaps regarding migratory eel encounters of, and their response to the altered EMF environment as they swim through it, are addressed and reported here.

This project was funded by the Bureau of Ocean Energy Management to conduct research towards understanding the potential for impacts on American eel (*A. rostrata*) movement and migration from EMFs emitted from high voltage direct current (HVDC) cables. Presently HVDC cables associated with leased OWFs in the USA are rare. Inter-array cables between turbines, are and will likely continue to be predominantly lower capacity High Voltage Alternating Current (HVAC) cables. The HVAC cables are also presently more common in leased projects as export cables unless long cables are required in which case HVDC will be used (e.g., Sunrise Wind Project, New York). Presently HVAC cables are also more commonly used in the EU and UK however HVDC cables are more frequently used where distances from shore are greater (Soares-Ramos et al., 2020). Large-scale offshore wind farm developments in the US are anticipated to be higher capacity and deployed at greater distances offshore than the majority of those in Europe and the UK. Therefore, as US offshore wind farms move further from shore, HVDC will become a more economical option for export cables. The use of HVDC is generally considered most optimal to facilitate higher capacity energy transmission over greater distances to onshore grids, comparative to HVAC technology (Soares-Ramos et al., 2020). Therefore, it is anticipated that in future, HVDC EMFs may be more frequently encountered by magnetoreceptive migratory species such as American eels in transitionary coastal waters. The specific goals of this project were to characterize the EMF emissions from an existing HVDC cable in USA coastal waters, set within the context of the local

geomagnetic field and determine both the potential encounter and responses of migratory American eels, to assist in the determination of potential impacts of cable EMF on the eels. As there were no large-scale OWFs with HVDC cables in USA waters, the study focused on an HVDC transmission cable called the Cross Sound Cable, which has similar characteristics to those that are anticipated to be used in future OWF developments.

The report presents the research background, methodology, analysis and interpretation in the following sections. Section 1.2 first provides a broad background for the reader. The growing need for renewable energy resources, the anticipated expansion of the offshore wind sector in the US and the resultant efforts to understand the potential environmental impacts of these developments, including EMFs, is provided (Section 1.2.1). The importance of natural electromagnetic fields and the ecologically important cues they provide to marine species is highlighted (Section 1.2.2) as a precursor to explaining the anticipated proliferation of subsea cabling and associated emission of EMFs (Section 1.2.3). These sections are followed by a brief review of the framework to assess the potential impacts of EMFs by adopting the vantage point of the receptive species (Section 1.2.4) before a detailed overview of the project aims and objectives (Section 1.3).

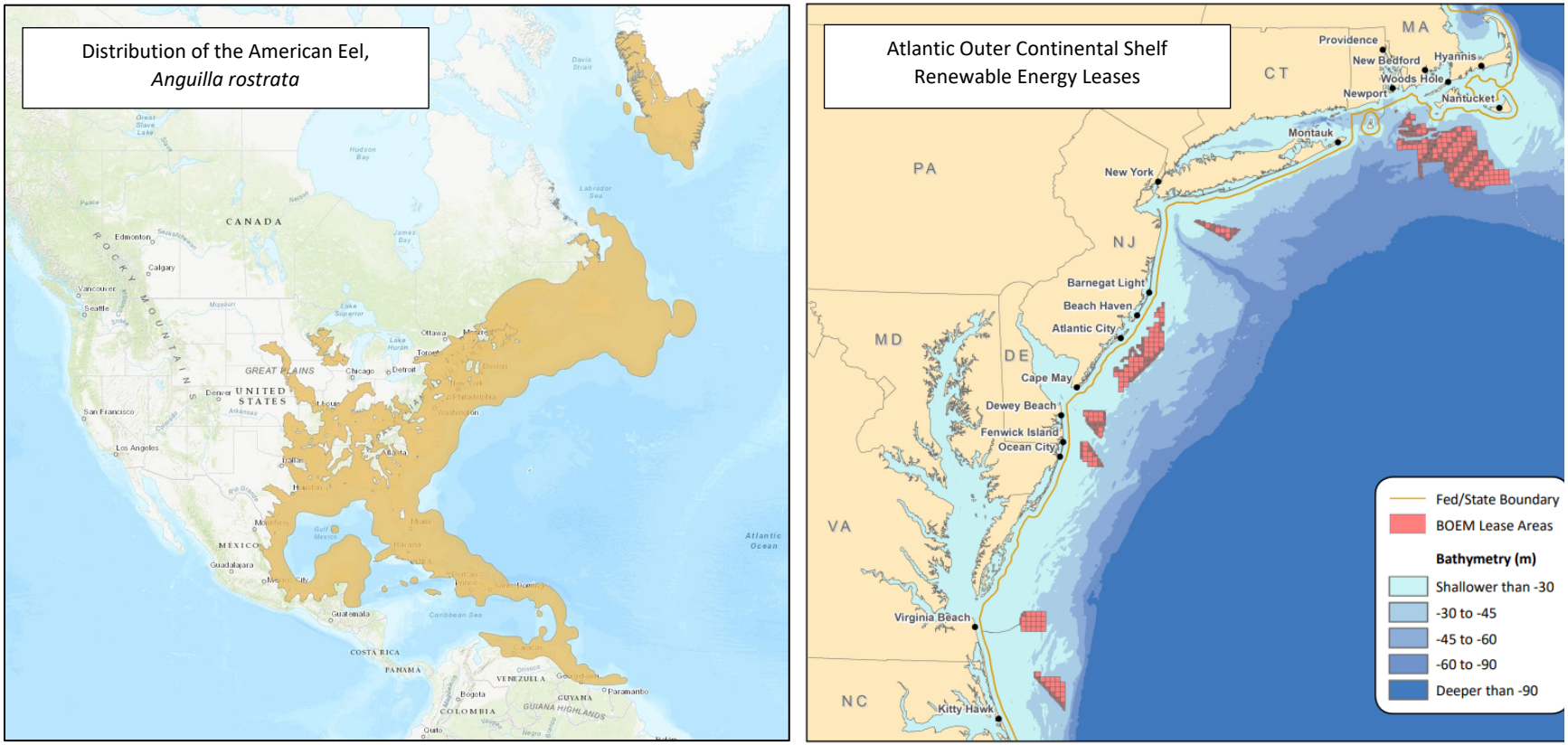

Figure 1.1. The American eel, Anguilla rostrata, distribution and overlap with upcoming offshore wind developments in the US. The geographical range of *A. rostrata* (left) is the Northwest to western Atlantic incorporating the south of Greenland, along the Atlantic coast of Canada through the USA to Panama, the West Indies and Trinidad. The species spawn in the Sargasso Sea. Image compiled by ASSG (Jacoby et al., 2017). The active commercial and research leases (right) for offshore wind developments along the Atlantic coast of the US (BOEM, 2021) overlaps with the geographical range of *A. rostrata*.

1.2. Background

1.2.1. Expansion of renewable energy

With the global move to reduce carbon emissions in a bid to reduce climate change there is a strong emphasis on the need for green energy resources. Between the period of 2000 to 2018, the US commissioned 156 GW of wind and solar power which provided nearly 9% of energy generation in 2018 (Shearer et al., 2020). The US joins many other countries in the goal of net zero carbon emissions by 2050 (GWEC, 2021). With such high precedence to reduce emissions, the use of renewable power generation must increase and much of the available space for wind power is offshore. Globally, 4.8% of installed wind power capacity (743 GW) is presently offshore, of which 6.1 GW was installed during 2020 and annual installations are expected to quadruple by 2025 (GWEC, 2021). The first commercial offshore wind farm in the US was the 30 MW Block Island Wind Farm, off Block Island, Rhode Island which became operational in 2016, followed by the 12 MW pilot Coastal Virginia Offshore Wind Farm, Virginia in 2020. As the US embarks on an ambitious plan for utility-scale offshore wind power along the Atlantic Coast, with many projects under development, the marine management authorities recognize the need for critical research and monitoring of the environmental effects on marine resources (Twigg et al., 2020; BOEM, 2021).

The environmental effects of offshore energy on marine systems are diverse and there are multiple efforts within the US to enhance knowledge and address knowledge gaps which remain, complementing years of research and monitoring within European and UK offshore wind farms. The first US offshore wind farms were monitored by the Real-time Opportunity for Development Environmental Observations (RODEO and RODEO II) program, developed to provide more accurate assessments of the environmental effects of a biological and physical nature in a US context (e.g., HDR, 2020a, 2020b). Through the Memorandum of Understanding between the National Oceanic and Atmospheric Administration (NOAA), the Bureau of Ocean Energy Management (BOEM) and the Responsible Offshore Development Alliance (RODA), a collaborative effort, the 'Synthesis of the Science' was undertaken to synthesize information with a particular focus on the interaction of fisheries and offshore wind energy[1]. This initiative instigated international collaboration to address the ecosystem effects (benthic and physical habitat, physical processes, fishery species, plankton), socio-economics (fishing operation, economy, socio-cultural effects) as well as cumulative impacts with a focus on regional issues and management. In parallel, the New York State Environmental Technical Working Group launched a 'State of the Science' initiative with a focus on cumulative impacts within which they focused on receptor groups (benthos, fish and mobile invertebrates, birds, bats, marine mammals, sea turtles, physical environmental change)[2].

Within these aforementioned initiatives to synthesize knowledge and identify prominent knowledge gaps, the potential impacts of EMFs from sub-sea cables on marine species is repeatedly identified as an area of high uncertainty and low confidence (e.g., Degraer et al., 2021).

[1] https://rodafisheries.org/portfolio/synthesis-of-the-science/
[2] https://www.nyetwg.com/2020-workgroups

1.2.2. Marine species derive ecological cues from electromagnetic fields

Species with the sensory capability to detect electric fields or magnetic fields and derive information from them are considered electro-receptive or magnetoreceptive, respectively. Specialist sensory physiology allows the electric and/or magnetic fields to be detected. Electro-reception is most widespread in aquatic taxa since water is a good conductor of electric fields although terrestrial examples do exist (e.g. bees) (Clarke et al., 2013; Newton et al., 2019). In marine species, electroreception is facilitated by ampullary organs which are relatively well defined within the chondrichthyans (sharks, skates, rays, chimaeras) (Newton et al., 2019). In contrast, magnetoreception is very widespread within terrestrial and aquatic taxa, however the precise sensory mechanisms are not as well understood (Nordmann et al., 2017). Presently three theories of magnetoreception exist which include a light sensitive chemical-based receptor, a mechanically sensitive biogenic magnetite-based receptor, and electromagnetic induction such as that in the ampullary organs of chondrichthyans (Nordmann et al., 2017). The latter two theories are presently considered more applicable to aquatic species (Formicki et al., 2019; Nyqvist et al., 2020).

The most dominant natural EMF in the marine environment is the geomagnetic field from the Earth which, globally, ranges from 25 to 65 μT (Finlay et al., 2010). Movement of conductive water (by currents, tides, or object such as a fish) through the geomagnetic field induces electric fields (typically <10-100's nV/cm) (Nyqvist et al., 2020 and references therein). The solar wind perpetuates a low magnetic field (1-10 nT) with occasional solar storms two orders of magnitude lower than the geomagnetic field and electrical lightning storms generate electric fields (Gill et al., 2014). Bioelectric fields from living organisms result from muscular contractions and cellular processes where they play important roles in biological function, development and regeneration (Bedore and Kajiura, 2013; Harris, 2021). For example, the muscular contraction of a fish may present bioelectric fields of <10 – 100's μV/cm, at <10 Hz, although injured specimens may be up to 500 Hz (Bedore and Kajiura, 2013).

Electro-receptive and magnetoreceptive species are able to derive ecologically important information from natural EMFs. Electro-receptive species may detect the bioelectric fields of predators, prey, mates or use them in communication (Bedore and Kajiura, 2013; Newton et al., 2019). Magnetoreceptive species are able to derive locational information using either a 'magnetic map sense' which defines the ability of the animal to determine their position relative to a goal or a 'magnetic compass sense' enabling an animal to orientate and maintain a heading relative to magnetic north (Lohmann et al., 2008; Putman, 2021). Therefore, these sensory abilities and electromagnetic cues play diverse and important roles in animal ecology.

Anthropogenic changes to the natural electromagnetic environment occur through the introduction of metal, shipping and survey activities, marine and coastal constructions, such as bridges, and the transfer of power through subsea cables (Gill et al., 2014; Klimley et al., 2017; Wyman et al., 2018; Hutchison et al., 2020b; Nyqvist et al., 2020). There is a recognized need to understand how anthropogenic EMFs change the natural EMF environment and potentially disrupt important cues (Formicki et al., 2019; Newton et al., 2019; Hutchison et al., 2020a; Nyqvist et al., 2020). Section 1.3 explains the anticipated increase of subsea cabling and EMFs in the context of the offshore wind industry.

1.2.3. Subsea power cables and electromagnetic field emissions

In offshore wind farms, subsea power cables (hereafter 'cables') are used to transfer the power harnessed by the turbines to the onshore grid. This system of cables typically includes inter-array cables and export cables and often substations for intermittent power collection. For example, Block Island Wind Farm operates with 34.5 kV cables and has 3.2 km (2 miles) of inter-array cables between the 5 turbines. The 10 km (6.2 mile) export cable, runs from the northernmost turbine to the onshore Block Island substation with a subsequent bidirectional transmission cable running 35.1 km (21.8 miles) from Block Island to the Rhode Island mainland (Tetra Tech, 2012). Naturally, with larger windfarms which have more turbines, there are a greater number of inter-array cables and in some cases several higher power rated export cables used for the transfer of power to shore (**Figure 1.2**).

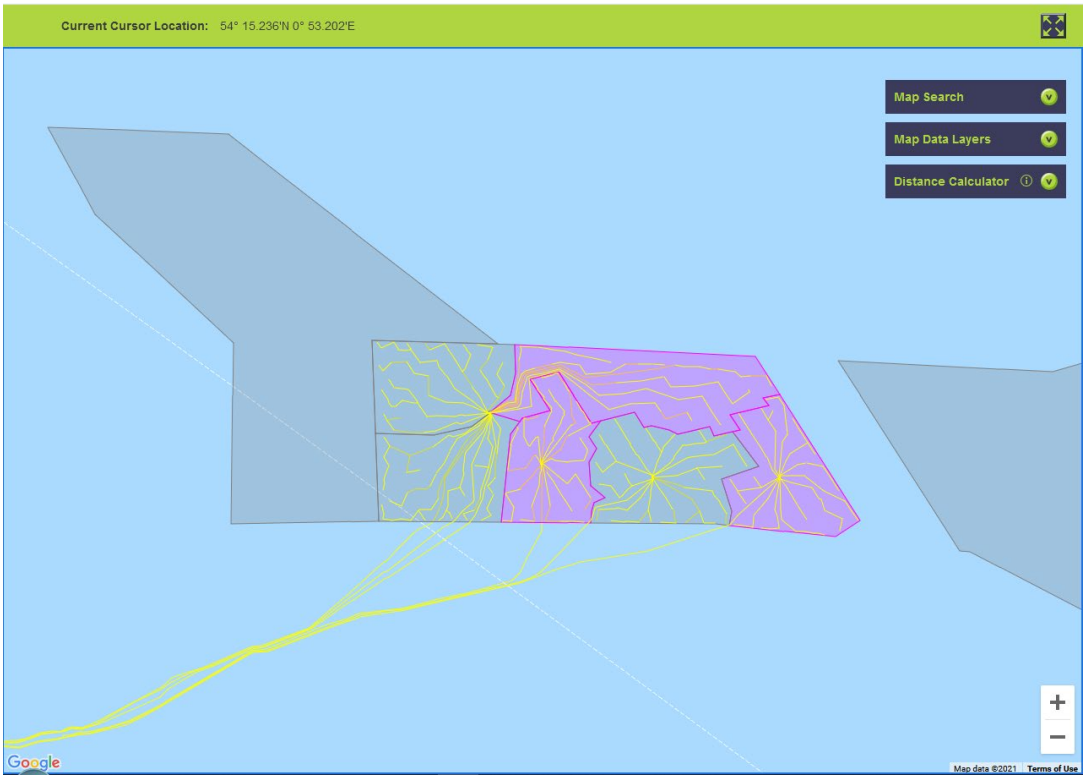

Figure 1.2. An example of inter-array and export cables from a European large-scale offshore windfarm. The cable network shown here is from the 'Hornsea One' (165 turbines, 1386 MW) and 'Hornsea Two' (174 turbines, 1218 MW) offshore windfarms in the southern North Sea off the east coast of England, UK. Image sourced from kis-orca.org and turbine information from 4coffshore.com (accessed February 2021).

Cables from turbines are typically directed by J-tubes down to the seabed where they are often protected by rock armor or concrete mattresses and then buried in the seabed. The majority of export cables are also often buried in the seabed where local geology allows, and if needed, concrete mattresses or rock armor is used as an alternative or in combination (Sheehan et al., 2020; Taormina et al., 2020). These cable protection options for bottom-laid cables protect the cables from abrasion and

third-party damage (Det Norske Veritas AS, 2016; Taormina et al., 2018; Dinmohammadi et al., 2019). Although bottom-laid cables are most common, the development of floating wind energy has also introduced dynamic cabling to the pelagic environment.

Cables associated with offshore wind farms may carry alternating current (AC) or direct current (DC) and may employ substations with transformers. Inter-array cables are typically AC cables however export cables may be AC or DC cables. Presently there are more AC cables employed in offshore wind farms globally, however DC cables offer advantages in reducing electrical losses where the transfer of power occurs over longer distances (Kalair et al., 2016). For example, Germany presently has the greatest number of DC cables associated with offshore wind farms since they exist at greater distances from shore and require longer export routes (Soares-Ramos et al., 2020). At present, operational and leased OWFs in the US, use AC cables for inter-array and export purposes unless longer export routes are required. For example, the leased Sunrise Wind Project in New York (924 MW) is further from shore and will use HVDC technology accommodating an approximate 100 mile cable route. In Europe, there is a decadal trend of OWFs moving further from coasts into deeper water as well as increasing the power capacity of individual turbines (Soares-Ramos et al., 2020). Developments in the US will be further from shore than is typical in Europe and will take advantage of improved modern technology employing large turbines with high power capacities. With this comes the proliferation of cables in the offshore and coastal environment which introduce EMFs to the marine environment raising concerns of their potential impact on marine species (Boehlert and Gill, 2010; Taormina et al., 2018; Hutchison et al., 2020a).

The EMFs from cables and their interaction with the natural EMF in the marine environment is described by Gill et al., (2014). Electromagnetic fields are emitted from cables as a result of electrical charges being passed through the core of the cable. The current describes the rate at which the electrical charge flows, the voltage describes the difference in potential between two points, therefore the power is the product of the current and voltage. In a perfectly grounded cable, the electric field is contained within the cable shielding, however, the generated magnetic field is emitted into the surrounding environment. This observation is true for both AC and DC cables, however their properties differ. In a DC cable, the emitted magnetic field is static (constant), however in the AC scenario the magnetic field occurs in a time-varying state and therefore also generates an induced electric field (also known as ‘back EMFs’).

In the marine environment, the conductivity of the medium (seawater or seawater within the seabed) will influence the spatial propagation of the induced electric field (Gill et al., 2012). Additionally, the conductive environment means that motion, either from the water, or an object such as an animal passing through the magnetic field, results in a motionally induced electric field (motionally induced voltage) (**Figure 1.3**) (Sanford, 1971). The intensity of the EMFs decreases approximately inversely to the distance from the source. However, the EMF is strongly influenced by the properties of the cable (Gill et al., 2014). **Figure 1.4** provides an overview of EMFs from different cable configurations from both fixed and floating wind including options for export cable routes as offshore wind developments become more numerous.

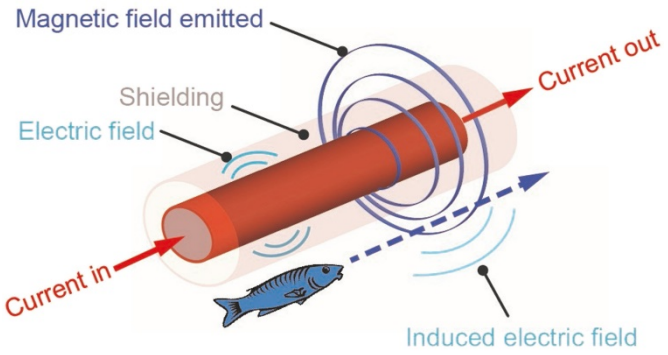

Figure 1.3. A simple representation of a subsea HVDC cable and emitted EMF. The electrical current passes through the cable conductor. The electric field is contained within the cable shielding, but the magnetic field is emitted into the surrounding environment. The motionally induced electric field arising from a fish passing through the emitted magnetic field is also shown. Single-core DC cables can be paired or bundled with another cable. Note that if the cable were HVAC, an induced electric field would also be emitted by the asymmetric rotation of the magnetic field during transmission of the electrical current. Reproduced with permission from Hutchison et al., (2021).

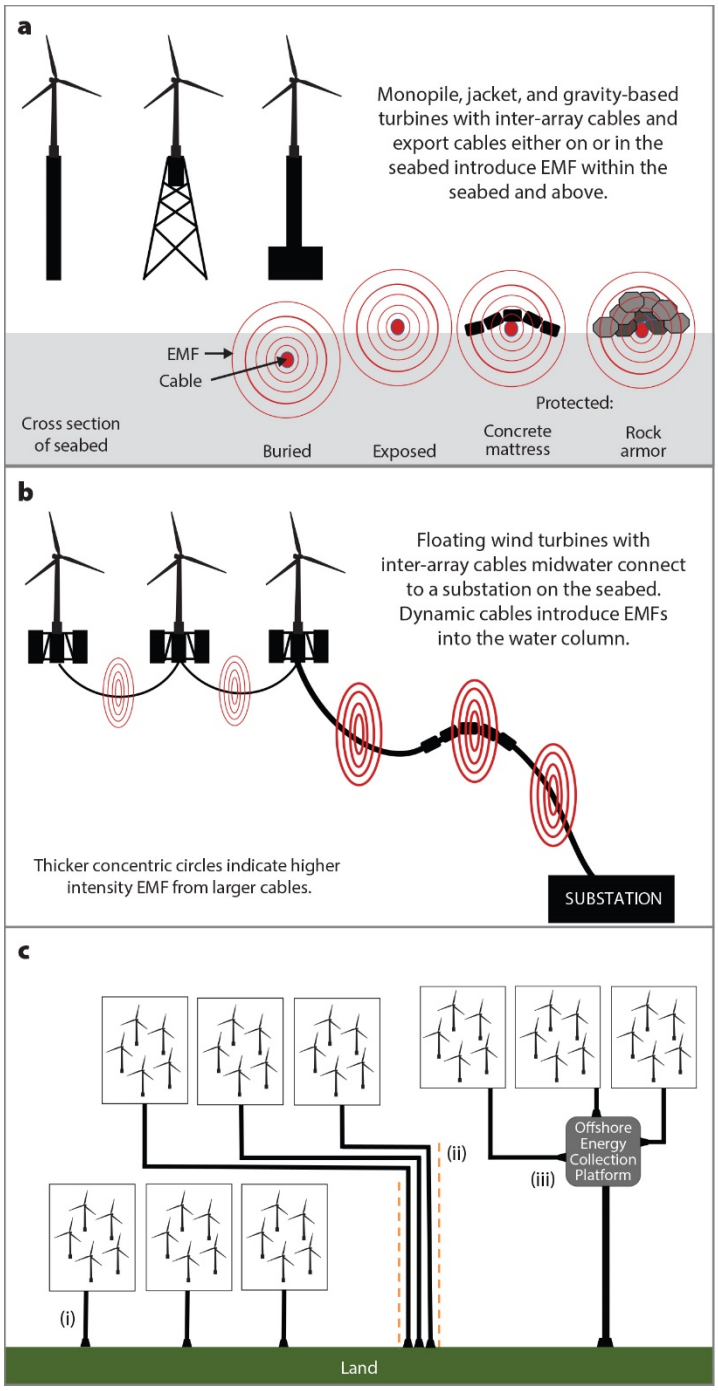

Figure 1.4. Subsea cables introduce electromagnetic field (EMF) emissions. (a) Benthic EMFs are emitted from export cables and inter-array cables that serve fixed foundation devices, either buried in or laid on the seabed with protection. (b) EMFs are emitted into the pelagic environment from dynamic cables of floating offshore wind projects. (c) Cable route configuration options as arrays increase in coastal waters include (i) simple individual exports from each array, (ii) multiple cables that may be in corridors, or (iii) offshore collection platforms that employ higher capacity export cables. From Hutchison et al., (2020a) used under the creative commons license.

Electromagnetic fields are typically modeled and rarely measured *in situ,* although there are some examples in the literature and a range of methods for measurement. These methods are summarized in **Table 1.1**. Measurements of EMFs from offshore wind farm cables have taken place in Belgium (export and inter-array cable, buried 1.0-1.5 m (3-5 ft)) and at the Block Island Wind Farm (export cable, buried 1.2-1.8 m (4-6 ft)) (Thomsen et al., 2015; Hutchison et al., 2018). In both circumstances, measurements were taken on low wind days to accommodate the deployment of a measuring device from a vessel (**Table 1.1**). Therefore, measured EMFs were of low intensity due to low operational power levels. However, it is noteworthy that there was still a measurable EMF from the cable despite the wind farm in Belgium not being operational (i.e., turbine blades were not turning); this results from the maintenance charge retained in the cable despite there being no energy to transfer (Thomsen et al., 2015). The EMFs from Block Island Wind Farm were also of low intensities, however, they were measurable despite a degree of self-cancellation owing to cable properties (Hutchison et al., 2018).

There have been more measurements of cable EMFs taken at non-offshore wind farm cables. Of particular relevance is the characterization of the EMFs from two HVDC cables in the US which employed the same methods of measurement as the aforementioned offshore wind farms. These include the buried Cross Sound Cable, in Long Island Sound, Connecticut and the Neptune Cable, New Jersey, which each had targeted burial depths between 1.2-1.8 m (4-6 ft) (Hutchison et al., 2020b). During operation, these cables emitted an EMF which was detectable at the level of the seabed and within biologically relevant intensities (i.e., within the expected range of the magneto-sensory and electro-sensory capacity of marine species (Tricas and New, 1997; Walker et al., 1997; Albert et al., 2020). The spatial extent of the measured DC magnetic field emitted by the cable was within 5-10 m either side of the cable which aligned with expectations from models. However, the *in situ* measurements also revealed an unexpected strong AC field, associated with both HVDC cables. The spatial extent of the AC magnetic field ranged between 5-10 m of the cable, but the AC electric field was present over a greater spatial extent of 80-100 m from the buried cables. *In situ* measurements have further exemplified the three-dimensional interactions of the emitted cable EMF with the local geomagnetic field which result in positive and negative anomalies as a result of their superimposition (Kavet et al., 2016; Hutchison et al., 2020b). Therefore, the interaction of the cable EMF with the local geomagnetic field must be considered in environmental assessments of potential impacts since some animals rely on the natural electromagnetic environment for ecologically important cues (Hutchison et al., 2020a).

Table 1.1. Measurements of electromagnetic fields from subsea power cables. Cables reported may be considered a proxy for similar capacity to export cables of future OWF scenarios. The Block Island Wind Farm (BIWF) sea2shore cable is also reported. Table modified from Gill and Desender (2020).

Cable Cable & Location	Specifications	Type	EMF Measurements Method	Magnetic field	Electric Field	Spatial Extent	Ref
Belgian OWF (Preliminary trial of SEMLA device) **Use:** OWF inter-array (C-Power) & export cable (Northwind) **Position:** both buried	Inter-array: not powered Export: 70 A	AC	**Platform:** vessel towed/suspended Swedish Electromagnetic Low-noise Apparatus 'SEMLA' (sledge). **Measured:** electric & magnetic fields, 3D. **Position:** on the seabed (magnetic sensor, 0.15m above seabed, electric sensors 0.52-1.04m above seabed).	Max: 4 nT inter-array cable (OWF not operational; device suspended) Max: 17 nT export (at 15 m distance)	Max: 0.3 mV/m inter-array (not operational) Max: 1.5 m/V export (at 15 m distance)	n/a 10's m	1
Cable near the Naval Surface Warfare Centre, South Florida Ocean Measurement Facility, South Florida, USA* **Use:** naval test site **Position:** buried	2-2.4 A, 0.98-1.59 A, 60 Hz	DC AC	**Platform:** AUV towed device **Measured:** magnetic fields, 3D. **Position:** 2.2 m above seabed. **Measured:** electric fields, 3D. **Position:** 4 m above seabed.	**Powered:** Max 150 µT positive deviation, -50 µT negative deviation from ambient. **Not powered:** Mean 30 nT above ambient n/a	n/a **Powered:** 60µV/m Mean 32 µV/m. **Not powered:** 10 µV/m	~10's m (estimated) ~150 m (estimated)	2
Trans Bay Cable (85 km), San Francisco Bay, California, USA** **Use:** domestic **Position:** buried	Max rating: 200 kV, 400 MW (variable power during survey)	DC	**Platform:** vessel towed drop-down device. **Measured:** magnetic field. **Position:** Surface tow (c.a. 14 m above seabed) and deep tow (c.a. 8 m above seabed).	**Surface tow**: mean 117.0 nT (sd = 22.1) **Deep tow**: mean 300.5 nT (sd = 130.5)	n/a	~80 m (40 m either side of cable)	3
Basslink (290 km), Bass Strait, Tasmania, Australia **Use:** state transfer **Position:** buried	592 A, 237 MW (1500 A, 600 MW)	DC	**Platform:** vessel towed drop down device. **Measured:** magnetic field, 2D. **Position:** 5, 10, 15, 20 m above seabed.	**Range:** 57.2 – 61.5 µT (background 61.6 µT) **At 5 m height:** 57.9 µT (background, 58.3 µT)	n/a **At 5m**: 5.8 µV/m***	up to 20 m from seabed & 10-15m either side of cable horizontally	4

Cross Sound Cable (40 km), Connecticut, USA **Use:** domestic **Position:** buried	0-345 A (300 kV, 330 MW)	DC	**Platform:** vessel towed Swedish Electromagnetic Low-noise Apparatus 'SEMLA' (sledge). **Measured:** electric & magnetic fields, 3D. **Position:** on the seabed (magnetic sensor, 0.15m above seabed, electric sensors 0.52-1.04m above seabed).	**DC:** 0.4-18.7 µT (expected) **AC:** max 0.15 µT (unexpected) (background, 51.3 µT)	n/a **AC:** max 0.7 mV/m	Magnetic fields: 5-10m. Electric field: up to 100 m (either side)	5,6
Neptune Cable (105 km), New Jersey, USA **Use:** domestic **Position:** buried	500 kV, 660 MW	DC	As above	**DC:** 1.3-20.7 µT (expected) **AC:** max 0.04µT (unexpected)	n/a **AC:** max 0.4 mV/m	Magnetic fields: 5-10m. Electric field: up to 100 m (either side)	5,6
BIWF Sea2shore (32 km), Rhode Island, USA **Use:** OWF export **Position:** buried	502 A, 30 MW	DC	As above	**AC:** 0.005 - 3.0 µT	**AC:** 0.02 - 0.25 mV/m	Up to 100 m either side of cable	6

*Magnetic and electric field measuring devices were towed independently while the cable was powered and unpowered with AC or DC currents. **Mean anomalies accounting for total range for positive and negative deviations, in absence of bridges. ***Motionally induced electric field arising from water movement through the measured magnetic field, calculated at 0.1m/s water flow. References: 1. Thomsen et al., 2015; 2. Dhanak et al., 2015; 3. Kavet et al., 2016 & supp. Material; 4. Sherwood et al., 2016, 5. Hutchison et al., 2020b; 6. Hutchison et al., 2018.

1.2.4. Assessing an Impact

Within the literature there is recognition of stressor-receptor relationships whereby an anthropogenic activity results in a stressor (or pressure) which may change or impact an environmental component (Bergström L. et al., 2014). In the case of the eels as the receptor the subsea cable EMF is the potential stressor. In some cases, the change is deemed an effect and to be an impact there must be additional consideration of the severity, intensity or duration of the effect (Boehlert and Gill, 2010). Furthermore, it is of note that an effect or impact may be deemed to be positive or negative or may be both in the context of cascading (indirect) effects (Dannheim et al., 2020). A further consideration is the potential cumulative effects and impacts which are of particular importance when assessing environmental effects at a regional scale (Willsteed et al., 2018). Cumulative effects may be most simply considered as the direct and/or indirect effects which may occur over greater spatial and temporal scales (Boehlert and Gill, 2010). However, within these broader scales the complexity of interacting effects can lead to individual minor effects becoming accumulative (i.e. additive, interactive, synergistic or irregular) and therefore become significant to the receptor over different spatial or temporal scales (Harriman and Noble, 2008; Willsteed et al., 2017).

Whilst the literature separates out these elements of environmental impact, in the USA, all environmental evaluations follow the regulations as specified by the National Environmental Policy Act (NEPA). Where the regulations are straightforward and explicitly state that effect and impact are synonymous and may include direct, indirect and cumulative effects of a beneficial or detrimental nature (40 CFR 1508.8).

In this context, we consider effect to be equivalent to an impact with undefined severity and therefore any resultant change in the eel receptor from encounter with the cable EMF is regarded as an impact. To determine the consequence or severity of an impact of EMF on eels requires knowledge of the different components that describe the EMF and the likelihood of the eels encountering the EMF. (**Figure 1.5**). The EMF must be considered from the vantage point of the receptive species; this requires consideration of the species perception of the EMF in space and time (Hutchison et al., 2020a). This approach requires appropriate knowledge of their sensory ecology, and consideration of their life history and movement ecology (**Figure 1.5**). The characterization of the EMF will require knowledge of the cable position in the marine environment, the specific cable attributes, energy supply which will be temporally variable and the type of current within the cable. **Section 1.5** explains how knowledge from the pressure and receptor are drawn together within this report to determine the potential impact of EMFs on migrating American eels.

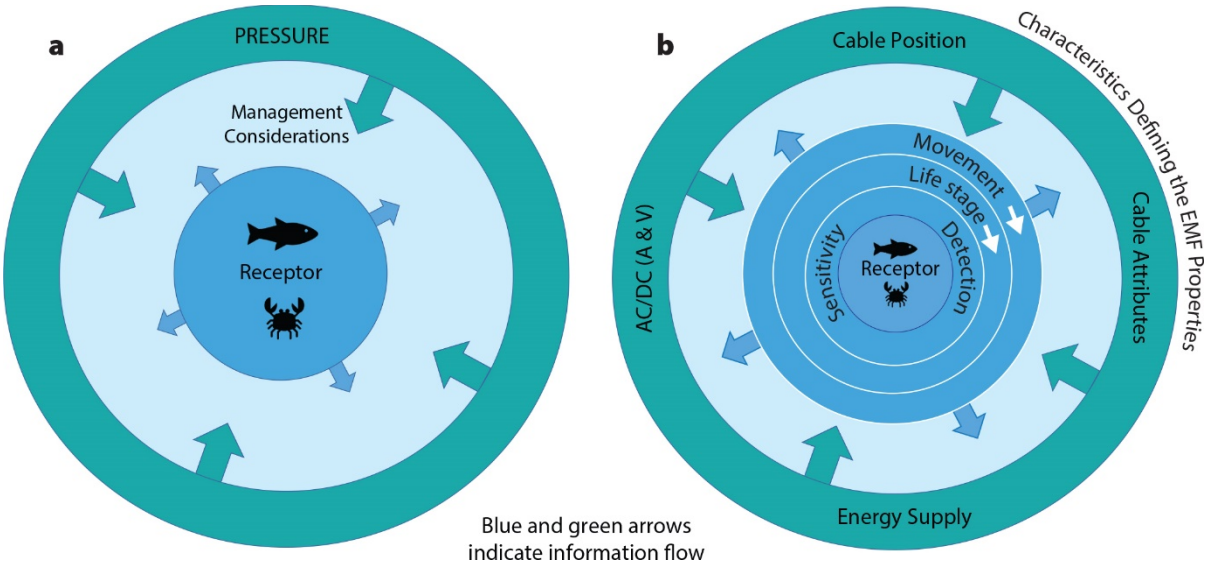

Figure 1.5. Vantage point of the receptor species. (a) Management must be informed by characteristics defining the pressure (here, EMF) and receptor response. (b) Sensory capabilities and detection thresholds are at the core of receptor species attributes and must be considered through the integration of life history ecology. Simultaneously, EMF characteristics must be known so that exposure levels can be determined, and management can consider the likely encounter rate and potential consequences of exposure. A = Current (amps). V = Voltage (volts). From Hutchison et al., (2020a).

1.3. Project aim, objectives and report outline

The aim of this project was to improve the scientific understanding of the potential impacts of electromagnetic fields emitted from an HVDC subsea cable, the Cross Sound Cable (CSC), on the American eel (*A. rostrata*). The study was completed on a HVDC cable because migratory eels were more likely to encounter export cable EMFs which may be AC or DC in nature. An HVDC cables was selected on the basis that the HVDC cables have greater operational capacity and theoretically emit greater EMFs providing a greater chance of detecting a measurable change in behavior. The CSC was considered a proxy for future HVDC offshore wind export cables and therefore provides valuable context regarding the anticipated EMF emissions, their effects on marine species and if mitigation measures may be required. The approach taken was to apply a scientifically robust methodology and analytical approach to determine the HVDC cable EMF environment, the EMF encountered by American eels when entering an area where subsea HVDC cable EMF is expected, and the effects on the movement behavior of the eels during their outward migration through coastal waters to sea. The knowledge gained from this project further provides valuable context for the management of the potential impacts of EMFs, to a number of marine species, by characterizing the three-dimensional properties of the EMF and their interaction with the local geomagnetic field.

To fulfill the above aim, several interlinked objectives were developed and undertaken in parallel. The objectives were:

1. Building on previous work on the HVDC CSC, further characterize the emitted EMF using custom equipment enabling three-dimensional measurements of the magnetic and electric fields.

    a. A detailed characterization of EMFs in the selected area for the eel study, in conjunction with Objective 2.
    b. Characterization included EMF measurements along the length of the HVDC cable to better define the DC and AC fields emitted by the cable.
2. To develop a free-ranging tracking study employing novel tagging technology to determine individual eel proximity to the cable and enable fine-scale (2D and 3D) movement behaviors and responses to the EMF be assessed.
    a. Development of the tagging study including a testing and refinement phase.
    b. In conjunction with Objective 1a, define the EMF encountered by individual eels based on their proximity to the buried cable and the operational characteristics.
    c. Based on the encountered EMF (Objective 2b) determine if the eels respond to the cable EMF in an ecologically meaningful way.

The HVDC CSC is a domestic energy transmission cable which transfers electrical energy between the Halvarsson converter station in New Haven, CT and the Tomson converter station in Shoreham, Long Island, NY (Cross Sound Cable Company, 2020). The characterization of the EMF was undertaken on a significant stretch of the HVDC CSC, reaching into the middle of Long Island Sound. A more focused characterization was undertaken on an area of the HVDC cable within the New Haven Harbor, between Sandy Point and Fort Nathan Hale, where the eel free-ranging tracking study was undertaken. **Figure 1.6** details the HVDC CSC and the project study areas.

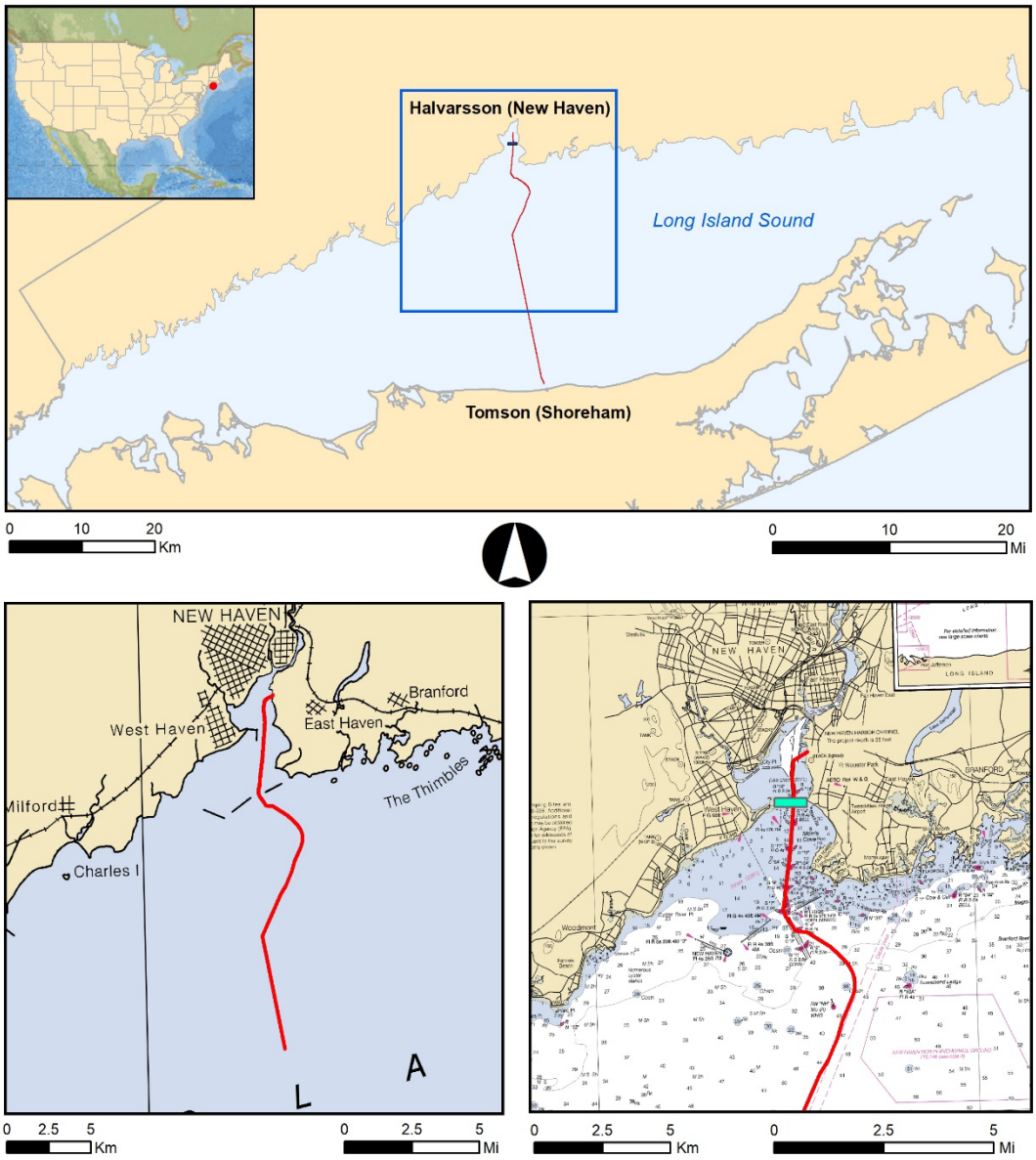

Figure 1.6. The HVDC Cross Sound Cable study sites. Top panel: the HVDC Cross Sound Cable transfers electrical energy between the Halverson converter station in New Haven, CT and the Tomson converter station in Shoreham, Long Island, NY. Lower left panel: a significant stretch of the HVDC cable was surveyed to characterize the EMF, extending into Long Island Sound. Lower right panel: the HVDC cable EMF was characterized in greater detail in the eel study area (green box) where the migratory eels were most likely to encounter the cables path on their outward migration. Image created using basemap sources from ESRI ArcGIS Online (including 'US States', 'National Geographic', 'NOAA Raster Nautical Charts').

Section 2 describes the systematic approach taken to combine measurements of the DC and AC fields with models to characterize the EMFs emitted from the HVDC CSC, in general and in detail for the eel study area. The approach to determine the position (depth) of the buried HVDC cable and subsequently model the EMFs in the water column to enable the EMFs encountered by eels to be derived, is also

described. Section 3 introduces the importance of the American eel (*A. rostrata*), and modern pressures on the population as well as the present state of knowledge regarding the anguillid magnetoreceptive abilities and the role in their migratory ecology. The novel approach to determining the encountered EMFs and the behavioral response of American eels to the EMF is fully detailed and discussed. The integrated nature of the project is detailed in **Figure 1.7**. Section 4 then summarizes the conclusions of Section 2 and 3 in the broader context of environmental effects of EMF from offshore wind farm cables.

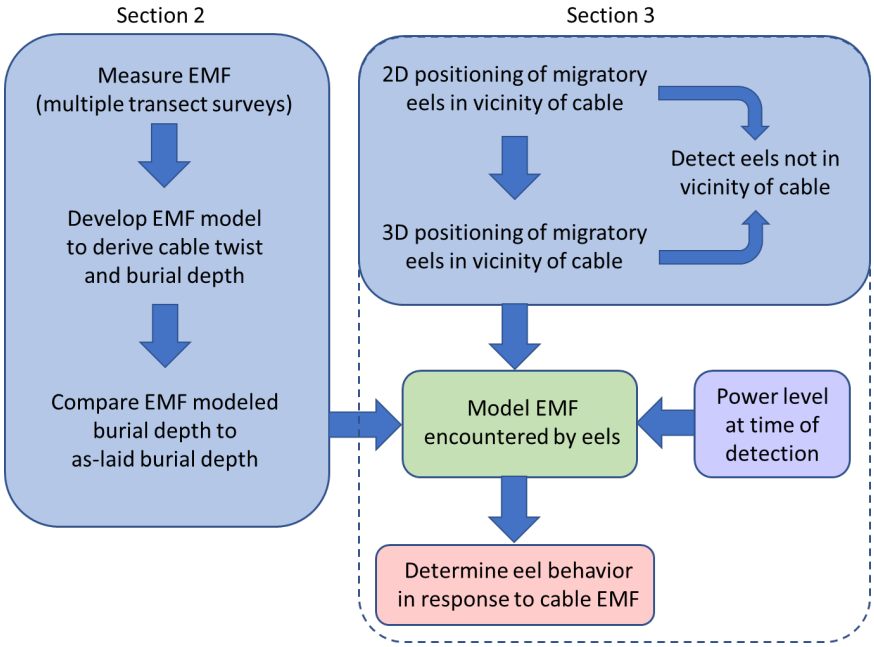

Figure 1.7. The integrated approach to determine the response of eels to the HVDC cable EMFs. The steps take to measure and model the EMFs are detailed in **Section 2**. The steps taken to determine behavioral response of eels to the HVDC cable EMFs, required the fine-scale positioning of eels and modeling the encountered EMFs based on the power level and are described in **Section 3**.

2. Characterizing Electromagnetic Fields from the Direct Current Cross Sound Cable

2.1. Introduction

The electromagnetic environment in the sea is attributable to natural sources (e.g., the earth's magnetic field) and anthropogenic sources (e.g., subsea cables). Therefore, when considering the potential effects of electromagnetic fields (EMFs) on receptive organisms it is important to be able to define the individual components that contribute to the EMF environment. Here, we set out the approach taken to determine the EMF that would be encountered by migratory eels, when passing a subsea high voltage direct current (HVDC) cable in transitionary waters, through a combination of models and *in situ* measurements.

2.1.1. Introduction to electromagnetic fields generated by cables in the sea

Electromagnetic fields (EMFs) consist of both electric and magnetic fields. When transmitting electricity through subsea power cables, a static current (direct current, DC) flowing in the cable core creates a DC magnetic field in the environment around the cable. If the electric current is time varying (alternating current, AC), then a magnetic field and induced electric field are present around the cable, and they are related, as described by Maxwell's equations (Panofsky and Phillips, 2005). In terms of the environment that the cables are located within, the presence of conducting media, such as the saline seawater, propagates induced electric currents (eddy currents). This observation implies that the electric currents are restricted to the conductive layers in the environment, e.g., the seawater and conducting sediments. The DC magnetic field is not directly affected by saline water and if no magnetic material, e.g., iron ore, is in the vicinity, the DC magnetic field propagates undisturbed in the sediments, ocean and in the air.

There are two types of transmission systems for transferring power in nearshore environments. If the power is generated close to the land, then AC power systems are generally used, where the current varies sinusoidally at 60 Hz (USA power frequency). If the power is transferred over a longer distance, then DC power systems are used, where the current is static but regulated at predetermined intervals. In the case of the Cross Sound Cable (CSC), the power and thereby the current, is regulated at the full hour; the reading and recording of the current for the CSC is done once every hour, at approximately five minutes past the full hour. DC transmission cables are often used because of the lower power loss in comparison with AC systems, but initial infrastructure costs are usually higher for DC cables. There are a number of high-power cable types available on the market. The cables differ for AC and DC transmission in that the former requires three conductors were as the latter two. For a bundled DC cable, the twist does not decrease the fields. Increased burial depth will decrease the maximal DC field at the level of the seabed due to increased distance from the cable but has no major effect on the amplitude of the AC fields that were observed to have a wider spread from the cable. Switching from bundled to coaxial cable would drastically decrease the AC and DC fields but only for DC cables since there are no three conductor coaxial cables on the market for AC cables.

2.1.2. The HVDC Cross Sound Cable (CSC) Power

The HVDC CSC power system is based on a bipolar transmission, in which the DC current is fed into one cable and the return current is in a second parallel cable. The two electrical cables are bundled together with a fiber-optic cable into one subsea cable that extends for 24 miles (39 km) buried in Long Island Sound, connecting the electric grid of New England to Long Island (New York, NY) (Cross Sound Cable Company, 2020). Commercial operation of the HVDC CSC started in 2003. The cable runs from the Halvarsson Converter Station in New Haven (Connecticut, CT), through New Haven Harbor, crosses Long Island Sound, and enters the Tomson Converter Station in Shoreham (NY). The HVDC CSC transmits a maximum power of 330 megawatt (MW) at a voltage difference of 300 kilovolt (kV). The maximum rated current is 1175 amp (A). At the feed end, the AC power from the power grid is rectified into DC power and transferred as DC current and DC voltage in the subsea HVDC cable. At the other end, the DC current is reconverted into AC current before being fed to the consumer grid. The electric current in the HVDC cable generates EMFs in the sea. The AC-DC-AC conversions are known to produce side harmonics starting at 60 Hz that are superimposed on the DC current. Hence, the HVDC CSC transmission should be regarded as a line source generating both AC and DC currents that in turn are expected to generate DC and AC fields in the ocean (Railing et al., 2004).

2.1.3. Previous work on the HVDC Cross Sound Cable

The EMFs of the HVDC CSC were characterized in situ in an earlier study (Hutchison et al., 2020b). The EMFs outside the breakwater of New Haven were measured at 32 transects crossing the cable using the same method and equipment as in the present study. The DC magnetic field, the AC magnetic and AC electric field components of the EMF were measured for three different modes of operation: cable offline, cable online but with no power transmission, and with 345 A running in the cable. The maximum DC magnetic field deviation was 14 μT (at 345 A) and the average deviation of the DC magnetic field was 4 μT. In the Hutchison et al., (2020b) study, a magnetic-field model for the DC magnetic field was used to determine the burial depth of the cable based on the measured EMF and electric current in the HVDC CSC. The results showed that the burial depth varied between 2 and 5 feet (0.6 and 1.5 m), in line with the recorded 'as-laid' burial depth (Cross Sound Cable Company, 2002). The 2 feet (0.6 m) burial depth was found for the observed maximum DC magnetic field. The AC fields for both the magnetic and electric fields were also measured. Spectral analysis of the AC fields measured at the seabed showed that there were side harmonics generated from 60 Hz up to at least 2500 Hz. The average total amplitudes of the observed AC components were 0.7 mV/m and 0.15 μT with 345 A running in the cable.

Key Information Box 2.1

- The Cross Sound Cable (CSC) is a high voltage direct current cable (HVDC) with a maximum operating capacity of 330 MW (1175 A)
- The HVDC CSC has an AC-DC-AC transformer to convert transmitted energy
- The EMF from the HVDC CSC has been previously characterized and has a measurable DC magnetic field, an AC magnetic field and an AC electric field
- The present work was to further characterize the EMF in general and also in the area of the eel study so that the EMF encountered could be modeled (see **Figure 1.7**)

2.1.4. Present work on the HVDC Cross Sound Cable

The primary aim of measuring and modeling the EMF emissions from the HVDC CSC was to characterize the EMFs that migratory eels encountered on their outward migration to sea (Section 3). A secondary aim was to better characterize the emitted DC and AC fields along the HVDC cable route by obtaining *in situ* measurements of the EMFs from the upper reach of the cable, extending into Long Island Sound.

2.2. Methods

2.2.1. Transect surveys to collect EMF data from the HVDC Cross Sound Cable (CSC)

A total of 22 straight line transect surveys were undertaken in and outside the New Haven Harbor to measure the EMFs by crossing the cable in as near to perpendicular an orientation to the buried HVDC CSC as possible (**Figure 2.1**). Eighteen transects were undertaken in the eel study area (described in full in **Section 3.2**), located between Sandy Point and Fort Nathan Hale to characterize the EMF in the tracking area of the eels. Four additional transect surveys were undertaken along the cable route to investigate any changes in the DC and AC fields along the cable route. One transect was undertaken in front of the Halvarsson Converter Station (track 1), one outside the breakwater (track 20) and two near to the midpoint between Long Island and New Haven (track 21 and 22; **Figure 2.1**).

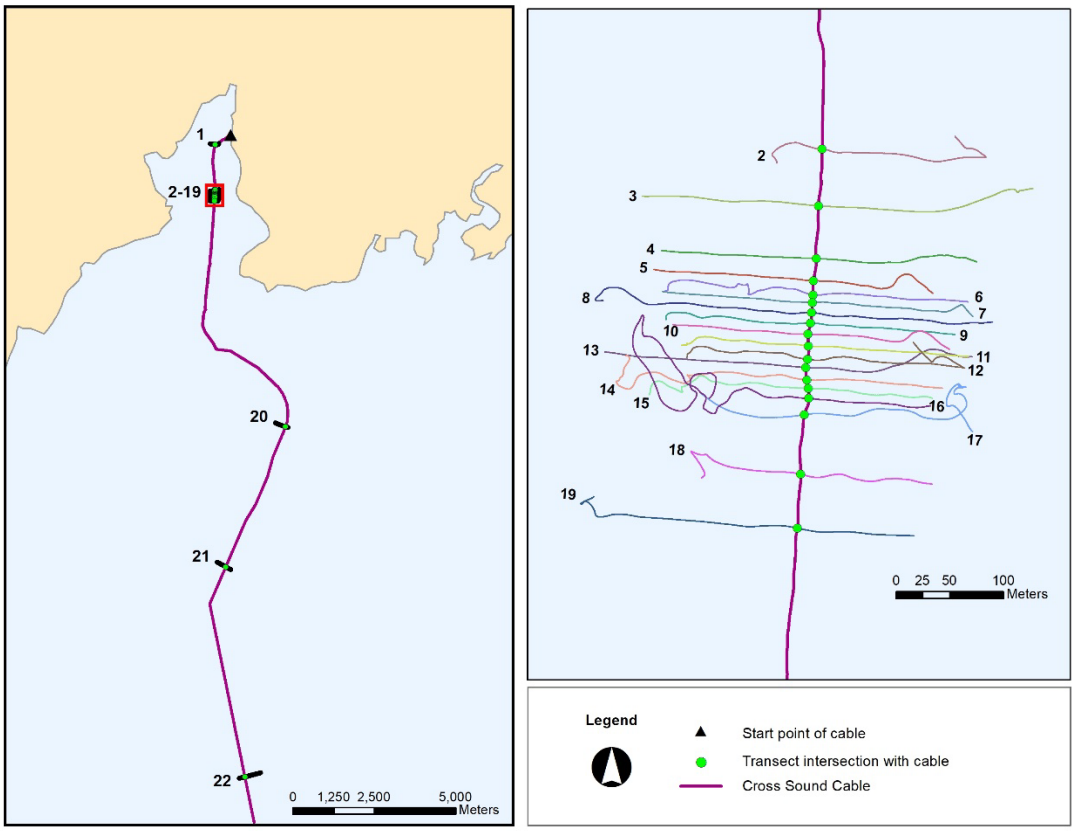

Figure 2.1. Chart showing the survey transects. Left panel: Northern stretch of the HVDC CSC route starting at New Haven. The triangle shows the position of the Halvarsson Converter Station. The line shows the cable route and the red box indicates the eel study area where a high density of transects were undertaken. The labels numerate the surveys in north to south order (track 1-22). Right panel: the eighteen surveys conducted in the eel study area (track 2-19).

2.2.2. Measuring the EMF from the HVDC Cross Sound Cable (CSC)

Measurements of EMF used a custom sensor platform, the Swedish Electromagnetic Field Low-Noise Apparatus, known as the SEMLA (**Figure 2.2**). For a detailed description see Hutchison et al., (2018). The magnetic field was measured using a three axial magnetic fluxgate sensor. The sensor platform was also equipped with electric sensors for characterizing the electrical field generated by the buried cable. The magnetic sensor was mounted on the lower part of the platform 0.15 m above the seabed keeping the sensor as near to the buried cable as possible. The electric field sensors were mounted on the top of the platform forming a cross. The center of the horizontal cross was mounted 0.52 m above the seabed and the center of the vertical was 1.04 m. The sensor signals were pre-amplified at the sledge and transferred to the boat unit by an electric cable running from the sensor platform to the towing boat. On the boat, the analogue sensor signals were low-passed filtered at 1 kHz to avoid signal aliasing before being sampled at 5 kHz with a 24-bit Analog-to-Digital Converter.

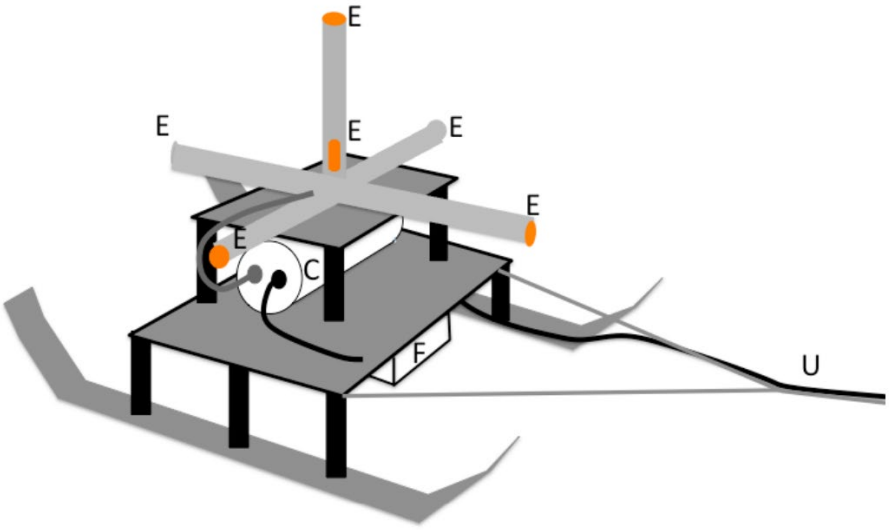

Figure 2.2. Swedish Electromagnetic Field Low-Noise Apparatus. *E's* mark the location of the six electrodes, *F* indicates the location of the fluxgate sensor, *C* is the cylindrical casing where the subsea electronics were stored and *U* the cable that connected the SEMLA with the boat unit. Image from Hutchison et al., (2018).

All analyses used the total field component of the magnetic fields, which were derived using

$$B_{tot} = \sqrt{(B_x + F_x)^2 + \left(B_y + F_y\right)^2 + (B_z + F_z)^2} \qquad (2.1)$$

where *B* denotes the magnetic field from the cable and the index of the component relative to the sledge, *F*, denotes the Earth's magnetic field and the subscript denotes the components relative to the sledge. The Earth's local magnetic field was 51.4 μT.

The measured signals of the magnetic field were processed in several consecutive steps. To obtain the DC magnetic field, the measured signal was low passed filtered with a threshold of 40 Hz. The total field, B_{tot}, was deduced by adding the three orthogonal vector components of the low-passed filtered signals using Equation 2.1.

The AC magnetic field was obtained by high pass filtering the measured signal at 40 Hz to include the 60 Hz and higher frequency components. The maximal amplitude was extracted using a sliding window of 0.5 s. The signal was smoothed using a sliding median window of 1 s. Finally, the total field was deduced by adding the magnetic components using Equation 2.1 with the Earth's magnetic field set to zero. The AC electric field was obtained using the same steps as for the AC magnetic field.

2.2.3. Modeling the EMF encountered by eels passing the HVDC Cross Sound Cable (CSC)

To determine the EMF encountered by the eels, a modeling approach was applied to calculate the DC magnetic field for each three-dimensional eel position relative to the buried cable. A simpler approach was taken in order to calculate the AC magnetic field encountered as there is currently no equivalent model to apply in the context of a HVDC cable.

2.2.3.1. Modeling the encountered DC magnetic field by eels passing the HVDC CSC

The DC magnetic field that the eels were exposed to was predicted, for each position in the water column, based on the measured DC magnetic field on the seabed by applying an EMF model. Two cable parameters had to be determined: the twist (the rotation angle of the two cables in the vertical plane) and the burial depth.

To explain this approach, the theoretical starting point is an infinite wire carrying current within the subsea HVDC bipolar cable. The magnetic field generated by a DC current from an infinite straight wire is expressed by:

$$B_T = \frac{\mu_0 I}{2\pi r} \tag{2.2}$$

where B_T is the tangential magnetic field, r is the distance from the wire and μ_0 is the magnetic permeability of free space. By adjusting the equation for two cables carrying the same current but in opposing direction, and with an offset, a, relative to the center, the DC magnetic field of the HVDC CSC is derived as:

$$\bar{B}_T = \frac{\mu_0 I}{2\pi(\bar{r}-\bar{a})} - \frac{\mu_0 I}{2\pi(\bar{r}+\bar{a})} \tag{2.3}$$

where the bar indicates a vector entity. Equation 2.3 was used to estimate the burial depth and the cable twist from the measured amplitude of the total DC magnetic field. The only unknown parameters were the burial depth, d, of the HVDC bipolar CSC as well as the relative twist of the two cables in the vertical plane, whereas the current, I, and the separation, a, of the two cables were known. Equation 2.3 was derived with the assumptions that the two wires (two cables) have infinite straight length and that the two wires do not twist in the vertical plane. This assumption will introduce an error since in reality the cable does not consist of infinite straight wires. However, an estimate of the error introduced by a finite and twisted cable is of the order of only a few percent (Pettersson and Schönborg, 1997). A property of the DC magnetic field generated by two parallel cables is that the shape of the measured DC magnetic field is solely dependent on the twist of the two cables in the vertical plane, while the amplitude is solely dependent on the burial depth and the current at the particular time.

Equation 2.1 shows that the Earth's magnetic field contributes to the measured DC magnetic field and that the resultant total magnetic field will be an integrated product between the components of the cable emitted magnetic fields and the Earth's magnetic field. The components of the Earth's magnetic field, F_x, F_y and F_z were determined by taking the measured values of the three individual magnetic field components, obtained at the beginning of a transect where the influence from the cable was negligible; thus, only the Earth's magnetic field contributed to the measurements. The low and high frequency components of the magnetic fields were separated by filtering and resulted in a DC magnetic field where the Earth's magnetic field was present, and the AC magnetic field where 60 Hz and higher frequencies were present.

For each survey transect, at the crossing of the cable, the cable twists and burial depths were modeled from the EMF measurements. The modeled cable twist and burial depth was achieved by numerical optimization where the parameters were iteratively changed to obtain the best fit for the measured DC magnetic field. Of the total 18 transects measured in the eel study area, 11 were used for estimating the magnetic fields. The other seven transects gave results which were considered as too unrealistic to be reliable (see Section 2.4.1 for further explanation). To extend the analysis to the whole water volume,

the twists and depths along the cable route between transects were derived by interpolating the EMF modeled twists and depths. With a full set of both modeled and interpolated twists and depths, it was possible to predict the DC magnetic fields that the eels were exposed to in the water column at a particular time.

2.2.3.2. Modeling the encountered AC magnetic field by eels passing the HVDC CSC

At present there is no AC magnetic field analytical model, similar to the DC magnetic field model, for determining the amplitude of the AC field as a function of twist, distance and power level in relation to an AC emitting cable such as CSC HVDC cable. Instead, the measured AC magnetic field was used to determine the amplitude in the eel study area by linear interpolation between the transects, both as a function of position along the cable and distance from the cable. The same 11 transects were used as those for the DC magnetic field. This interpolation scheme did, however, presuppose that the strength of the AC magnetic field was correlated with depth as well as the current in the cable. A statistical analysis of the relation between the amount of electric current in the cable and the amplitude of the AC magnetic field was not possible to perform, since the surveys in New Haven Harbor were all obtained at full power (1175 A). In this study it is heuristically assumed that the amplitude of AC magnetic field scales with the current in the cable, i.e., lower current gives rise to lower amplitudes and vice versa.

Key Information Box 2.1.

- A device called the 'SEMLA' was used to measure the EMF *in situ* in terms of the magnetic field (DC and AC) and the AC electric field; the components were measured simultaneously
    - Measurements were taken to characterize the EMF in the eel study area
    - Measurements were taken to characterize the EMF along the route of the cable
- The measured DC magnetic field was used in a previously verified model to determine the burial depth of the HVDC cable at the point of the SEMLA crossing the path of the cable
- Models were used to determine the magnetic field (DC and AC) encountered by an eel at a specific position in space and time (i.e., based on the 3D proximity to the cable and the power level in the cable at the time)
- Further work is required on the AC model to verify its suitability to a HVDC cable in relation to burial depth, twist and power level

2.3. Results

2.3.1. Characterization of the EMF from the HVDC Cross Sound Cable

The DC and AC magnetic fields and AC electric field were measured in the eel study area and outside the breakwater of New Haven harbor. In total 22 transects were conducted, 18 within the eel study area and four along the length of the cable. The primary focus for the eel study area, given the magnetoreceptive abilities of eels, were the DC and AC magnetic fields however the AC electric fields are also reported for the purposes of full characterization. As an example, the measured DC and AC fields are shown for transect 12 in **Figure 2.3**. The AC magnetic field appears to be wider than the DC

field. However, the DC magnetic field is dominated by the main peak at the crossing point of the survey that appears to obscure the deviation at greater distances. The AC electric field is observed to be wider than the AC magnetic field. A possible explanation is that the induced electric field is driving eddy currents to flow in the water and by Lentz's law these are distributed so as to encompass the AC magnetic field and thus giving rise to an apparent wider peak. To resolve this question an AC model is required for both the AC magnetic field and AC electric field from the HVDC cable.

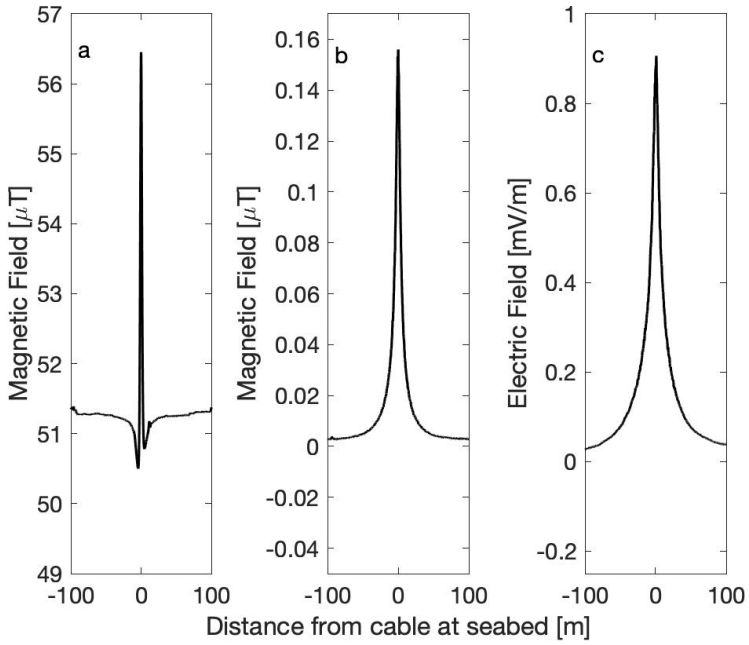

Figure 2.3. An example of the AC and DC fields measured within the eel study area. a) The observed DC magnetic field obtained at transect 12. b) The observed AC magnetic field obtained at transect 12. c) The observed AC electric field obtained at transect 12.

Key Information Box 2.2

- The EMF of the HVDC Cross Sound Cable was characterized
- The amplitude of the DC magnetic field was greater than the AC magnetic field
- The spatial extent of the DC magnetic field and the AC magnetic field were similar
- The AC electric field has a greater spatial range

2.3.1.1. Observed amplitudes of DC and AC EMFs from the HVDC CSC within the eel study area

The amplitude of deviation of the magnetic fields within the eel study area, based on the results of the surveys of the DC and AC magnetic fields are summarized in **Table 2.1**. Maximum DC and AC amplitudes were extracted by taking the maximum measured amplitude, which corresponded to the SEMLA being positioned on top of the cable (Closest Point of Approach). The average positive deviation of the DC magnetic field in the eel study area was 2.8 μT (±2.5), the average for the AC magnetic field was 0.10 μT

(±0.05) and for the AC electric field 0.51 mV/m (±0.23). The maximal observed deviation of the DC magnetic field in the eel study area was 7.5 μT, obtained at transect 8; the maximal AC magnetic field was 0.19 μT, obtained at transect 13; and the maximal AC electric field was 0.90 mV/m, obtained at transect 12. The twist angle of the two cables varied between 0.53 (30) and 1.6 (92) radians (degrees). The burial depth as estimated from the measured DC magnetic field varied between 1.8 and 8.2 m, however, discounting the unrealistic burial depths, the true range of burial was between 1.8 and 3.7 m (**Table 2.1**).

Key information Box 2.3.

- Within the eel study area, the burial depth of the cable was between 1.8 and 3.7 m
- Unrealistic burial depths were easily identified as being over 4.0 m
- From the SEMLA surveys in the eel study area
    - DC magnetic field deviations could be positive or negative relative to the geomagnetic field
    - The maximal DC magnetic field deviation was 7.5 μT (7500 nT)
    - The maximal AC magnetic field was 0.19 μT (190 nT)

Table 2.1. Summary of obtained results from the EMF surveys. The amplitudes of the DC and AC magnetic fields and the estimated cable depth and twist obtained by using the measured magnetic DC magnetic field. Transect marked with grey were excluded from the analysis since the modeled depth was too unrealistic. All fields were obtained at full current (1175 A). Values marked with a '*' were scaled to full current.

Transect Location	No.	Max DC magnetic field [μT]	Depth [m]	Twist [radians]	Max AC magnetic field [μT]	Max AC electric field [μV/m]
Upfront power station New Haven	1	3.5	2.3	0.83	0.11	1100
eel study area	2	7.2	1.8	0.91	0.18	250
eel study area	3	0.4	7.5	0.83	0.05	170
eel study area	4	2.3	3.4	0.85	0.11	350
eel study area	5	1.1	4.6	0.84	0.08	700
eel study area	6	1.7	3.7	0.78	0.1	840
eel study area	7	0.42	7.5	0.82	0.045	500
eel study area	8	7.5	2.1	1.1	0.17	480
eel study area	9	0.35	7.9	0.73	0.04	460
eel study area	10	0.35	8.2	0.86	0.04	420
eel study area	11	3.2	2.7	0.53	0.12	750
eel study area	12	6.5	2.1	0.69	0.16	900
eel study area	13	6	1.8	0.94	0.19	450
eel study area	14	2.3	3.3	0.53	0.1	670
eel study area	15	1.6	3.7	0.61	0.09	650
eel study area	16	4.8	2.3	0.82	0.15	790
eel study area	17	0.51	7.1	0.91	0.05	280
eel study area	18	3.8	2.5	1.1	0.15	250
eel study area	19	0.85	5.1	1.6	0.06	200
Outside breakwater	20	5.5	2.1	1.6	0.13	850
Middle Long Island Strait	21	5.3*	1.9	0.77	0.17*	940*
Furthest away towards Long Island	22	0.6*	6.4	0.75	0.04*	380*

2.3.1.2. The AC magnetic field along the HVDC cable path

The AC-DC-AC conversion technique is known to generate both AC and DC currents within an HVDC cable. In terms of the EMF being emitted into the surrounding environment, there are several electrical pathways (circuits) that could contribute to AC fields in the water, such as grounding points resulting in earth currents. These would be localized near to the converter stations and as a result the AC field would monotonically change as a function of distance from the converter stations. To test this hypothesis additional surveys in close vicinity to the Halvarsson Converter Station, outside the breakwater and near to the midpoint of the Long Island Sound were conducted (**Table 2.1**, **Figure 2.1**). The measured amplitude obtained at transect 22 was low resulting in a modeled burial depth of 6.4 m and since this depth was unreasonably large it was excluded from the analysis. For the hypothesis to

hold, the amplitudes of the AC magnetic field would be expected to be higher at the converter station and lower in the surveys further along the cable in Long Island Sound, or for the inverse relationship to be true. Based on the results in **Table 2.1**, there is no evidence of any monotonic change in the AC field amplitude with distance from the converter station.

Key information Box 2.4.

- The potential for the AC magnetic field to diminish along the length of the HVDC cable route was explored
- There was no evidence of this relationship

2.3.2. Determination of the cable burial depth to model the encountered EMF for eels

The results from the EMF modeling to estimate cable burial depth and twist showed that the model outputs were strongly affected by the measured amplitudes of the magnetic field. Low measured amplitudes resulted in large modeled burial depths. Burial depths much larger than the as-laid depth and those not typical of burial depths in general, were excluded from the analysis. The deviation between as-laid depth and modelled depth is discussed in **Section 2.4**. One plausible explanation is that the cable was not on full power when the sledge crossed the cable as suggested by the power reading which was reported on the full hour. The actual power was possibly lower at the time of crossing of the cable due to power level fluctuations, but the model used the reported full power (full current) and had to increase the depth of the cable to compensate for the amplitude of the magnetic field.

The relationship between the modeled burial depth, and the measured amplitude of both the DC magnetic field and the AC magnetic field is shown in **Figure 2.4**. EMF modeled burial depths larger than 4.0 m were excluded (seven in the eel study area and one outside the breakwater, see **Table 2.1**). The correlation coefficient, R^2, for the burial depth and the DC magnetic field was 0.88, indicating that there was a strong relationship between the burial depth and the amplitude of the DC magnetic fields. The correlation coefficient, R^2, for the burial depth and the AC magnetic field was 0.94, also suggesting a strong relationship between the burial depth and the amplitude of the AC magnetic field.

Since the burial depth and amplitude of the DC magnetic field were interrelated, the measured AC magnetic field could be used to test the consistency of the model. The AC magnetic field showed a strong correlation with modeled burial depth (**Figure 2.4**), suggesting a consistency in burial depth and both AC and DC magnetic field amplitude, but also provided some confidence to the modeled depths.

The modeled EMF burial depths and as-laid depths are shown in **Table 2.2** for the eel study area. The as-laid depths vary between 2.6 and 4.0 m while the EMF modeled depths vary between 1.8 and 8.2 m. Excluding the unrealistic depths (i.e., all depths larger than 4.0 m in the eel study area) brings the modeled burial depths of the remaining 14 transects within reasonable range of the as-laid depths obtained by the cable company (based on the depth reach at the time of deployment of the cable). However, there were differences in the calculated burial depth for some transects ranging from 0.2 to 1.1 m (**Table 2.2**).

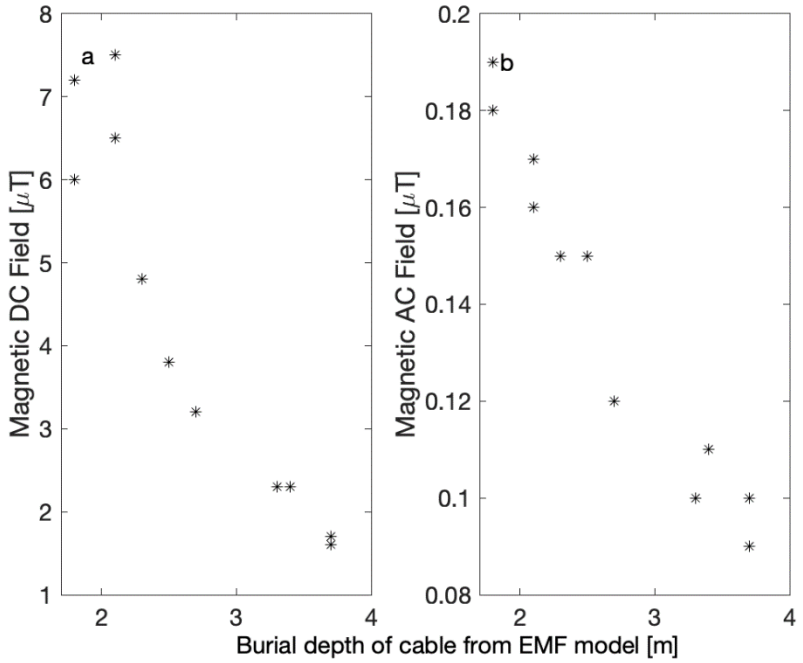

Figure 2.4. Correlation between cable depths and magnetic fields. a) The DC magnetic field dependence on the estimated burial depth using the DC EMF model. The correlation, R^2, was 0.88. b) The AC magnetic field dependence on the estimated burial depth applying the AC EMF model. The correlation, R^2, was 0.94. Unreasonable burial depths (i.e., those greater than 4.0 m) were excluded from the graph.

Table 2.2. As-laid depths and EMF modeled depths in the eel study area. Comparison between as-laid burial depth obtained by the cable laying company and the burial depth estimated by using the DC magnetic field in the eel study area. Seven transects, marked with grey, were excluded due to unrealistic burial depths indicating they were incorrect.

Transect	Depth from EMF model [m]	As-laid depth [m]
2	1.8	2.8
3	7.5	3.5
4	3.4	3.6
5	4.6	3.2
6	3.7	3.3
7	7.5	3.2
8	2.1	3.2
9	7.9	3.3
10	8.2	3.2
11	2.7	3.1
12	2.1	2.7
13	1.8	2.6
14	3.3	2.6
15	3.7	2.8
16	2.3	3.4
17	7.1	3.3
18	2.5	4.0
19	5.1	3.7

The application of the model to the eel positions, to determine the encountered EMF is reported in Section 3.

Key information Box 2.5

- There was a strong relationship between the modeled burial depth and the amplitude of the DC magnetic fields
- There was a strong relationship between the modeled burial depth and the amplitude of the AC magnetic fields
- The EMF modeled burial depths were compared to the 'as-laid' burial depths, that is the recorded burial depth at the time of cable-laying
- The modeled burial depths of the HVDC cable were within reasonable range of the as-laid burial depths after unrealistic depths were excluded
- The as-laid burial depths were not sufficiently accurate to model the encountered EMF for the eel study

2.4. EMF Discussion

To characterize the EMFs relevant to the EMF environment that the eels would encounter, a series of field measurements were taken and the data were also used to develop bespoke DC and AC field modeling. The *in situ* EMF survey covered a total of 22 transects, 18 of which were used to estimate the EMF within the eel study area and four to investigate the EMF characterization along the length of the cable. As the cable depth and any twisting are key factors in the EMF intensity in the water column, a DC EMF model was developed to determine the twist and the burial depth of the HVDC cable through numerical optimization of the measured and modeled DC magnetic field. The same model was then used to predict the strength of the DC magnetic field in the water column (i.e., where the eels would be moving through) using the predicted twists and depths.

In situ measurements of the DC magnetic field used within the model showed that burial depth was estimated to be in the same range as the as-laid depth. These depths were however not correlated with the as-laid depths. The most likely explanation is that the thickness of the sediment on top of the cable may well have changed since the cable was laid in 2003, as a result of dredging, sediment transport and deposition in the area.

For modeled depths larger than 4.0 m, this sediment thickness change over time cannot realistically be the explanation given that the cable EMF was measured in a maintained shipping channel and therefore they were excluded from the analysis. Further, the same year (2018) as the in situ measurements were undertaken, the US Marine Corps performed a bathymetric survey of the New Haven Harbor and no undulations were found in their data (US Army Corps, date 5th June, 2018). The present study cannot explain what the cause was for the large depths obtained at apparent full power. However, it is possible that the electrical current in the cable was lower at the time the transect was surveyed than the reported current by the grid operator, which is reported on the full hour. A possible solution would be to use a higher temporal resolution of reported operational current to use in the analysis which may capture fluctuations in power inferring greater depths of burial.

When considering the EMF environment for mobile receptive species (such as eels) that move over periods of seconds through an area requires a higher sample rate of the applied power in the cable to reflect the actual EMF more accurately in encounter models. A higher sampling rate of the operational current would provide more representative data on the power in the cable at the time of the animal passing therefore maximizing accuracy. Additionally, this would also help in understanding any fluctuations in the operational electrical load which may have influenced the measured EMFs and derived burial depths that were considered unreasonable. It is recommended to obtain representative DC magnetic field level data, based on power recorded at least once per second. This approach however would not be appropriate for determination of the representative AC field. A much higher sampling rate is needed to resolve the AC components. For the HVDC CSC the side harmonics dictates the needed sampling rate. To measure the first and second harmonics, 60 and 120 Hz, would require at least 240 Hz sampling rate. However, to determine higher harmonics would require even higher rates.

Whilst it has been shown that DC magnetic fields generated by a bundled cable can be modeled, there is no corresponding model for the AC fields for a bipolar HVDC cable. This lack of an AC model for HVDC bipolar cables, limits the ability to assess the full EMF environment experienced by receptive species.

Our recommendation is that in order to estimate the AC fields in the water column a model needs to be developed for a HVDC bipolar cable, which can integrate AC field measurements.

It was hypothesized that the AC magnetic field would reduce along the route of the HVDC cable with distance from the converter station. However, the measured AC magnetic fields along the HVDC cable route did not decrease, they stayed similar in relation to the estimate burial depth and cable twist. Therefore, the occurrence of AC magnetic fields measured in the water also needs to consider the different pathways that the AC magnetic field can potentially take from the AC-DC-AC conversion point. In the converter station, high-pass filtering is used to decrease the AC content in the cable. There are however several grounding points both on the AC and DC side of the converter at either end of the cable (Railing et al., 2004) that could feed AC currents into the HVDC cable and therefore the marine environment. In order to determine the likely source of the AC fields, it is recommended that high power system experts investigate the pathways of side harmonics of the AC to DC conversion.

3. Behavioral Response of American Eels to the Cross Sound Cable Electromagnetic Fields

3.1. Introduction

The enigmatic life history of anguillids has fascinated researchers for years. Recent scientific advances have supported the hypothesis that anguillid eels migrate to and from their natal rivers to offshore spawning grounds in the Sargasso Sea with the assistance of a 'magnetic map' and 'magnetic compass' sense (Durif et al., 2013; Béguer-Pon et al., 2015; Cresci et al., 2017b, 2019; Naisbett-Jones et al., 2017). This long-distance migration takes place through coastal and offshore environments that are increasingly the focus of human activity (such as the rapidly expanding offshore renewable energy industry). Owing to the conservation concern for all anguillid eels, the potential for eels to be affected by human activity is an important consideration. From a magnetic-based eel migration perspective, the potential for anthropogenic electromagnetic fields (EMF) from subsea cables (e.g. electricity transmission cables associated with the offshore wind industry) to affect the eels must be assessed (Ohman et al., 2007; Westerberg and Lagenfelt, 2008) in order to determine if there is any impact to the eels. In a broad context, eel interactions with subsea cable EMFs are expected to be most likely to occur in shallow coastal and transitionary waters and in some locations where cables run up or across rivers that eels may migrate through. The focus of interest has been on marine power transmission cables and OWF export cables that connect to on-shore grids of which the greatest number are in the coastal zone.

Section 3.1.1. introduces the life history and modern pressures that anguillid eel populations face before providing an overview of the present knowledge base on the physiological magnetoreception and behavioral magnetic orientation in anguillids in Section 3.1.2 and evidence for responses to anthropogenic EMFs in Section 3.1.3. We then consider the movement ecology of the migratory eel while outlining the approach undertaken to assess the likely encounter of a cable EMF and the individual eel response to the encountered cable EMF in Section 3.1.4.

3.1.1. The modern life of an eel

Anguillid eels are catadromous fish which means they spend most of their lives in freshwater and once mature, migrate to sea to spawn. Eggs hatch as leptocephalus (larvae) and are transported by ocean currents while metamorphosing into glass eels (post-larvae) (Tesch, 2003; Miller, 2009). They eventually arrive at coastal brackish waters transforming into elvers (pigmented juveniles) and migrate through freshwater tributaries where they grow into yellow eels (juvenile, non-mature adults) and then silver eels (mature adults) (Haro and Krueger, 1988; Tesch, 2003; Durif et al., 2005). However, anguillids can exhibit a high degree of plasticity in their life history and may reside in, or interchangeably inhabit freshwater, estuarine, and marine habitats, and are therefore considered facultatively catadromous (Lamson et al., 2006; Marohn et al., 2013). Eels may even cross terrestrial ground to transfer between aquifers (Redmann et al., 2020). The time to reach sexual maturity can be from 5 to 25+ years depending on their habitat conditions (Jessop, 1987; Tesch, 2003). For example, northern populations of *A. rostrata* maturing in freshwater may take up to 40 years to reach sexual maturity but those in estuarine or marine water mature faster due to more food and faster growth (Jessop, 1987; U.S. FWS, 2015). There is strong sexual dimorphism with females being much larger than males and sexuality is density dependent with higher densities leading to a greater number of males (Krueger and Oliveira,

1999; Oliveira and McCleave, 2002; Jessop et al., 2004). A sexually mature silver eel then undertakes the outward migration to the Sargasso Sea to spawn and then die (Schmidt, 1923; Béguer-Pon et al., 2015, 2018). Anguillids are believed to be panmictic meaning that they breed randomly which is thought to help maintain the high ecological plasticity (van Ginneken and Maes, 2005; Côté et al., 2014; Enbody et al., 2021).

Throughout their life cycle anguillid eels play an important role in the ecosystem. Young eels prey on a variety of benthic fauna including insects, polychaetes, mollusks such as snails and bivalves, crustaceans and fish and can strongly influence lower trophic levels (Busch et al., 1998; Stranko et al., 2014). Eels also serve as common prey to larger fish (e.g., haddock, striped bass, bluefish), and may be preyed on by watersnakes as well as birds (e.g., herons, osprey) (Haro, 2014). Migrating silver eels may also be an important food source to higher tropic levels. For example, the predation of *Anguilla anguilla* by mammals, most likely toothed whales, was captured in the mesopelagic zone of the east Atlantic (Wahlberg et al., 2014). Similarly, *A. rostrata* have been reported to be predated by tuna and sharks and may represent a reliable food resource to porbeagle sharks in the Gulf of St. Lawrence (Béguer-Pon et al., 2012, 2015).

As well as natural predation, anguillid populations are under threat from additional anthropogenic pressures throughout their life cycle (**Figure 3.1**). It is noteworthy that in the USA, the American eel is not considered a threatened or endangered species under the Endangered Species Act of 1973, as amended (Act) (Fish and Wildlife Service, 2015). However, in 2013, the declining population of the American eel (50 - 60% over 3 generations) was recognized as an endangered species on the advisory International Union for Conservation of Nature Species (IUCN) Red List of Threatened Species (Jacoby et al., 2017). Population declines are for several reasons. For example, a changing climate influencing the oceanic processes may be influencing the recruitment of glass eels to coastal habitats and the salinity fronts used by silver eels in oceanic migrations (Drouineau et al., 2018). Biological and chemical impacts such as the persistence of the introduced nematode parasite, *Anguillicoloides crassus*, and the presence of persistent organic pollutants are contributing factors (Byer et al., 2015; Hein et al., 2016). Glass eels remain a culinary delicacy and small yellow eels have been important as bait, however the collection of glass eels is now prohibited in US states, apart from in Maine and South Carolina, and there was a coastwide cap put in place in 2014 to help manage the yellow eel fishery (ASMFC, 2017). Despite this, there has been an increased demand on glass eels due to tighter restrictions on the European and Japanese eels. In contrast, silver eel fisheries are restricted to the Delaware River (NY). From 2000-2009 exports from the USA were between 1,660 – 3,683 tonnes per year (Monticini, 2014), however since 2012 there have been no fresh or frozen exports, only live exports are permitted (ASMFC, 2017).

Changes to natural systems such as the introduction of dams and management of water systems have presented barriers to migratory movements and technological advancement has been required to facilitate migrations where natural passage has been impacted e.g., fish passes and airlifts (Haro, 2013; Haro et al., 2016; Pratt et al., 2021). Chaput et al., (2014) concluded that barriers to migration were likely the greatest threat across the species expansive range whereas other threats could be considered to have a more regional influence. The planned development of offshore wind in the US and the proliferation of subsea cables emitting electromagnetic fields may represent an additional pressure on the migratory phases of American eels due to the potential disruption of locational cues from the geomagnetic field (Ohman et al., 2007; Westerberg and Lagenfelt, 2008). While this is often described as a potential barrier to movement, the response to EMFs is unlikely to present as an absolute barrier

and therefore assessments must focus on fine-scale movements in response to the EMF encountered to determine if migratory eels may be impacted (Wyman et al., 2018; Hutchison et al., 2020a).

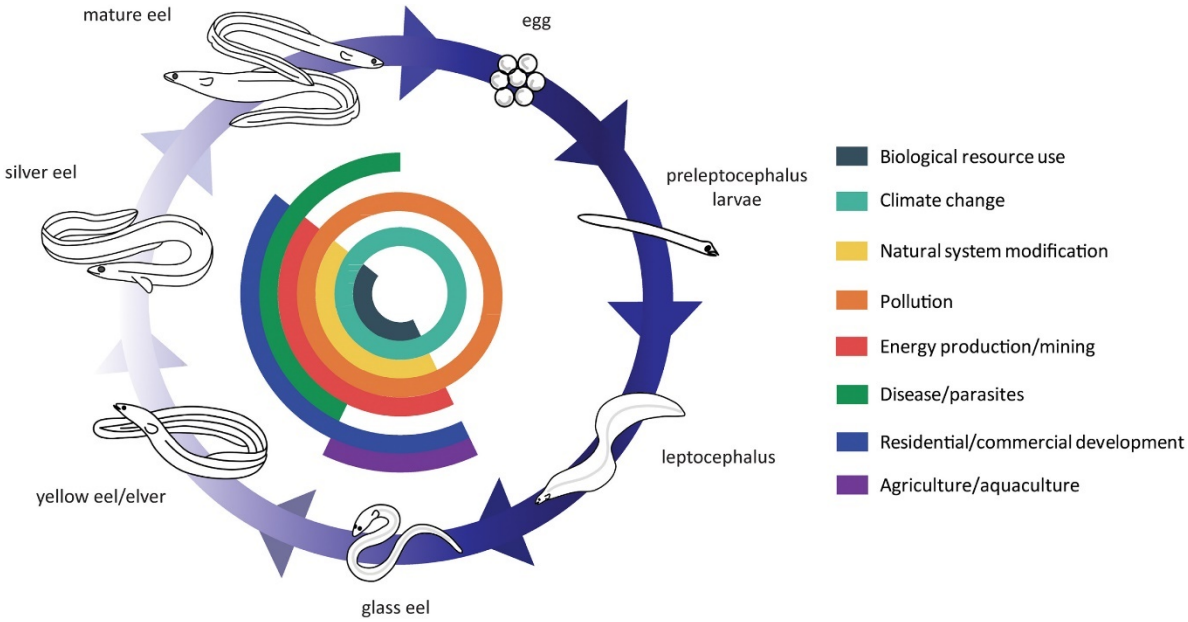

Figure 3.1. A schematic diagram of the life cycle of anguillid eels and pertinent threats. An illustration of how the different life stages are potentially impacted by a variety of threats according to the advisory IUCN categories. The darker blue arrows of the life cycle represent the oceanic phases and the lighter blue, the continental phases. From Jacoby et al., (2015), used under the Creative Commons license.

3.1.2. Evidence for magnetoreception in the American eel

Physiological magnetoreception

The hypothesis of biogenic magnetite as a probable mechanism of magnetoreception in teleost fish, has gathered the most evidence (Formicki et al., 2019). Early studies confirmed the presence of magnetic particles in *Anguilla anguilla* amongst other species (Hanson and Westerberg, 1987). Magnetic particles were found in the skull and vertebrate column along with magnetization of the connective tissues, however it was reported that it may be related to the production of new bone tissue rather than magnetoreception. Subsequently, the exploration of magnetoreception focused mostly on salmonids with evidence suggesting that magnetoreceptive cells exist in the olfactory organ (Walker et al., 1997; Diebel et al., 2000; Formicki et al., 2019), although there have been recent advances in anguillid magnetoreception. In Japanese eels, *A. japonica*, the magnetosensory apparatus is also thought to be in the nasal region since the conditioned cardiac response of eels to a magnetic field was lost in eels with olfactory inhibition (Nishi et al., 2005). More recent evidence, has reported magnetite material, most likely biogenic, in the lateral line of silver eels (*A. anguilla*) with a concentration around the mandibular canals (Moore and Riley, 2009). The authors further indicated a sensory ontogenic shift since the presence of magnetic material was more pronounced in silver eel tissues comparative to yellow eels. To

date, there are no studies into the magnetosensory cells in earlier life-stages although the earlier life-stages have largely been the focus of behavioral evidence for magnetoreception.

Behavioral magnetic orientation

Early studies to determine magnetoreception of the American eel (*A. rostrata*) focused on the elver life-stage and used maze studies comparable to those that had demonstrated magnetoreception in European eel (*A. anguilla*) elvers (Tesch, 1974; Zimmerman and McCleave, 1975). However, there was little evidence for American eel elvers orientating to the magnetic field yet preliminary evidence of a response to weak electric fields was found, leading the authors to suggest that perhaps elvers used the induced electric field arising from the geomagnetic field to orientate (Zimmerman and McCleave, 1975). Laboratory studies on *A. rostrata* had also indicated cardiac responses to weak electric fields and only ambiguous evidence for responses to magnetic fields (Rommel Jr and McCleave, 1973). Later studies had supported the suggestion that induced electric fields from oceanic currents may facilitate orientation in *A. rostrata* elvers but not induced electric fields produced by their own movements (McCleave and Power, 1978).

The proposal of induced electric fields as indirect magnetoreception was disputed and further work demonstrated the directional preferences of both *A. anguilla* and *A. rostrata* silver eels in response to manipulated magnetic field components under laboratory conditions (Tesch, 1974). The directional preferences were indicated in freshwater but more pronounced in seawater for silver *A. anguilla* with similar responses in *A. rostrata* (Tesch, 1974). Karlsson (1985) later found the orientation of silver eels in a laboratory setting to be individual specific however also reported directional behavioral responses to manipulated geomagnetic fields. Similar aquarium experiments of *A. rostrata* showed a strong preference for the northeast however after exposure to experimental manipulations of the magnetic field, exposure to control conditions resulted in preference for north and northwest (Souza et al., 1988). Later, experiments using yellow and silver eels (*A. anguilla*), demonstrated that swimming behavior mimicked the change in direction of the geomagnetic field (approximately 90°), responded to the reversal of magnetic north and also changes in the inclination and reduction of the total intensity (Tesch et al., 1992). Seasonality in directional orientation has also been demonstrated in studies of yellow eels (*A. anguilla*) with greater orientation to shelters experimentally aligned with the direction of the Sargasso Sea during fall (Van Ginneken et al., 2005). It was believed that the yellow eels studied would reach sexual maturation and therefore become migrants within 2 years of the study and may be supportive of the hypothesized ontogenic shift in anguillid magnetoreception. Durif et al., (2013) also tested the ability of maturing yellow eels (*A. anguilla*) to orientate after displacement, in altered magnetic fields representative of the geomagnetic field (north, east, south, west). They demonstrated in controlled conditions that eels were able to memorize and orientate to their magnetic field position prior to displacement while differences in the orientation linked to temperature were indicative of seasonal behaviors.

Research efforts have also focused on the abilities of anguillids to use the magnetic field as an orientation cue during early life stage migrations. The magnetic map sense of glass eels was explored in magnetic displacement experiments, demonstrating the ability of eels to decipher altered magnetic intensities and inclinations, indicative of their ability to decipher positional information from the geomagnetic field, potentially as a bi-coordinate map sense (Naisbett-Jones et al., 2017; Putman et al., 2017). Coupled with a simulation of earlier life-stages, the authors demonstrate that the magnetic map sense experimentally derived in glass eels, would theoretically facilitate orientation of leptocephali

larvae to the Gulf Stream enabling passive migration facilitated by oceanic drift (Naisbett-Jones et al., 2017; Putman et al., 2017). Further consideration of the leptocephali larval stage and their magnetic map abilities would be required to confirm such abilities and help inform potential imprinting of geomagnetic information (Durif et al., 2017; Putman et al., 2017). However, research has retained focus on the glass eel life stage and explored the tidal influence on magnetoreception. Using a drifting circular arena in a fjord channel and in a controlled laboratory setting, the common orientation of glass eels (*A. anguilla*) during the ebb tide was demonstrated (Cresci et al., 2017b). Since the laboratory testing was completed in the absence of the tidal influence, it is suggested that the magnetic orientation was based on an endogenous circa-tidal rhythm and further, the magnetic orientation was maintained under a manipulated magnetic field. Cresci et al., 2019 then demonstrated that glass eels memorize and orientate to the magnetic field of the tidal direction of the estuary that they recruit to by exploring orientation in glass eels from different estuaries under manipulated magnetic fields. The authors proposed that this ability may be a form of imprinting providing important directional information to glass eels as they migrate upstream but also later life during their outward migration as silver eels, however they also discuss the possibility of continuous ongoing learning providing a flexible memory of magnetic orientation to the water flow. These theories require further work to elucidate the precise use of the magnetic field in eel orientation throughout the life-cycle and further emphasize the need to take the vantage point of the species, that is to consider their sensory perception in space and time, when considering the effects of anthropogenic EMFs for species which rely on natural EMF cues (Hutchison et al., 2020a).

3.1.3. Evidence for responses to anthropogenic electromagnetic fields

The majority of studies of magnetoreception in eels have focused on manipulations of the geomagnetic field (Section 3.1.2). Recent literature has turned focus to effects of anthropogenic electromagnetic fields which have practical benefits. For example, the use of industrial magnets in fishing have been demonstrated to increase *A. anguilla* silver eel catch (Tanski, 2014 cited in Formicki et al., 2019). Most recently, interest in the response to EMFs has been explored regarding the potential of electrical guidance within dam passage but was not deemed to be a suitable method (Pratt et al., 2021).

There have been efforts to determine the responses of anguillids to cable EMFs. Öhman et al., (2007) first discussed the issue of EMFs from cables resulting in a divergence in the migratory path of European silver eels on the basis of early work by Westerberg and Begout-Anras (2000). They detected eels traversing the HVDC Baltic Cable in the Southern Baltic Sea during their outward migration using ultrasonic transmitters and found results consistent with the eels following a magnetic compass course but a deviation from the straight course was detected in the vicinity of the cable. The resolution of the tracking was of insufficient detail and lacked a vertical profile to determine the response of the eels or indications of the potential EMF encountered. The HVDC cable (130 kV) which typically operates with 1000 A (maximum capacity of 1300 A) was reported to emit a magnetic field of 5 µT at 60 m from the cable (Westerberg and Begout-Anras, 2000; Westerberg and Lagenfelt, 2008).

The best available information to date, regarding the potential responses of anguillid eels to a cable EMF is from a subsequent study by Westerberg and Lagenfelt (2008) on a buried AC cable in the Kalmar Strait of the Baltic Sea. The specifics of the EMF are not reported in terms of the emitted intensity or the

spatial extent, however the current in the three-phase twisted AC cable when the eels passed was between 140 - 300 A. Using an acoustic telemetry array, four transects of receivers detected the presence of eels north of the AC Kalmar Strait cable, in the vicinity of the cable and south of the cable (**Figure 3.2a**). Following the release of 60 silver *A. anguilla* eels, the water current corrected speed of movement within transects segments was measured for 46 eels demonstrating a slower speed within the vicinity of the AC Kalmar Strait cable. Based on the speed of movement, it was reported that some eels stopped for periods of time which was not indicated as a result of the AC cable EMF, rather, was considered typical movement for the species. However even on removal of those eels, the remainder still demonstrated significantly slower speeds of movement within the vicinity of the cable. Further analyses indicated that the reduced swimming speed was weakly related to the increased current in the cable (140-300 A). The authors concluded that the reduced speed was indicative of a response to the AC Kalmar Strait cable EMF however suggested that better evidence be obtained by finer resolution tracking and further understanding of sensory perception would require laboratory and sensory deprivation experiments.

Subsequently there were laboratory studies of *A. anguilla* silver eels exposed to an AC magnetic field of 9.6 µT from Helmholtz coils (Orpwood et al., 2015) (**Figure 3.2b**). A total of 28 eels were tested individually in 4 hour exposures but only 10 eels were active. The active eels passed through the magnetic field between 1 and 43 times and there was no apparent evidence of a startle response or change in behavior associated with the magnetic field, however, the authors noted the small sample size and also that eels tended to reduce activity over time indicating they may not have acclimatized to their surroundings.

Despite these efforts to determine if silver eels respond to DC and AC cable EMFs *in situ* and AC magnetic fields from Helmholtz coils in laboratory settings, there is insufficient evidence to confidently decipher the behavioral response to cable EMFs in the context of AC or DC cables. Where magnetoreception species derive locational cues from the geomagnetic field, the EMF from a DC cable is most similar in that they are both static fields (approximately); the geomagnetic field does change over long time periods (Skiles, 1985). The EMF from an AC cable is less similar due to the time-varying nature of the EMF, which in the US is at 60 Hz. However, a species encountering the EMF of a cable will encounter the total EMF environment and it is not known how or if magnetoreceptive species decipher the geomagnetic field signals in the presence of anthropogenic magnetic fields. Nor is it known if magnetoreceptive species are responsive to only some anthropogenic fields e.g., DC or AC, or both. It is noteworthy that the total EMF environment of the HVDC Cross Sound Cable includes both DC and AC fields (see Section 2). It has been experimentally derived that an electro-receptive species (catsharks) are able to distinguish between AC and DC electric fields but not natural and anthropogenic DC electric fields (Kimber et al., 2014). Comparable evidence for magnetoreceptive species is lacking and the sensory purpose of electro-receptive and magnetoreceptive species are very different, which prevents confident cross-interpretations.

(a)

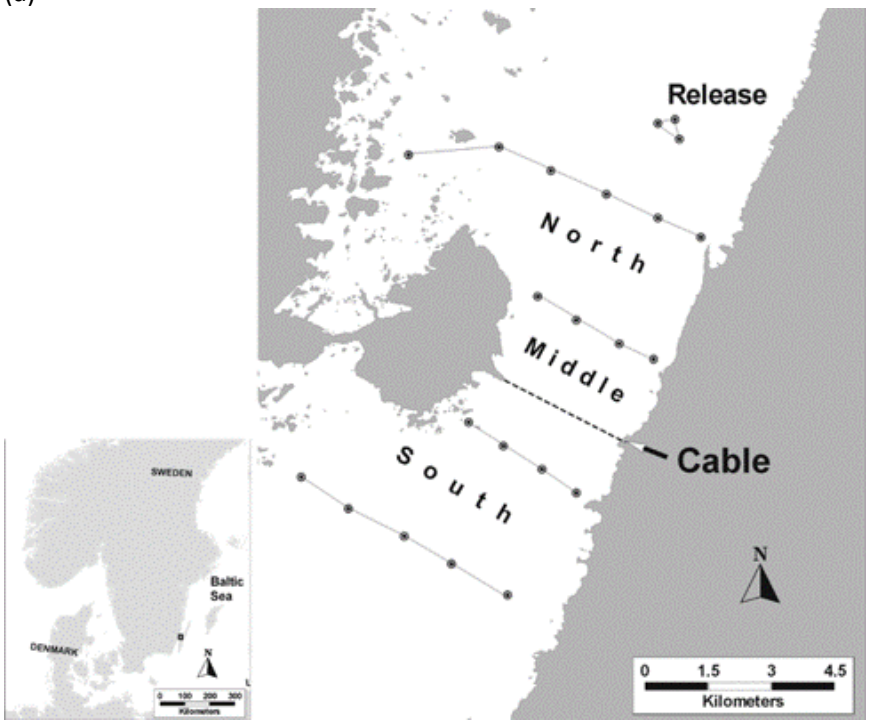

(b)

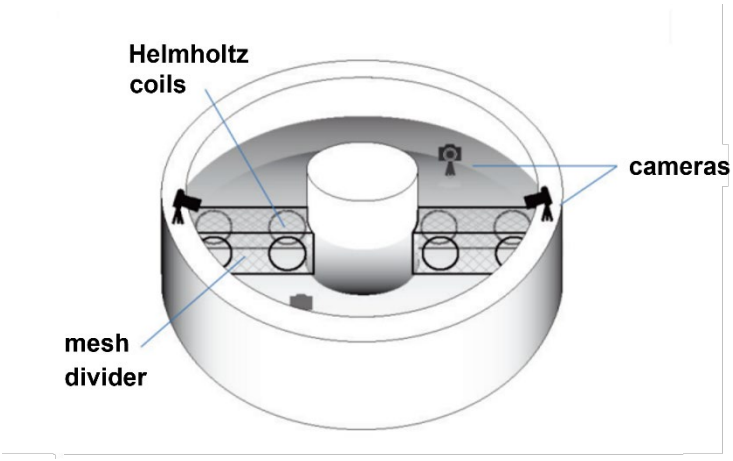

Figure 3.2. Efforts to establish the response of the European eel to cable type EMFs. (a) Four transects of acoustic hydrophones enabled the swimming speed of the *A. anguilla* to be compared in the vicinity of the three-phase AC Kalmar Strait Cable in the Baltic Sea (operating with 140-300 A) with swimming speeds north and south of the cable (Westerberg and Lagenfelt, 2008). (b) A laboratory experiment determining the response of *A. anguilla* to AC magnetic fields using Helmholtz coils (Orpwood et al., 2015). Images (a) reproduced with permission (Westerberg and Lagenfelt, 2008) and (b) reproduced under creative commons license.

3.1.4. Aims of this study

Building on the present knowledge base of potential anguillid responses to cable EMFs, we developed an *in situ* observational experiment focusing on the outward migration of the silver American eel (*A. rostrata*). Here, we focus on the HVDC Cross Sound Cable which has DC and AC EMFs associated with it (Section 2). The first aspect in assessing if there is a response by eels to the HVDC cable EMF is to determine if the migratory eels are likely to encounter the HVDC cable EMF. As highlighted by previous efforts, the fine-scale behavioral movement is important in determining the interaction with the cable EMF (Westerberg and Lagenfelt, 2008). Such studies of animal movement are typically undertaken in two-dimensions. However, the third dimension (vertical movement) is of particular importance in being able to decipher the EMF encountered since it is the distance from the cable of the receptive species (the EMF source) that is the most relevant in the exposure to the emitted EMF. Both the movement ecology of the receptive species and the burial depth of the cable are therefore significant factors in determining the distance from the cable and these factors may change along the route of a cable (Hutchison et al., 2021) (**Figure 3.3**). While yellow eels are considered benthic, silver eels are considered oceanic diel vertical migrators (Tesch, 1978a; Brown and Castro-Santos, 2009; Béguer-Pon et al., 2015). There is less available information on the vertical movements of migratory silver eels in transitional coastal waters (Brown and Castro-Santos, 2009; Béguer-Pon et al., 2014, 2015), however vertical dives likely begin as water depth increases. Advancing the work of Westerberg and Lagenfelt (2008), we use fine-scale telemetry to explore the interaction of silver eels with HVDC cable EMFs.

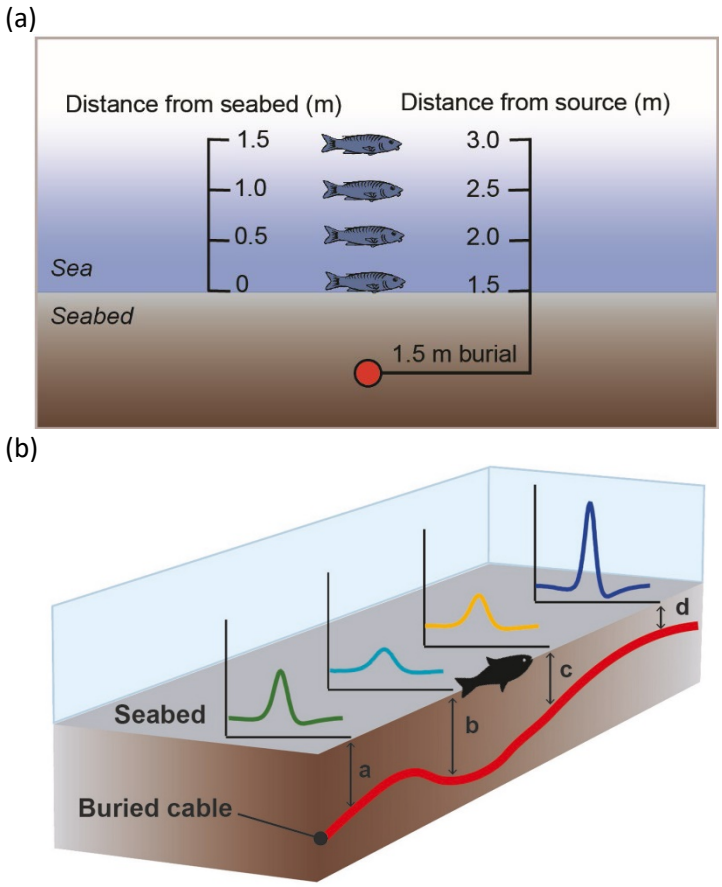

Figure 3.3. Exposure of a receptive species to cable EMF is dependent on the distance from the cable. (a) The animal's position in the water column influences the distance from the cable (EMF source). (b) The cable burial depth may vary along a cable route. For a species moving along the seabed, the variable burial depth of the cable, changes the distance from source and exposes the animal to variable EMF intensities. Burial depths depicted are approximations and not to scale; (a) 2.0 m, (b) 3.0 m, (c) 2.5 m, (d) 1.5 m. Image (b) reproduced from Hutchison et al., (2021).

In year 1 of this study, we developed and tested the ability of an acoustic array system to provide fine-scale two-dimensional positional data in the vicinity of the buried HVDC Cross Sound Cable (CSC). Using translocated silver eels, we focused on the upper reach of the cable in the narrowest part of New Haven Harbor between Sandy Point and Fort Nathan Hale where there was the greatest likelihood of detecting tagged eels in the area where the EMF of the HVDC CSC was located.

Based on the successful testing in year 1, we advanced the system to provide finer-scale three-dimensional positional data for eels in the vicinity of the HVDC cable. In conjunction with the methods described in Section 2.2.3, we modeled the encountered EMF during the silver eel escapement on their outward migration to sea. Using this novel approach to determine the encountered EMF, we assess the behavioral modes of silver eels during their escapement and if they respond to the HVDC cable EMF by slowing down to explore it.

3.2. Methods

In 2018 and 2019, a Vemco (Innovasea Systems Inc.) acoustic array was used to detect silver American eels (*A. rostrata*) on their outward migration to sea over the HVDC Cross Sound Cable, New Haven, CT. A high-definition array around the HVDC cable enabled fine-scale behavioral movements of the eels to be detected where they may interact with the cable EMF, and a presence/absence array covered areas outside the high-definition array. The presence/absence array allowed the eel migration to be monitored even if they did not encounter the high-definition area. The whole acoustic array was set up between Sandy Point and Fort Nathan Hale in New Haven Harbor and translocated eels were collected from Groton-Poquonnock River system, CT and released in the upper stretch of West River, CT. Translocated eels were used since there was a regularly monitored population, regarded as healthy, and with known availability from the Groton Eel Abatement Program[3] whereas there was no available data on eel populations in rivers joining the New Haven Harbor area. An overview of the study area is provided in **Figure 3.4**.

[3] https://grotonutilities.com/water/all-about-eels/

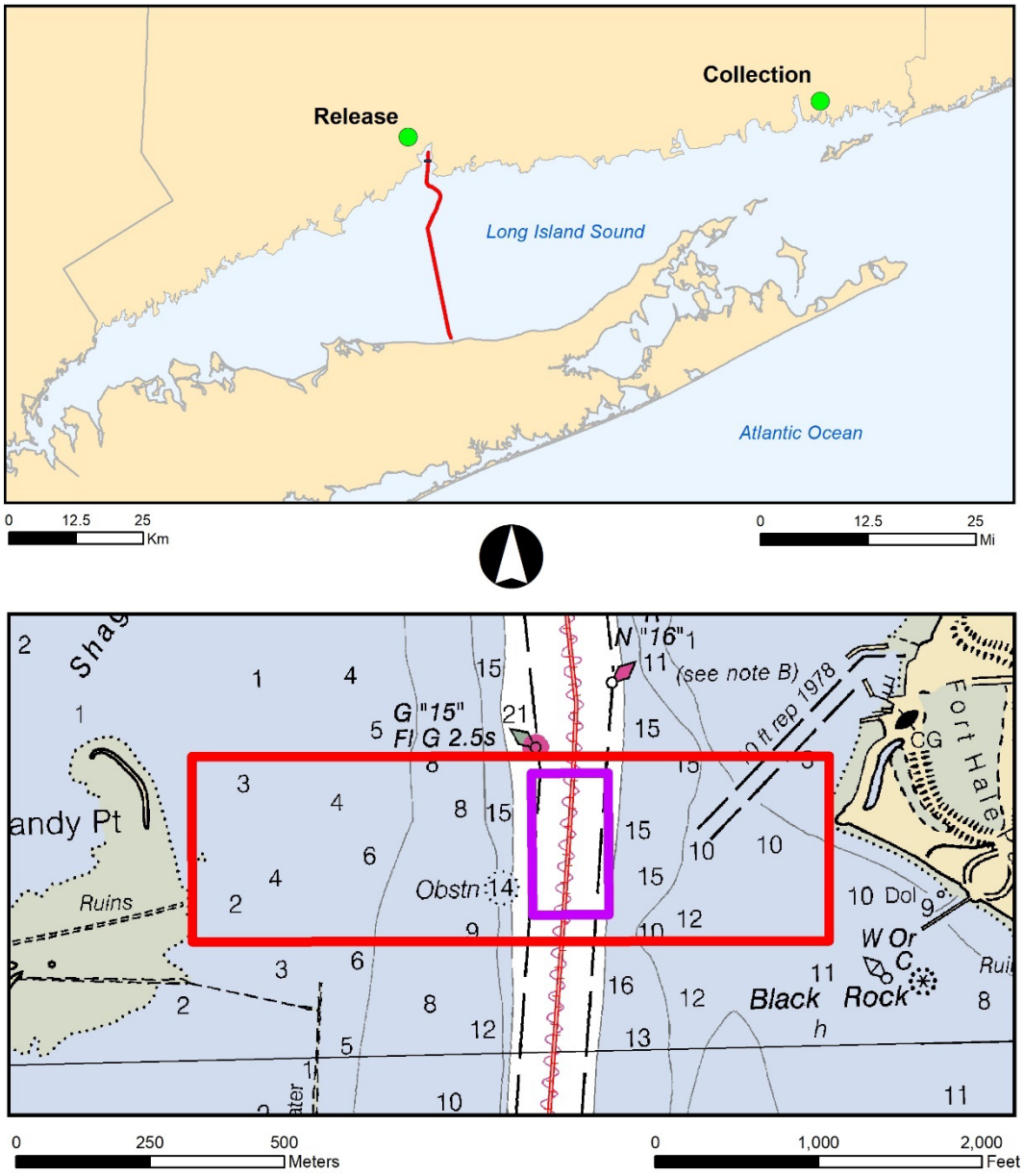

Figure 3.4. An overview of the eel study area. The eel collection point from Groton Utilities and release point in the upper stretch of West River are indicated in the upper panel. The release point was 6.2 km (3.9 miles) from the acoustic array between Sandy Point and Fort Nathan Hale in New Haven Harbor, CT, where a high-definition array (small purple box, lower panel) around the HVDC Cross Sound Cable was accompanied by a presence-absence array east and west of the cable (large red box, lower panel). Map created with ESRI ArcMap (version 10.8.1) using basemap 'US States' and 'NOAA Raster Nautical Charts'.

3.2.1. Acoustic Receivers and Tags

A combination of two types of acoustic receivers were used. Within the channel, to obtain fine-scale positioning of eels within the vicinity of the HVDC cable, a Vemco Positioning System (VPS) was used

employing High Residency receivers (model HR2-180hHz, HR). Outside of the channel, to detect eels that had migrated through the area without interacting with the VPS, VR2W receivers (VR2W-180kHz) were used to provide presence/absence data. Receivers were turned on and off, and data accessed via VUE (version 2.6) and Fathom (version 2.3.0) software and receiver firmware were maintained as updates became available.

In Year 1 (2018) of the study, V9-180 tags (n=100) were used to provide two-dimensional data and in Year 2 (2019) V9P-180 tags (n=200) were used to provide three-dimensional data with the incorporation of a pressure sensor. The tags were very similar in size with V9 being 26.1mm and the V9P being 26.5 mm, both with a diameter of 9 mm and the weight in water being 2.0 and 2.2g respectively. In each year of the study, stationary reference tags of the aforementioned models with a cap for attachment, were deployed with the acoustic array (Section 3.2.3-4). All tags were switched on when required using a handheld device, Vemco Tag Activator (VTA, model VTA-180k-V9), which could also check whether the tag was operational prior to attachment (Section 3.2.6).

A dual tag ID programming approach was used (**Table 3.1**) and within the time specifications, unique identifiers were provided enabling each individual eel to be identified, even if present at the same time, regardless of density. The Pulse Position Modulation used an A180 code allowing the VR2W receivers to detect eels. However, the VPS using HR receivers adopts a faster transmission system using the H170 code but also detected the A180 codes. The tag programming selected was designed to maximise the resolution of the positional data enabling the finest scale behavioral assessments possible (i.e., sub-second, **Table 3.1**). The frequency was increased for the V9P tag programming used in Year 2. The duration was estimated by Vemco based on the programme adopted and was balanced with the anticipated period of eel migration for the eel population under study (late September to December). For the eel tags, a single step was used meaning that when the tags were turned on, they operated consistently as programmed. Reference tags (hereafter 'Ref') had two steps facilitating a higher ping rate within the first 4 days of operation and then a slower ping rate for the remaining time to conserve battery life.

Table 3.1. An overview of the tag programming for the V9 and V9P tags. Single steps were used for tags attached to eels and a dual step was used for reference tags ('Ref') of each model. Dual codes were used to accommodate detections by the VR2W and HR receivers.

		Step 1			Step 2		
Tag	**Code**	**Duration (d)**	**Min Delay (s)**	**Max Delay (s)**	**Duration (d)**	**Min Delay (s)**	**Max Delay (s)**
V9	A180	51	18	30	-	-	-
	H170	51	0.8	1.0	-	-	-
V9P	A180	51	18	30	-	-	-
	H170	51	0.6	0.8	-	-	-
Ref	A180	4	45	75	735	270.0	330.0
	H170	4	8.0	12.0	735	25.0	35.0

3.2.2. Deployment method

Receivers and reference tags were mounted on fibre glass posts held within concrete blocks, therefore reducing any interaction with electromagnetic fields from the use of metal anchors. In both cases, it was ensured that the sensors of receivers and tags were above the fibre glass posts to maintain a clear path of transmission. Following the initial range test (Section 3.2.3), concrete blocks were strapped to broader wooden bases to prevent the possibility of sinking into the soft sediment seabed and maximising stability for longer term deployment. Additional environmental stations using the same non-magnetic anchor system were included; a sonde (In Situ Inc. Troll 9000 Pro) was deployed in the channel to collect temperature, oxygen, and salinity data (5 minute frequency) and data loggers (HOBO Water Temp Pro v2, onset®) were used east and west of the channel to collect temperature data only (5 minute frequency).

A scientific dive team from URI deployed and recovered the equipment in conjunction with a pontoon vessel crew. The pontoon vessel was used to accommodate the shallow waters outside of the channel. Full dive plans were approved for each phase of the study by the URI Diving Safety Board. The pontoon vessel manoeuvred into position using the POS MV GPS system for a highly accurate locational reference. The anchor was lowered to the seabed, with a buoy attached. The deployment location was recorded so that the buoy could be removed and the anchor relocated by divers at the end of the study. The divers descended with the receiver or tag, attached the item securely with zip ties, removed the buoy line and ascended. The receivers and tags remained in the shipping channel with no surface markers for the duration of the eel study. For recovery of all items, the deployed GPS locations were used. A shot line was deployed at least 1 m away from the targeted item to prevent potential damage. The divers descended the line, and using a circular search, recovered the item, attached a lifting line to the anchor and ascended with the item. The crew then lifted the shot line and after recording the GPS location, the anchor was then lifted. Planned, deployed and recovered GPS positions were included in the specifications provided to Vemco for data processing. All diving and equipment deployment was approved by the US Coast Guard. Local shipping companies were informed daily of diving activities and provided anticipated shipping schedules to accommodate planning. During diving activities in the shipping channel, a designated person acted as a lookout for unscheduled shipping.

3.2.3. Pre-deployment Range Test

In consultation with Vemco, a temporary array deployment was undertaken to determine the most suitable spatial arrangement of receivers for the full deployment, specific to the study area. Due to the restrictions of working in the shipping channel, the range test was undertaken on the flat seabed east of the channel, close to where the full deployment was anticipated **(Figure 3.5**). Four HR and four VR2W receivers were deployed with three reference tags positioned to test the detection performance over a range of distances from the receivers. The planned distances ranged from 14-89 m for the HR and 10-107 m for the VR2W receivers. Data were collected from September 27 to 30th, 2018. The water depth was 4.6 to 6.8 m, depending on the state of tide (chart MLLW 15 ft (NOAA, 2012)), the water temperature range was 20.5-21.1°C and salinity 27.5-29.5 ppt. Vemco assessed the quality of the detections and determined that the receivers had performed well. The full array was planned with 100 m spacing between VR2W receivers providing overlap in detection range of neighboring receivers

ensuring full transect coverage and the HR receivers had a 70 m square arrangement providing 99 m distance on the diagonal (**Figure 3.6**).

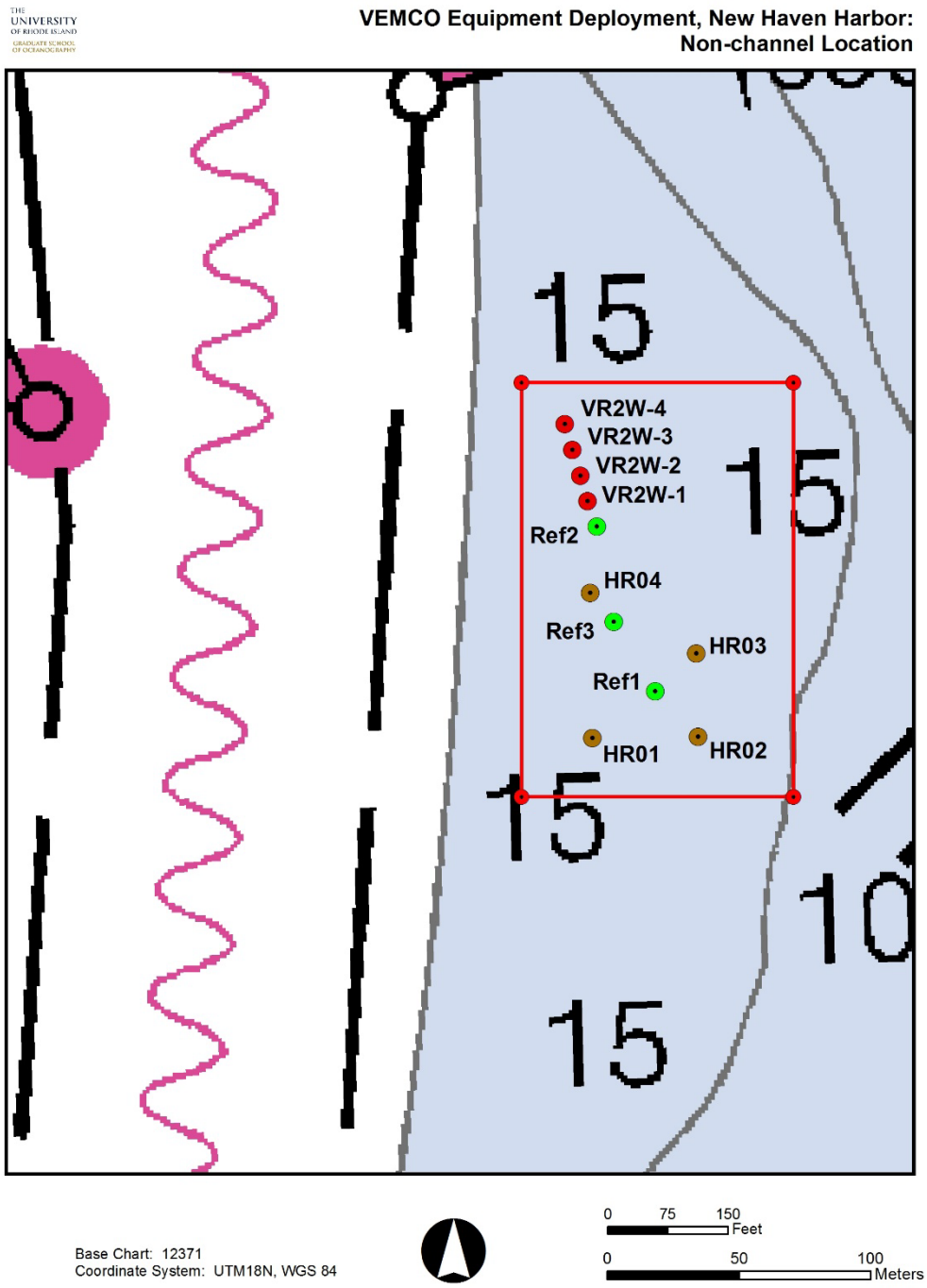

Figure 3.5. The acoustic array range test. Due to restrictions of working in the shipping channel, the range test was completed on flat seabed east of the channel (red box). Being close to the channel ensured relatively similar environmental conditions in shallower depths (15 ft MLLW) (NOAA, 2012). Four VR2W and four HR receivers were deployed with three reference tags to obtain a range of distances.

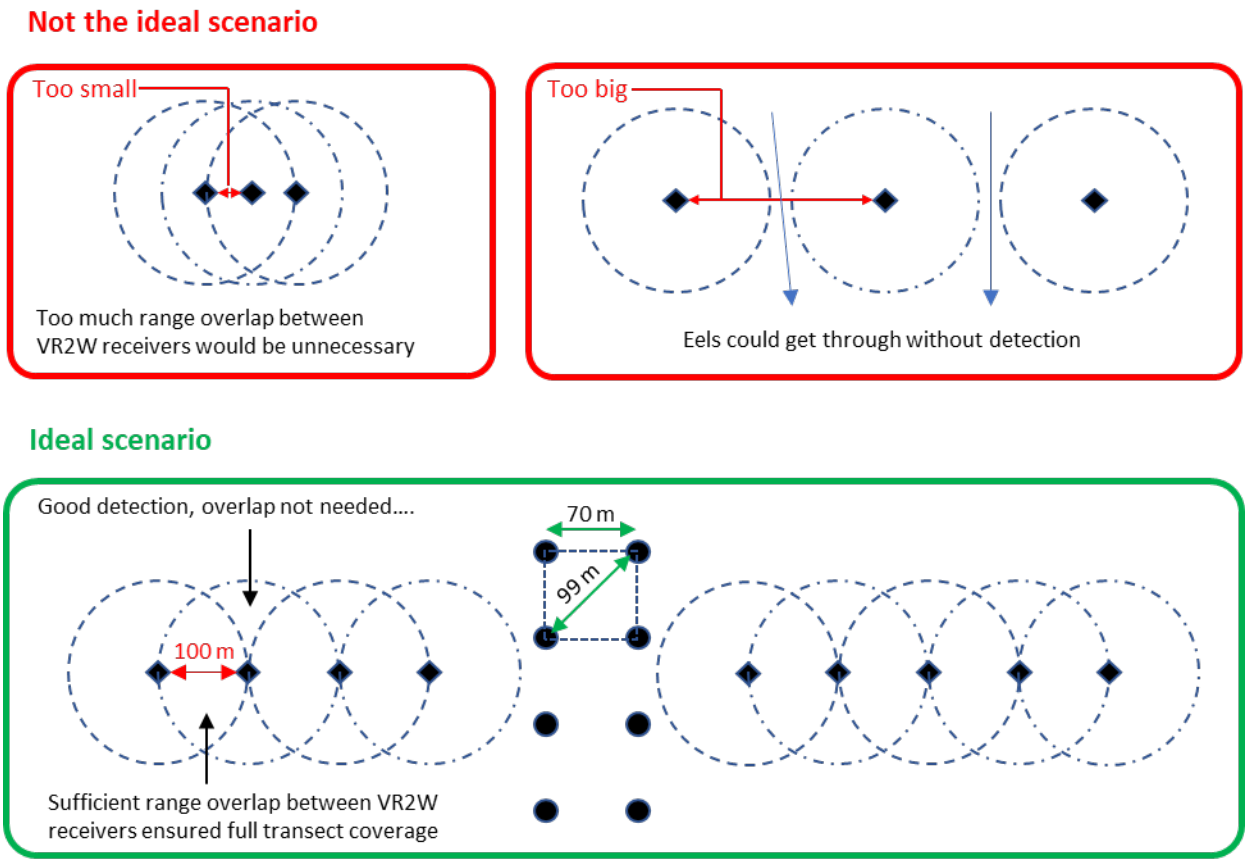

Figure 3.6. Ensuring appropriate acoustic receiver position to obtain full coverage across the harbor transect. (a) Having the receivers too close together would provide unnecessary overlap in detection. (b) Having the receivers too far apart would reduce the coverage such that eels may pass through the transect without being detected. (c) The ideal scenario provided sufficient overlap in detection to ensure full coverage of the transect area. The ideal coverage for the HR receivers (circles) in the central array provided overlap between three receivers enabling 2D and 3D triangulation of the eel tag position.

3.2.4. Full Array Deployment (Year 1 and 2)

An overview of the full array deployment is provided in **Figure 3.7**. Eight HR receivers were located in the channel and ten VR2W receivers were distributed either side of the channel creating a transect covering the full span of the harbor. The HR receiver array in the shipping channel enabled high resolution positional data to be collected allowing fine-scale interactions with the cable EMF to be assessed. The VR2W array allowed eel migrants that did not pass through the high-resolution area to be detected, providing important context regarding the total number of tagged eel migrants in each year. In year 1, data collected were in two-dimensions and in year 2, the data collected were three-dimensional due to the addition of a pressure sensor in the tag (**Section 3.2.1**). Reference tags were deployed within the channel as static control measures (**Section 3.2.5.1**) and while central positions within the receiver quadrants would have been preferred, they were off-center to accommodate

shipping at low tide reducing the risk of tags being disturbed. In year 1, the full data collection period was from 26th October to 5th December 2018 and in year 2 the full data collection period was 18th September to 4th December 2019.

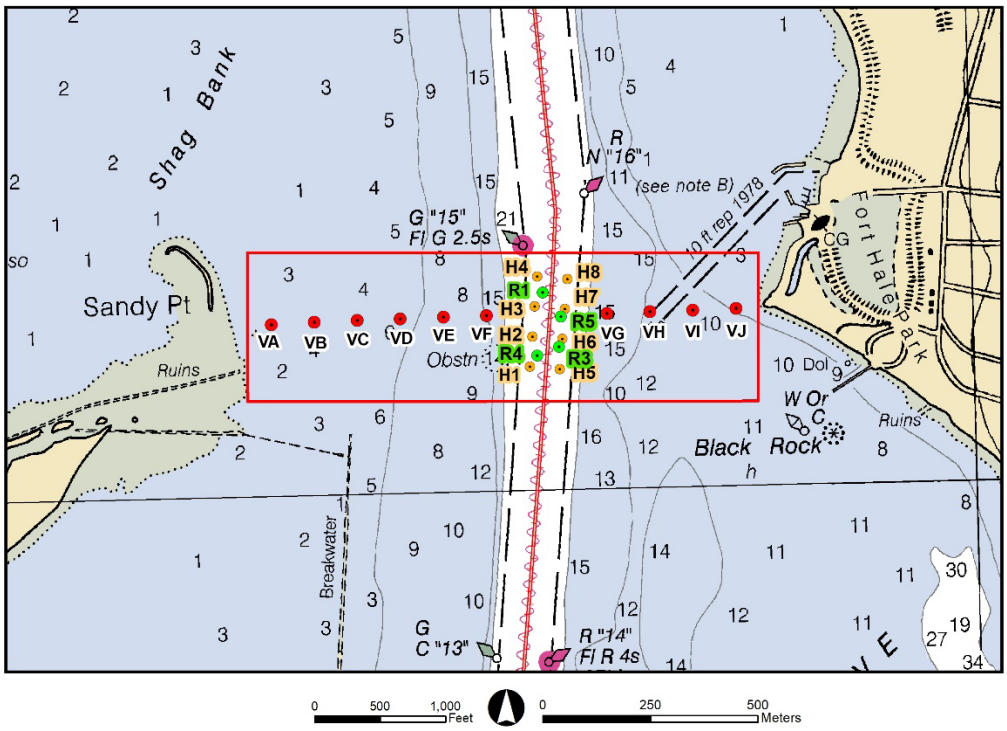

Figure 3.7. Full Vemco acoustic array deployment. Eight HR receivers were deployed within the shipping channel (H1-H8) creating a high-resolution detection area around the buried HVDC cable. Ten VR2W receivers (VA-VJ) were deployed outside of the channel, six on the west side of the channel and four on the east side of the channel. Two reference tags (R1, R3) and four reference tags (R1, R3, R4, R5) were deployed in year 1 (2018) and year 2 (2019) respectively. The basemap used is the 'NOAA Nautical Chart 12371'.

3.2.4.1. Control measures

Stationary Ref tags were deployed throughout the study period (**Figure 3.7**). In 2018, V9 tags Ref 1 and 3 were deployed (Ref 2 was unavailable). In 2019, Ref 1 and 3 were deployed again in the same locations and supplemented with Ref 4 and 5 which were V9p tags with pressure sensors.

In 2019, prior to reference tags being deployed at their stationary locations, three 'tag drags' were undertaken. Reference tags were attached to a line with known distances between the tags and deployed from a fixed point on the vessel with a weight at the base of the line. The vessel then drifted through the array at three locations; moving through upper, middle and lower quadrants of the HD array in the channel. A further tag drag was completed with four V9p tags through the middle quadrant of the array to provide a broader range of depth profiles.

3.2.5. Eel husbandry, tagging and release

Silver American eels, which had commenced their migration, were collected from an air lift assisted deep pass (Haro et al., 2016) at the Groton Utilities reservoir, CT. The air lift was in place to accommodate the physical barrier to their migration and the number of eels migrating each year was monitored by Connecticut Department of Energy and Environmental Protection (CT DEEP). Permits for eel collection for scientific use were approved by CT DEEP (SC-18023) and all methods were ethically approved by the URI Institutional Animal Care and Use Committee (Reference No. 1282655-8) and overseen by the URI Marine Science Research Facility (MRSF) management. Eels were transported to the MRSF (38 miles) and subsequently to their release site (90 miles) in large, aerated coolers (total translocation from catch site to release site was approximately 50 miles).

Within the MRSF, the eels were held in aerated aquarium tanks 1 m diameter with a semi-continuous flow of freshwater. Freshwater was collected from a local stream and held in a header tank (2.5 m diameter) that supplied water to an intermediate reservoir using a timed pump accommodating up to five, 1 hr inflows within a 24 hour period (c.a., 140 L, 75% volume replacement). Water depth was shallow (c.a., 0.16 m), and the tanks and outflow were covered with a net to prevent escapement. Eel density was variable, and parameters were monitored using a digital thermometer and an API Freshwater Master Test Kit (pH, ammonia, nitrite, nitrate) on a daily basis and the water inflow rate adjusted where necessary. Temperatures reflected the ambient conditions and an ambient light regime was maintained. The three tanks were used as a general holding, an intermediate reservoir and for post-tagging recovery, as required. Eels in holding tanks were provided with PVC pipe to provide covered resting areas.

Prior to eel tagging, tags were turned on, and attached to a customized plastic sheet tag (5/16" x 1-1/2", Floy Tag & Manufacturing, Inc.) with two holes to accommodate sutures. Eel tagging was completed using a staged cooling process to reduce the eel temperature to the point of low mobility allowing manual handling with minimal stress. Eels were lifted while covering the eyes and placed in an eel sizer which also accommodated the tagging process. The length of the eel was recorded, the eye was photographed and the tag was sutured anterior to the dorsal fin. The eel eye index was verified according to Pankhurst (1982). Eels were returned to an individual holding tank prior to being returned to the recovery tank with other tagged eels. Behavior was observed to ensure the eel accepted the tag. Where eels exhibited erratic swimming or figure of eight behaviors in attempt to remove the tag, eels were chilled, and the tag removed if necessary.

In 2018, five releases occurred between 3rd and 15th September (n=100), and in year 2, six releases between 16th October and 13th November (n=200) (**Table 3.2**). After transport, the eels were released following a brief acclimation period. The eel release site was in West River, south of Long Pond, CT at an approximately similar longitude to the collection point. The release site was approximately 6.2 km (3.9 miles) from the acoustic array allowing sufficient distance and time for eels to resume normal behavior prior to acoustic detection, even if they swam downstream immediately.

Table 3.2. An overview of the eel release dates and numbers in year 1 and 2 of the study.

Year 1		Year 2	
Release Date	**n**	**Release Date**	**n**
3rd November 2018	17	16th October 2019	35
6th November 2018	16	20th October 2019	33
9th November 2018	30	24th October 2019	32
13th November 2018	32	31st October 2019	15
15th November 2018	5	10th November 2019	42
		13th November 2019	43

3.4. Data Processing & Analyses

The telemetry data were assessed in two forms; the year 1 and year 2 data were qualitatively analyzed, and year 2 data only were quantitatively analyzed (**Figure 3.8**). The qualitative analyses (year 1 and 2 data) provided information on eel movements in coastal waters and the likelihood of encountering a HVDC cable EMF based on the 2D proximity to the cable. The quantitative analyses of the year 2 data used the 3D position and operational characteristics of the cable to provide information on the DC and AC EMF encountered as the eels passed through the study area. This analysis also considered if there was an ecologically meaningful change in the eel movement behavior. The data processing is described in **Section 3.4.1** and the qualitative and quantitative analyses are described in **Section 3.4.2**.

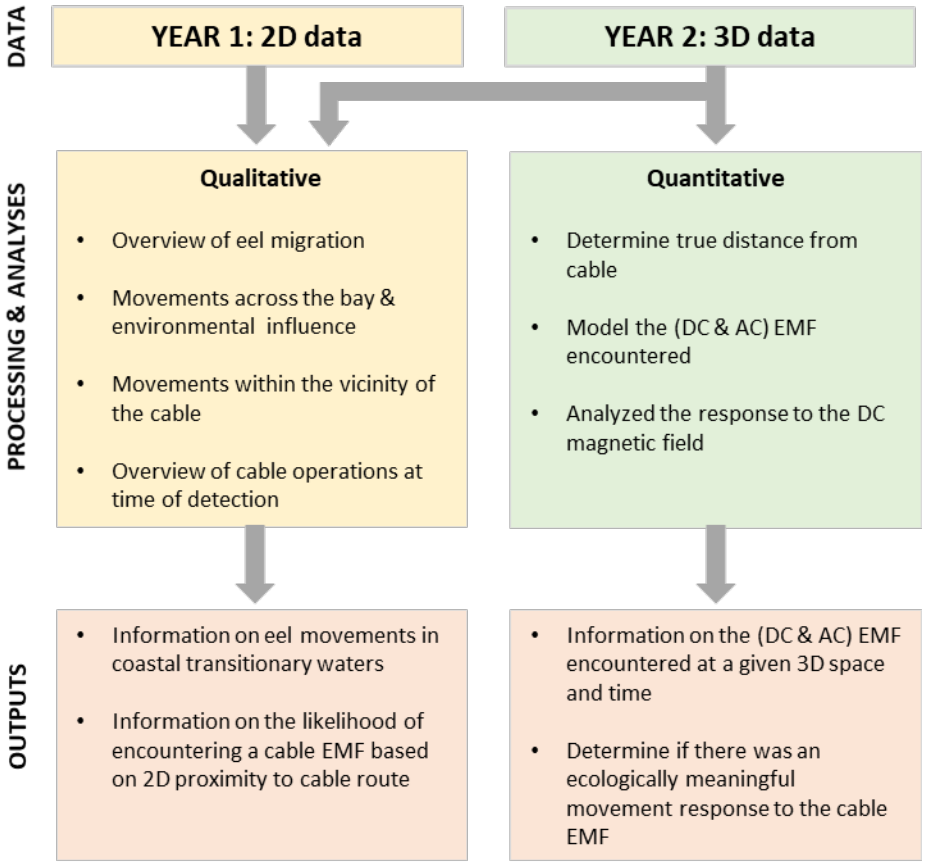

Figure 3.8. The eel telemetry data were analyzed qualitatively and quantitatively. Year 1 and Year 2 data were qualitatively analyzed (see Section 3.4.2.1) and the Year 2 data were quantitatively analyzed (see **Section 3.4.2.2** and **Figure 3.9** for an overview).

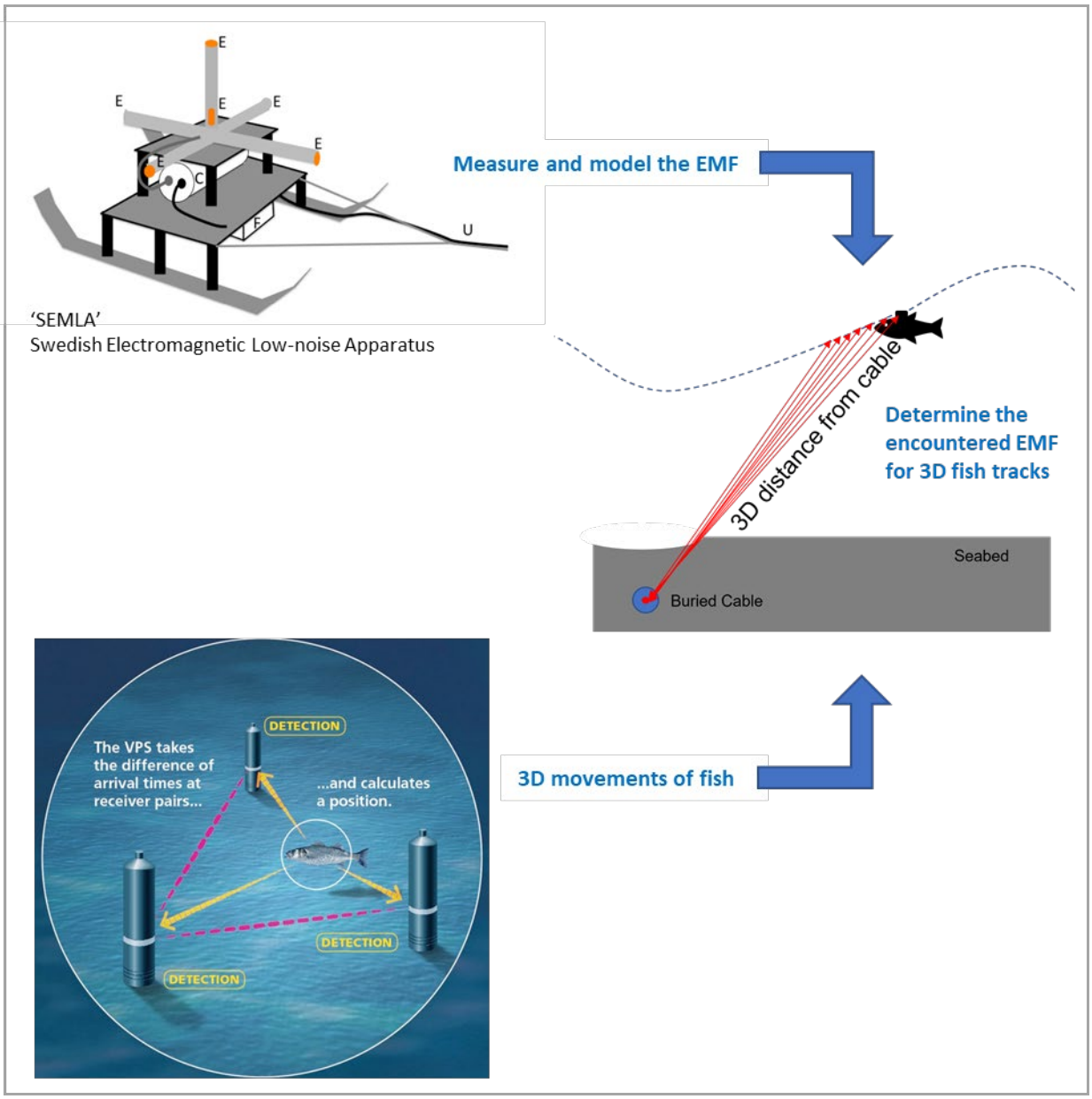

Figure 3.9. An overview of how data were combined for the quantitative assessment. The measurement and subsequent modeling of EMF is described in **Section 2**. The collection of 3D telemetry data as an eel passed over the HVDC cable is described in **Section 3.2**. The combination of these datasets with the specific operational characteristics of the cable at the time of the eel passing through the array, allowed the DC and AC EMF for each eel position to be determined. Subsequent statistical analyses allowed the behavioral response to the EMF to be determined. The image of the SEMLA is used with permissions from Hutchison et al., (2018) and the VPS image from Innovasea (2020) is used under the creative commons license.

3.4.1. Data Processing

For the qualitative and quantitative analysis of year 1 and year 2 telemetry data, error sensitivity filters were applied, described in brief in **Section 3.4.1.1**. For the three-dimensional data collected in year 2, the data were used to determine the true distance from the buried cable and subsequently the EMF encountered by the eels (**Section 3.4.1.2**).

3.4.1.1. Horizontal position error (HPE) filter determination

The horizontal position error (HPE) is a relative, unitless metric provided by Vemco for the analyzed data and is unique to each study, providing an estimate of error sensitivity for the hyperbolic positioning (Smith, 2013). The objectives of the HPE filtering were to balance (i) maximizing the volume of data retained and the number of eel tracks, (ii) minimizing the error sensitivity and (iii) retaining the depth profiles of the tracks. For the qualitative assessment, minimal filtering was used (HPE <10). To maximize accuracy and precision in positioning in the quantitative assessment, an HPE filter of <5 was applied. Application of the HPE <5 resulted in a median error sensitivity of 0.09 m in 2D. The vertical positioning was also assessed, and the error sensitivity was experimentally determined to be 0.10 m. The approach to determine the most suitable HPE filter and derive the error sensitivity in the 2D and for the vertical profile is described in full, in Appendix A.

3.4.1.2. Determination of proximity to the cable & calculation of EMF exposure

The V9p tags provided a positional water depth based on a pressure reading (i.e., distance from sea surface). However, the study area was influenced by the tidal regime which could be up to 7.5 ft (2.3 m) (www.USHarbors.com). Therefore, the inverse of the tag depth was not a true representation of the distance from the seabed. The V9p reference tags (Ref 4 and 5) were fixed points at a known height from the seabed and recorded the water depth. Therefore, a tidal range correction was applied to each eel position using Ref 4 tag as a reference point.

For each eel position, the true height from seabed was derived from the Ref 4 tag height above the seabed and the recorded water depth, interpolated from 30s intervals and smoothed (lag corrected moving average of 50). The nearest point on the cable was derived from the 2D as-laid cable burial data in ESRI ArcMAP (version 10.8.1). The bathymetry for the 2D cable position was obtained from the most recent bathymetric survey of the shipping channel area (US Army Corps, date 5th June, 2018). For each eel position, the present burial depth of the cable was derived from the EMF measurements by interpolating between the SEMLA transects in the eel study area (see **Section 2.3.3**). Together the known cable bathymetry relative to the assumed Ref 4 tag bathymetry, the EMF derived burial depth of the cable and the tide corrected height above the seabed provided the most accurate derivation of the vertical distance between the tag and the cable. This was then combined with the horizontal distance from the cable to determine the 3D distance from the cable using trigonometry. The 3D distance from the cable was used to model the EMF exposure (DC and AC magnetic field) for each eel position as described in **Section 2.3.3**.

The three-dimensional position was largely based on the telemetry data which had a 0.09 m accuracy in 2D and a vertical 0.10 m error sensitivity (see **Section 3.4.1.1** and **Appendix A**). The use of the bathymetry data may increase the error sensitivity and if the study were to be repeated, the collection of bathymetry data during the study should be considered. The EMF survey transects which were used

in the interpolation and EMF modeling were taken at approximately 10 m spacing. Reducing this spacing would improve accuracy, however, the gain in accuracy cannot be quantified without further surveys.

3.4.2. Data Analysis

Power transmission data from the real-time interchange, provided on an hourly basis (ISO New England), were used to describe the fluctuations in power level during the eel migration season for the study and prior years (2015-2019). The daily mean power level is presented for each year between September 01 and December 31 to provide context for the EMF environment that the eels would likely encounter (**Section 3.5.1**).

3.4.2.1. Qualitative Analysis of Eel Movements

The presence of migratory eels was derived from the transect area covered by the VR2W stations and the data were used to determine the total number of tagged eels that migrated during the periods of study in year 1 (2018) and year 2 (2019). A descriptive account of the use of the harbor area and their behavior is provided (**Section 3.5.2**).

The data (HPE <10) from the VPS array during year 1 (2018) and year 2 (2019) were used to give an overview of fine-scale eel movements within the vicinity of the cable. In Section 3.5.3, an overview of the tracks for eels detected in each year is presented together with a descriptive account of the timing of eel detections in relation to environmental variables. The spatial coverage of the telemetry array is also described.

3.4.2.2. Quantitative Analysis of the Encountered EMF and Behavioral Response

The Encountered EMF

The encountered DC and AC EMF was derived from the three-dimensional data, and the operational power level in the HVDC cable at the specific time of the eel passing through the study area (using the models described in Section 2). **Section 3.5.4** first describes the operational power level of the HVDC cable at the time of eels being detected in the study area in year 1 (2018) and year 2 (2019) and then focusses on reporting the encountered DC and AC EMF for the three-dimensional data collected in year 2 (2019) only. Based on the filtered data (HPE <5) of three-dimensional positions of eels in the vicinity of the HVDC cable, the encountered EMF was derived using the models described in Section 2 and the approach described in **Section 3.4.1.2**. For each eel, the encountered DC and AC EMF was modeled for each position over the recorded track. The encountered DC EMF is presented for the duration of the eel tracks and is shown in relation to the background geomagnetic field. The encountered AC EMF is shown for the duration of the track focusing on only the AC magnetic field and not the AC electric field. Hereafter, specific references to the DC magnetic field (DC MF) and the AC magnetic field (AC MF) are used where appropriate.

The Behavioral Response to EMF

Hidden Markov Models (HMM) were used to determine if there was an ecologically meaningful movement response by the eels to the HVDC cable EMF during their outward migration to sea. This section first introduces HMM before describing how they were applied to the three-dimensional telemetry and EMF data.

The movement of an animal is an observable result of underlying behavioral motivation and state (Nathan et al., 2008). Analyzing data on the sequential positioning of an animal, such as the acoustic

tracking data of the eels, provides an opportunity to link the movement pattern with behavioral responses to environmental conditions (Patterson et al., 2009). Hidden Markov Models are considered to be very useful for the analysis of movement data in terms of understanding the underlying behavioral states leading to meaningful inference from the observed movement (Patterson et al., 2009; Michelot et al., 2016).

An HMM is a time series model where each observed variable, i.e., the eel movement measured as step length in this study, arises from multiple probability distributions (Zucchini et al., 2016). An unobserved state variable determines which distribution is active at each time step, and the dynamics of this underlying state process are characterized by transition probabilities. The transition probabilities provide a likelihood of the animal remaining in the same behavioral state for the next step or moving into another state.

The analysis of the American eel data focused first on defining the movement behavior of eels in coastal waters using the 3D data (2019 data only) by fitting HMMs to define behavioral states and the transition probabilities. The influence of the encountered DC magnetic field within each behavioral state was then assessed. The encountered AC and DC magnetic fields were highly correlated, therefore only the encountered DC magnetic field was analysed. The HMM analyses were performed in R using the package 'momentuHMM' (McClintock and Michelot, 2018; R Core Team, 2020).

Step length (i.e., distance moved, m, in a given time) was the response variable in the HMM, as it is linked to movement speed and is often used to distinguish between different levels of activity or behaviors. It is typical to also use turning angle as the observed variable in HMM analyses, to model changes in the tortuosity of movement tracks. However, there is no unambiguous definition for turning angle in 3D tracks, and we therefore focused on step lengths here. The filtered data (HPE < 5, **Section 3.4.1.1**) had irregular time steps due to the unique identifiers programmed for each tag (**Table 3.1**). HMMs require regular time intervals, and therefore all tracks were interpolated on a regular time grid with a 5-second resolution (chosen as the 90th percentile of time steps in the original tracks) (**Figure 3.10**). This interpolation procedure can introduce large bias where there are long time gaps, so first the data were split into sub-tracks where there were gaps greater than 60 s. While the continuous-time correlated random walk, as implemented in the R package 'crawl', can be used to regularise 2D locations (Johnson et al., 2008), this method is not directly applicable to 3D data, therefore linear interpolation was used to regularise the 3D locations and the magnetic field anomaly observations to a regular 5-s time grid. The HMM applied to the 3D data used the relative change in x, y and z and therefore the tidally standardized depth value (**Section 3.4.1**) was not required. The standardized depth value was, however, used in **Section 3.5** to show the dive profiles on a common scale.

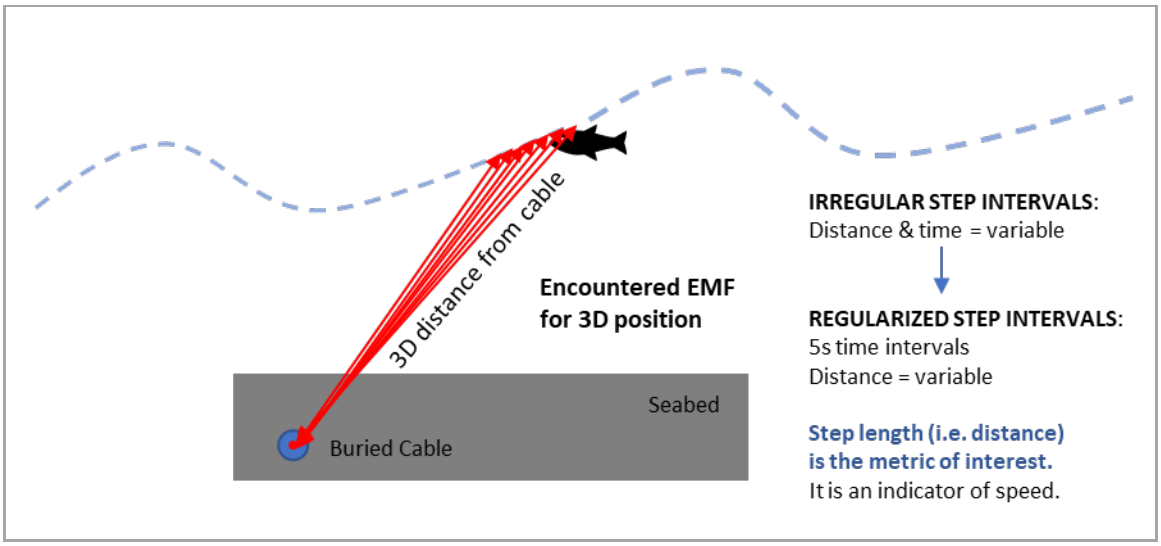

Figure 3.10. Regularized step intervals were used in the Hidden Markov Model. The telemetry data collected provided positions on an irregular step interval, i.e., positions which varied in distance (cm) and time (seconds). For the analysis, the positions and DC magnetic field encountered were regularized, providing positions every 5 seconds with step lengths which varied in distance. The step length (i.e., distance moved) was the metric analysed and was considered an indicator of speed. Note, that where tracks had intervals greater than 60s, sub-tracks were created to avoid bias in the analysis.

A model was fitted, with three states, as a trade-off between computational complexity, flexibility, and biological interpretability (Pohle et al., 2017). The state process (S_t) at each time t, was parameterized in terms of nine transition probabilities:

$$\begin{bmatrix} \gamma_{1\text{-}1} & \gamma_{1\text{-}2} & \gamma_{1\text{-}3} \\ \gamma_{2\text{-}1} & \gamma_{2\text{-}2} & \gamma_{2\text{-}3} \\ \gamma_{3\text{-}1} & \gamma_{3\text{-}2} & \gamma_{3\text{-}3} \end{bmatrix}$$

where the probability of a transition from state *i* to state *j* over one step is defined by:

$$\gamma ij = \Pr(S_{t+1} = j \mid S_t = i)$$

The HMM was fitted with a discrete random effect on the transition probabilities, with three mixtures. The choice of the number of mixtures was based on the best error prediction estimator Akaike Information Criteria (AIC), following McKellar et al., (2015). This approach imlpies that three transition probability matrices were estimated rather than just one and the eel sub-tracks were then assigned to one of three groups that best described their behavioral dynamics. The transition probabilities between states 1 and 3, were fixed to zero, following the assumption that eels always go through the intermediate state (state 2).

The model incorporated the one observed variable, the step length, employing gamma distributions with two parameters (mean and standard deviation). The observation model can therefore be written as:

$$Z_t \sim \text{gamma}(m_j, s_j)$$

in state $S_t = j \in \{1, 2, 3\}$, where m_j and s_j are state-dependent mean and standard deviation parameters, respectively. The encountered DC magnetic field anomaly was included as a covariate (linear effect) on the mean and standard deviation parameters in each state (see McClintock and Michelot, 2018).

Further covariates (temperature, state of tide, light/dark) were not required in the model but were considered in the discussion of the model results. This approach was deemed most appropriate based on the resolution of the covariable data compared to the high-resolution eel position and EMF data.

A summary of the Hidden Markov Model and its application to the eel telemetry and DC magnetic field data is provided in **Figure 3.11**.

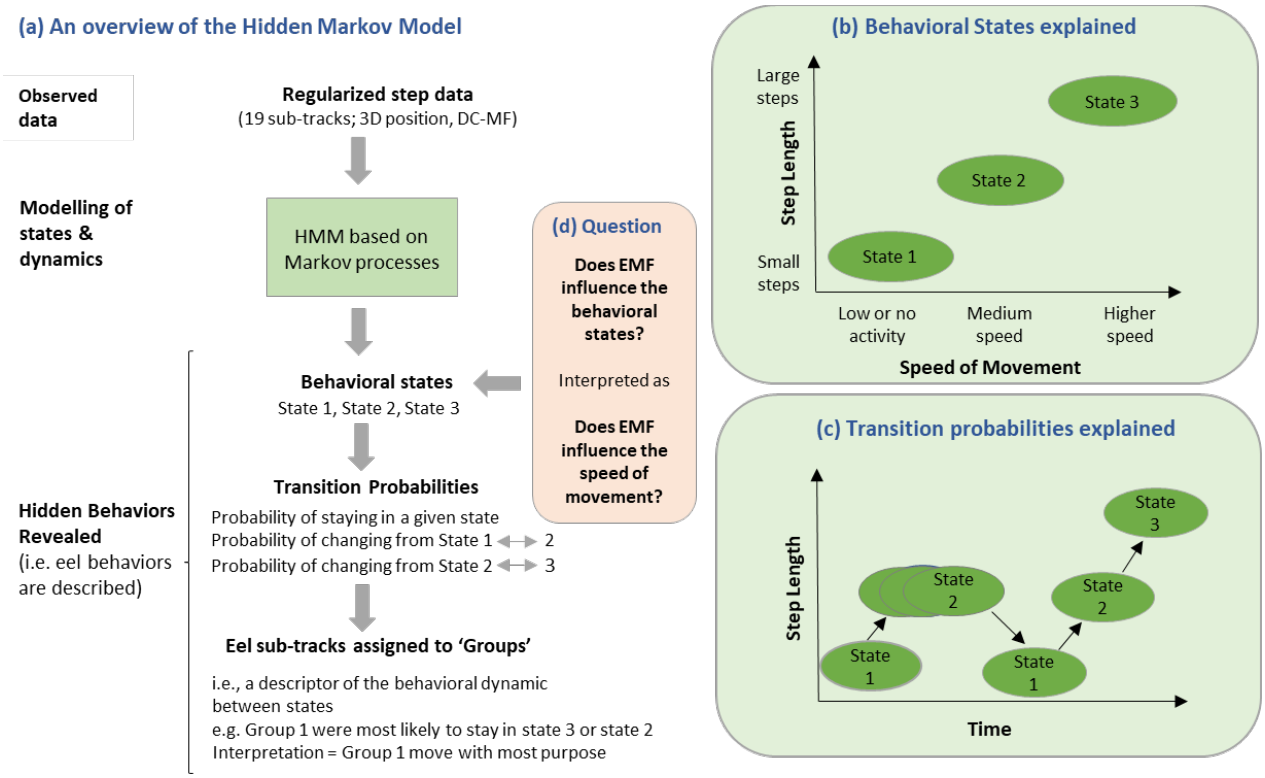

Figure 3.11. A summary of the Hidden Markov Model applied to the three-dimensional eel position data and encountered DC magnetic field. (a) The observed data were regularized to 5 second intervals allowing the step length (i.e., distance moved) to be used in the model (see **Figure 3.10** for an overview of regularization). The HMM was applied to the regularized observed data to determine the behavioral states and dynamics based on transition probabilities. Based on the transition probabilities, the behaviors of the eels were described facilitating the assignment of eels tracks to groups. (b) The behavioral states were based on the step length (i.e., distance moved in 5 s intervals). The HMM characterizes the behavioral states based on the regularized observed step length data (mean, sd, confidence intervals) and can be considered descriptors of low or no activity (small steps), medium speed (medium steps) and high speed of movement (larger steps). (c) The transition probabilities are also derived from the regularized observed data and are indicative of the behavioral dynamics within a track (i.e., probability of changing between states). For example, an eel may move from states 1 to 2 to 1 to 2 to 3 indicating low – medium – low – medium – high activity. The reverse pattern can also occur. A combination of patterns is possible, but eels cannot jump from state 1 to 3 and vice versa they must move through state 2. The change between states is characterized for the observed data in terms of probability of state changes for each eel track and based on the probabilities they can be grouped for their characteristic behaviors (a). (d) While the HMM describes the eel behavior in terms of the behavioral state, transition probabilities and groups the eel tracks accordingly, the question of if the eels respond to the DC magnetic field is assessed at the level of the behavioral state.

3.5. Results

Between the 15th November and 3rd December 2018, 25% of the eels released (n=100) were detected by the full array, and 21 % were detected by the high-resolution VPS array in the channel. In 2019 15.5% of eels (31 eels) released (n=200) were detected by the full array and 8.5 % (17 eels) were detected by the

VPS array in the channel. The 2018 and 2019 data were used in the qualitative analyses and the 2019 data were used in the quantitative analyses.

In this section, the power level in the Cross Sound Cable during the study is first described and compared to activity in previous years (**Section 3.5.1**). The results of the qualitative analyses are then presented. This includes a description of the presence of eels detected by the VR2W array for both 2018 and 2019 (**Section 3.5.2**). An overview of the fine-scale movements of eels obtained by the VPS array in the vicinity of the HVDC cable in 2018 and 2019 is also provided in **Section 3.5.3**. Note that this descriptive account is irrespective of the HVDC EMF.

The results of the quantitative analyses are then presented. This includes the DC and AC magnetic field encountered by eels in 2019 when they were in the vicinity of the HVDC cable (**Section 3.3.4**). The Hidden Markov Model results describing the behavioral states, transition probabilities and the influence of the DC magnetic field is provided in **Section 3.5.5**.

3.5.1. Cross Sound Cable Power Level

The power level in the Cross Sound Cable fluctuated between 0 and 300 MW based on domestic demand in the Long Island and New England grid. The American eel population under study typically start their outward migrating toward the end of September. Therefore, the patterns of power fluctuation were explored for the eel migration period and are shown in **Figure 3.12** for the two study years of the eel study and three years prior (2015-2019 inclusive).

In 2018, there was a period of greater power level (100-330 MW) in September followed by a period of 0 MW in late September to early October (**Figure 3.12**). The power was then typically between 100 and 330 MW for the majority of time until mid-November when the power reduces to 0 MW with only minor low-level fluctuations through December.

In 2019, the mean daily power level fluctuated but was typically above 150 MW until mid-October (**Figure 3.12**). There was only a minor period with a daily mean of 0 MW in early-October. The power level then increased and was typically above 200 MW for the remainder of October and into November after which it gradually decreased and was typically below 100 MW throughout December but only briefly at 0 MW.

Comparisons with years prior to the eel study, show that power is generally highest through September and lowest moving into the winter months, but there are typically brief periods of 0 MW with the power level being overall highly variable throughout the September to January period in any one year (**Figure 3.12**).

Key Information Box 3.1

- The operational power level in a cable is variable
- For the HVDC Cross Sound Power cable
    - the power level varied seasonally but also by hour as reported by the company
    - annual power level patterns were also variable

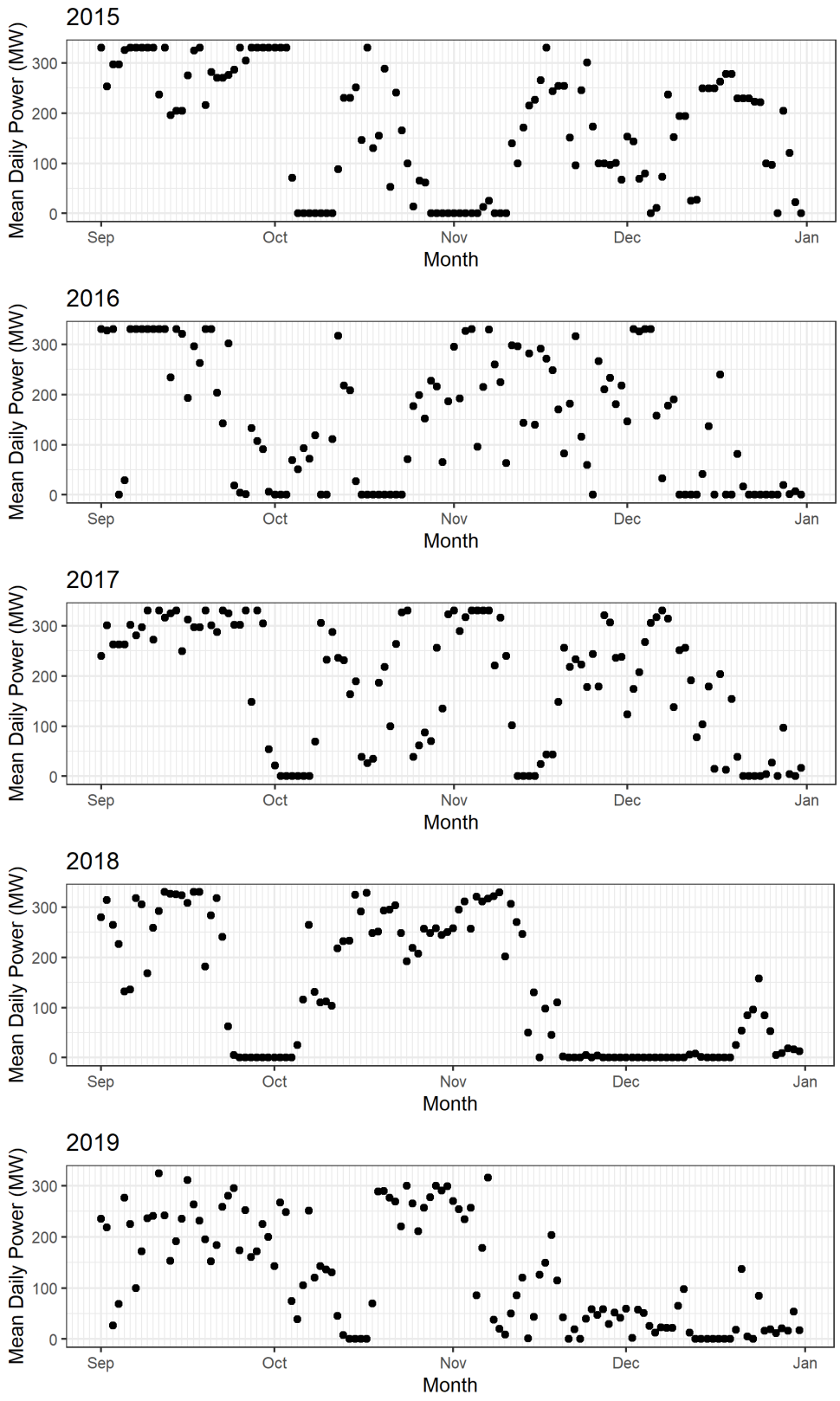

Figure 3.12. Cross Sound Cable power activity during the eel migration period in 2015-2019. The hourly power level (ISO New England) is shown as the mean daily power during the months of September through to the end of December between 2015 and 2019.

3.5.2. Eel Detections Across the VR2W Array (2018 and 2019)

In 2018, the total number of eels detected per VR2W station varied between four eels at station VJ and 18 eels at station VF. In 2019, the total number of eels detected varied between 2 eels at station VB and 16 eels detected at station VF (**Figure 3.13**). For reference, the VPS array was positioned in the shipping channel between VF and VG.

In 2018 and 2019, a greater number of eels were detected by stations positioned in the center of the array compared to those positioned at the edges of the array (**Figure 3.13**). The number of eels detected by station VB in 2019 is low compared to other stations. Referring to the field notes indicated that station VB was not vertical when recovered in 2019; situated in shallow water, it was likely knocked over by a boat during the course of the study. For both 2018 and 2019, the greatest number of eels were detected by station VF however, a greater number of detections occurred at stations VE, VF, and VG in 2018 and stations VG to VJ in 2019.

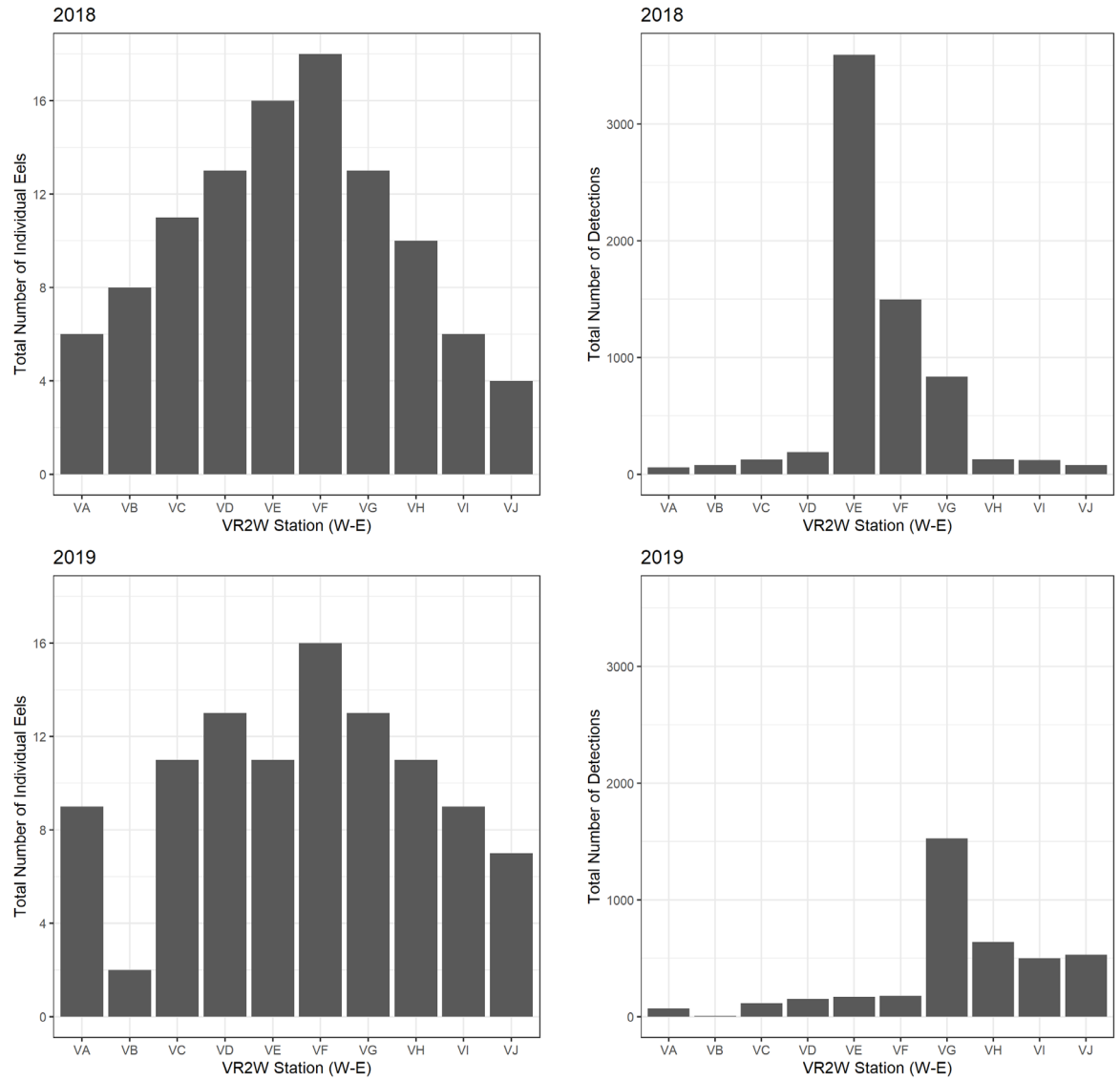

Figure 3.13. The number of individual eels and number of detections by the VR2W array. The VR2W receivers were positioned at stations (VA-VJ), west to east (W-E) either side of the channel and provided an indication of presence only. The number of individual eels (left) and number of detections (right) are shown for 2018 (upper panel) and 2019 (lower panel). For reference the VPS array was positioned in the channel between stations VF and VG.

The number of detections per eel tag by each station, provide an indication of the spatial use of the harbor area by migratory eels (**Figure 3.14**). Based on the detections of the reference tags positioned in the channel by neighboring VR2W receivers (data not shown), it can be inferred that eels within the channel may be detected by VR2Ws on either side of the channel (west VE, VF, east VG, VH).

In 2018, two eels (IDs 56, 79) were detected only on the west side of the channel and did not interact with the channel area. Ten eels were detected on the east side of the array, of which six were detected by the most easterly receivers VI and VJ. All ten of the eels detected on the eastern side of the array were also detected interacting with the channel area (i.e., detected by VE-VH). A total of 23 eels were

detected by receivers at stations VE to VH, indicating that they were close to the channel area of which nine were more confidently in the channel as indicated by dual detection by stations VF and VG. In 2018, 22 of the 25 eels were first detected during the hours of darkness and 3 were first detected during daylight. For most eels, detections ranged between 3 minutes and 1 hour 41 minutes, however there were three eels that made return visits to the array in the same day (IDs 44, 56, 81) and three eels that made return visits over a period of 2-5 days (IDs 8, 21, 65, 81). One eel was continuously recorded for 3 days (ID 99) by the same receivers suggesting it was briefly sheltering in place.

In 2019, seven of the eels (ID's 34, 109, 117, 134, 183, 190, 196) were only detected on the west side of the harbor and did not interact with the channel within the detection range of the array. Of the ten eels detected on the east side of the harbor, only one eel (ID 18) was detected with no prior detections within the vicinity of the channel, indicating that it crossed the channel north (or south) of the Vemco array. A total of 22 eels (of 31 detected) were detected in the vicinity of the channel based on the VR2W array. Eels with detections by both VF and VG provide greater confidence that there were eight eels present in the channel. In 2019, all eels were first detected during periods of darkness. Five eels were detected during daylight hours, of which, two eels (ID's 143 and 181) had a period of detection starting in the night but continuing during the day for prolonged periods. In 2019, most eel detection periods were between approximately 2 and 37 minutes, however one eel made a return visit within 4 hours the same day (ID 187), one made a return visit the next day (ID 113) and two eels had prolonged detections over 12-14 hours indicating brief residency in the area (ID's 143, 181).

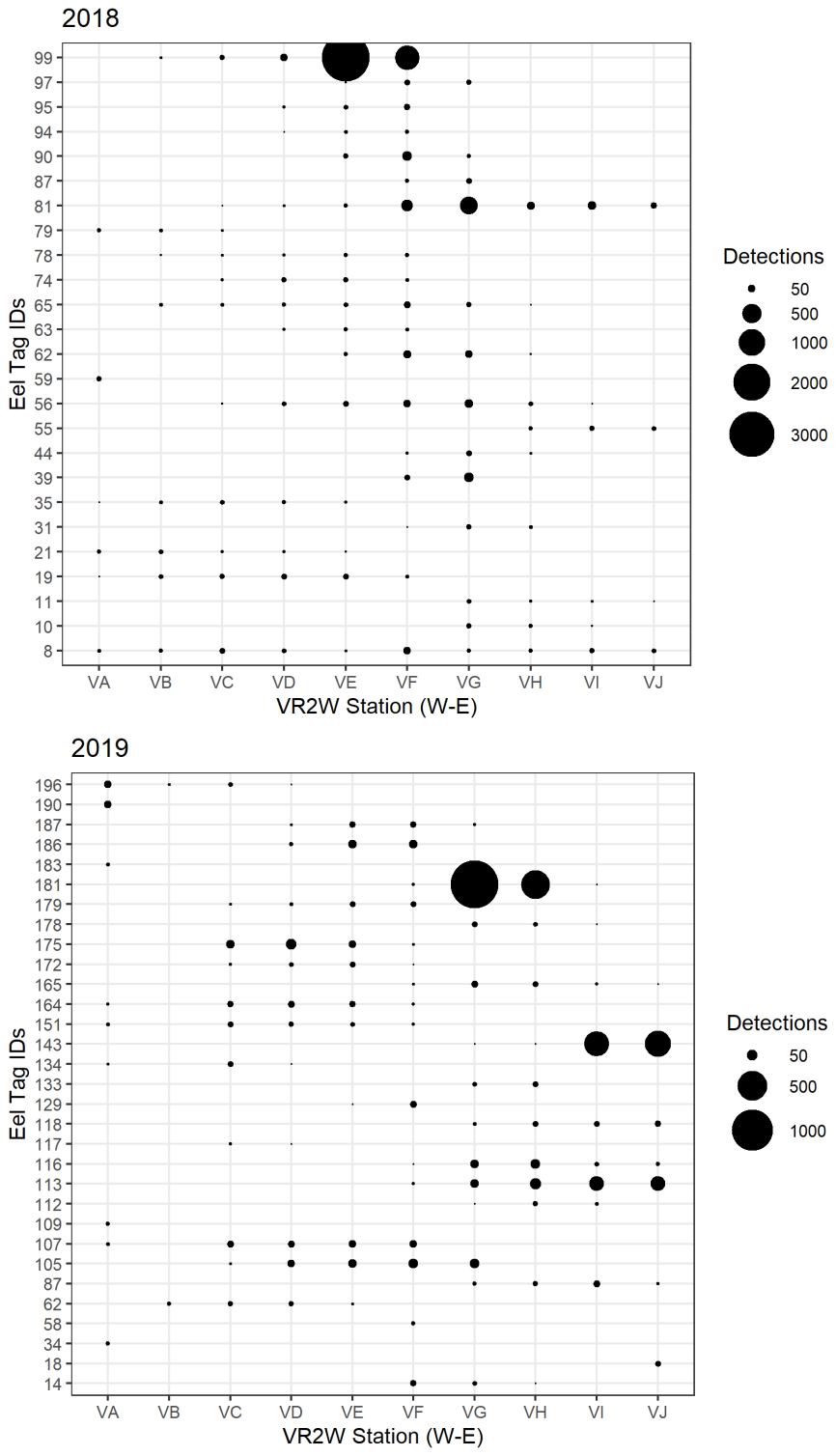

Figure 3.14. The number of detections per eel for each VR2W station in 2018 and 2019. The VR2W receivers were positioned at stations (VA-VJ), west to east (W-E) either side of the channel and provided an indication of presence only. For reference the VPS array was positioned in the channel between stations 'VF' and 'VG'. The number of detections for each eel (represented by black circles), and each station provides an indication of spatial use by individual eels within the array area. A larger number of detections is indicative that the eel spent more time near a station, within each year.

Detections of eels by station alone do not allow directional movement, only presence. However, based on the time of detection by the VR2W receivers some directional information on the movement of eels across the harbor can be derived. Examples of eel movements are provided from the 2019 release group (**Figure 3.15**). Eel 62 was initially detected by station VB and progressively moved through VC, VD, VE indicating a movement from west to east toward the channel over the course of approximately 7-8 minutes (**Figure 3.15a**). Similarly, eel 105 demonstrated a west to east movement over the course of 1.5 hr, initially detected by station VC, moving toward the channel and apparently straightening the trajectory since it was not detected by VH (**Figure 3.15b**). Eel 113 was first detected by VF, crossed the channel and beyond the VJ receiver was progressively detected moving east over the course of approximately 1 hr (**Figure 3.15c**). The eel moved outside of the range of detection returning approximately 2 hrs later moving in an east to west direction toward the channel over the course of approximately 40 minutes and was later recorded moving west 1 hr later (**Figure 3.15c**). Movements were not always able to be derived and may instead be representative of a stationary or relatively low activity in an eel, demonstrated by eel 181 where the detections are predominantly consistent between two receiver stations (**Figure 3.15d**). The density of detections and time can also provide indications of the speed of movement. For example, it can be inferred that eel 62 moved over a greater distance in a short period of time and therefore was moving fast relative to the movements of eel 105, 113 and 181 (**Figure 3.15**).

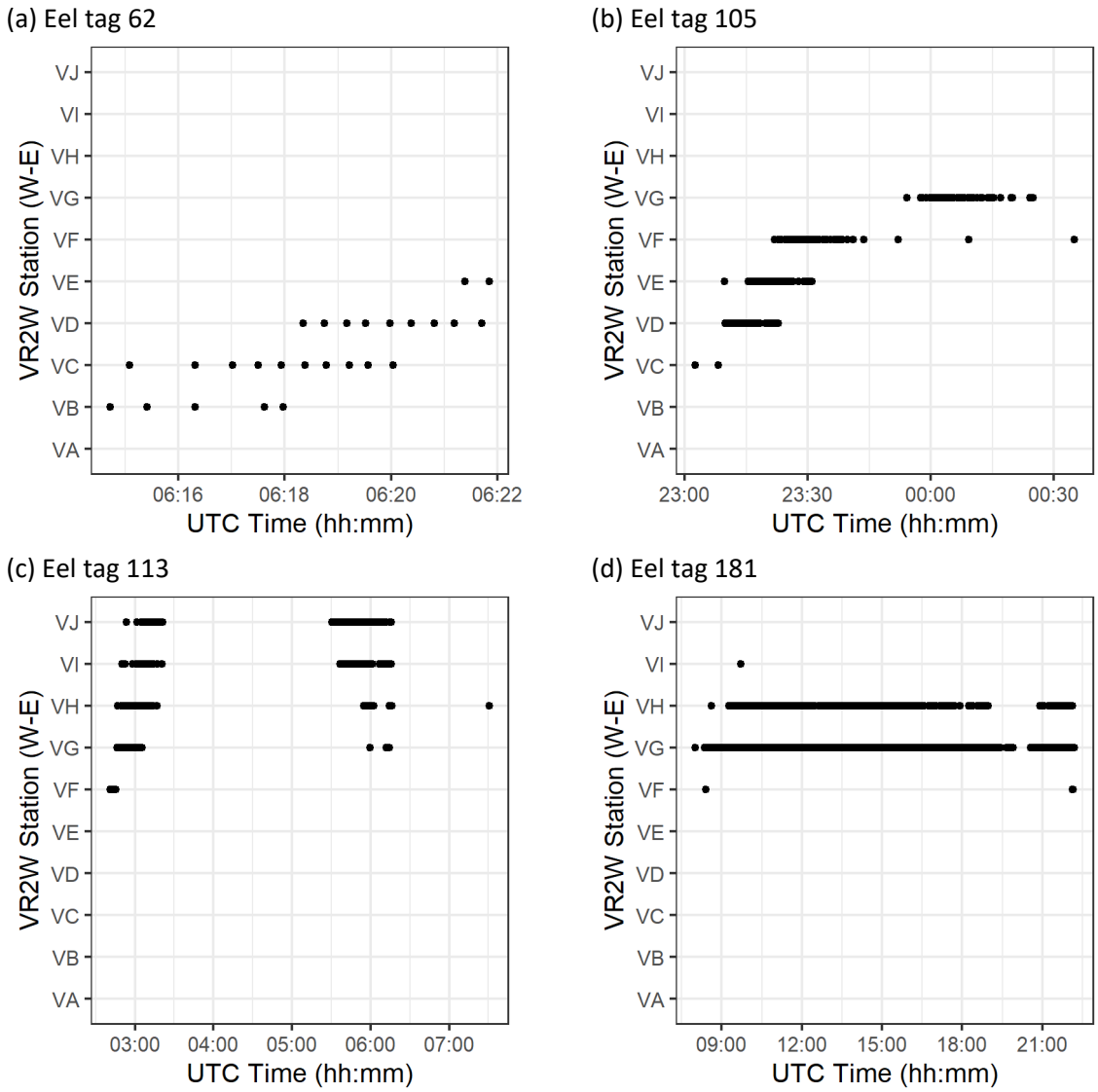

Figure 3.15. Eel movement inferred from the VR2W array. While data from the VR2W receivers only provides an indication of presence in the area, serial data from multiple receivers in a west to east array can provide an indication of movement across the harbor area and also relative speed of movement.

Key Information Box 3.2

- The VR2W array detected eels over the full span of the transect across the harbor
- Moving eels were detected for variable time periods (2 min to 1 hr 41 min)
- Some eels made return visits to the array over 1-5 days
- Brief residency (12 hr to 3 days) was observed
- Directional movements could be determined from the VR2W array
    - This lacked sufficient detail to derive the encountered EMF or determine responses

3.5.3. Fine-scale American Eel Movements detected by the VPS array (2018 and 2019)

In 2018, 28 tracks from 21 eels were detected by the VPS array in the vicinity of the cable. Following HPE filtering, five tracks were omitted due to a low number of positions. The remaining 23 tracks from 19 eels were include in the 2D analysis and are the focus of the following results (**Figure 3.16**). Five of the 19 eels made return visits to the study area, of which three eels had more than one track retained. Tracks ranged from 25 to 9871 positions over a period of a 1.3 minutes to 352.5 minutes (nearly six hours) (**Table 3.3**). The majority of eels in 2018, were detected during the hours of darkness at variable times throughout the night, however two eels were detected in daylight (ID 87 and 95). Fourteen of the eel tracks were obtained during an ebbing tide and eight during slack tide (**Table 3.3**).

In 2019, 19 tracks from 17 eels were detected by the VPS array in the vicinity of the cable. Six tracks from five eels were omitted due to a low number of positions remaining after HPE filtering. After HPE filtering a total of 13 high-resolution tracks from 12 eels were used in the analysis (**Figure 3.16**). Only one eel made a return visit to the study area and both tracks were retained. Tracks varied with between 37 and 1386 positions per track with durations ranging between 7.32 minutes and 96.26 minutes (**Table 3.4**). The majority of eels in 2019, were detected during the hours of darkness and varied throughout the night, apart from one (ID 187) that was first detected 38 minutes after sunrise, in full daylight (**Table 3.4**). The tidal state at the time of eel detections was variable with eight eels being detected during the ebbing tide (**Table 3.4**). One eel was detected just after slack tide at the beginning of an ebbing tide and four fully in a slack tide period.

It was anticipated that only eel positions obtained from within the triangulation of the HR receivers would be sufficient for high-resolution analysis. Therefore, the VPS array developed provided an anticipated spatial coverage of 14,700 m^2 based on the hydrophone area, covering 212 m of the CSC and 35 m on either side of the cable (**Figure 3.7**). However, sufficient resolution was also obtained for tracks outside of the array where there was sufficient detection range. Based on the HPE filtered tracks, the high-resolution data obtained was from an area of 129,839 m^2 covering 440 m of the CSC in 2018 and was similar, in 2019 with a spatial coverage of 114,583 m^2 covering 423 m of the CSC (**Figure 3.16**). The greater spatial coverage in 2018 is due to a greater presence of eels (**Figure 3.16**).

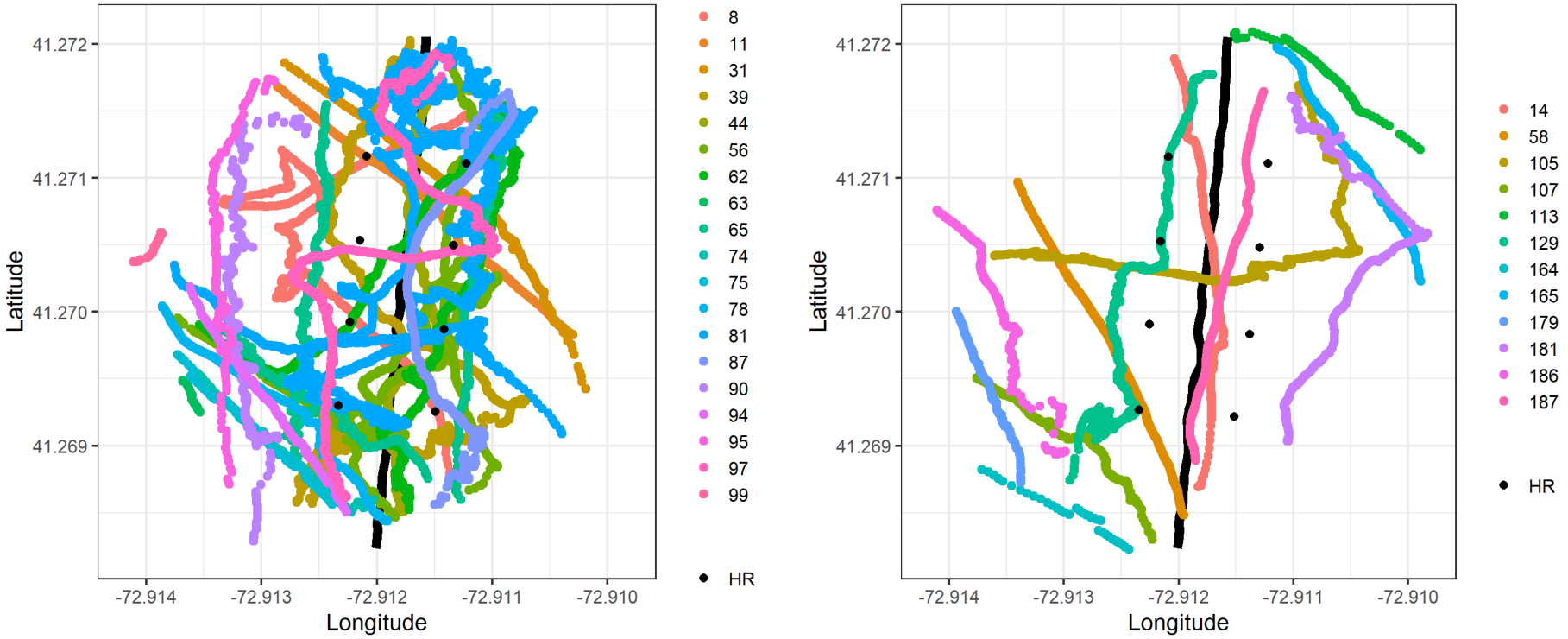

3.16. An overview of the eel tracks from the VPS array in 2018 and 2019. The Cross Sound Cable is indicated as a back line as a visual reference but was buried in the seabed. The VPS High Residency (HR) receivers are indicated as black dots. In 2018 (left) a greater number of eels were detected (n = 21) providing 28 tracks. In 2019 (right) fewer eels were detected (n=12), providing 13 tracks. The eel tracks are color coded by individual eel per year.

Table 3.3. An overview of the high-resolution two-dimensional eel tracks from year 1 (2018). A total of 19 eels were recorded, providing 23 high resolution tracks in the vicinity of the Cross Sound Cable. The Cross Sound Cable was not transferring power at the time of detection for all eels in 2018. Eel track numbers with lower case letters are separate tracks of the same eel.

Eel Track ID	Track duration (min)	First detection (Local time)		Positions	LL:DD*	Tidal Ref. (hrs)**	Tidal State
8	9.2	Nov 22	17:01 EST	1286	DD	-5.5	Slack
11	23.6	Nov 30	19:29 EST	320	DD	2.3	Ebb
31	121.2	Nov 28	19:24 EST	915	DD	4.3	Ebb
39	225.4	Nov 29	19:53 EST	2195	DD	3.7	Ebb
44	70.9	Nov 28	02:09 EST	1021	DD	-0.6	Slack
56a	26.7	Nov 24	17:39 EST	3143	DD	-0.3	Slack
56b	352.5	Nov 25	19:15 EST	680	DD	0.3	Slack
62	1.3	Nov 28	20:21 EST	2883	DD	5.3	Ebb
63	13.6	Nov 23	02:52 EST	25	DD	-4.3	Ebb
65a	11.9	Nov 16	18:09 EST	359	DD	0.2	Slack
65b	30.5	Nov 19	02:25 EST	362	DD	-5.5	Ebb
65c	10.4	Nov 22	18:09 EST	1062	DD	-4.4	Ebb
74	7.7	Nov 23	03:52 EST	275	DD	-5.3	Slack
75	8.8	Dec 07	23:15 EST	133	DD	-0.1	Slack
78	46.4	Nov 29	17:18 EST	351	DD	1.2	Ebb
81a	85.6	Nov 29	17:29 EST	3121	DD	1.3	Ebb
81b	290.4	Nov 30	19:55 EST	9871	DD	-3.7	Ebb
87	194.8	Nov 28	15:29 EST	969	LL	0.4	Slack
90a	54.9	Nov 28	17:27 EST	484	DD	2.4	Ebb
94	9.2	Nov 23	03:46 EST	334	DD	-5.2	Slack
95	20.2	Dec 03	09:54 EST	186	LL	2.2	Ebb
97	47.9	Nov 27	03:07 EST	1632	DD	1.3	Ebb
99a	8.2	Nov 27	03:06 EST	33	DD	1.3	Ebb

*LL or DD is considered the light or dark period based on the sunrise [06:51 ±11 min] and sunset [16:26 ±5 min] for the specific dates.

**Decimal hours relative to nearest high tide as per tidal charts (www.USHarbors.com), slack tide is considered ±1 hr relative to high/low tide.

Table 3.4. An overview of the high-resolution three-dimensional eel tracks from year 2 (2019). These tracks were used in the Hidden Markov Modeling to determine the response of eels to the EMF from the Cross Sound Cable. A total of 12 eels were recorded, providing 13 high resolution tracks around the Cross Sound Cable and the encountered magnetic field anomaly (AC and DC) was modeled (see **Table 3.5**). Eel track numbers with lower case letters are separate tracks of the same eel.

Eel Track ID	Track duration (min)	First detection (Local time)		Positions	LL:DD*	Tidal Ref. (hrs)**	Tidal State	Temperature (°C)
14	12.88	Nov 01	05:31 EDT	620	DD	2.68	Ebb	16.2
58	9.94	Nov 02	05:47 EDT	402	DD	2.05	Ebb	15.1
105	65.62	Nov 18	18:47 EST	1386	DD	3.20	Ebb	7.6
107	10.51	Dec 03	17:31 EST	404	DD	1.25	Ebb	5.1
113	14.60	Dec 03	21:45 EST	102	DD	5.48	Slack	5.0
129	52.89	Nov 24	23:15 EST	1314	DD	1.92	Ebb	7.4
164	7.32	Nov 24	20:24 EST	37	DD	-0.93	Slack	7.4
165	10.30	Dec 03	21:30 EST	309	DD	5.23	Slack	5.0
179	5.31	Dec 02	05:18 EST	194	DD	2.20	Ebb	6.1
181a	96.26	Dec 01	03:20 EST	209	DD	1.08	Slack/ebb	6.0
181b	19.82	Dec 01	16:56 EST	219	DD	2.45	Ebb	6.0
186	22.57	Nov 25	22:13 EST	247	DD	0.03	Slack	7.4
187	8.49	Nov 28	07:31 EST	513	LL	-4.53	Ebb	7.7

*LL or DD is considered the light or dark period based on the sunrise [07:02 ±21 min] and sunset [17:07 ±42 min] for the specific dates.

**Decimal hours relative to nearest high tide as per tidal charts (www.USHarbors.com), slack tide is considered ±1 hr relative to high/low tide.

Key Information Box 3.3

- The VPS array successfully provided high-resolution tracks for tagged eels
- The spatial coverage of the VPS array was greater than expected and varied each year based on eel presence
- In 2018, 21 eels were detected providing 28 tracks
- In 2019, 12 eels were detected providing 13 tracks
- Eels were predominantly first detected during the night and in an ebbing or slack tide

3.5.4. The encountered EMF for the eels

3.5.4.1. The operational activity of the HVDC cable when the eels migrated (2018 and 2019)

In 2018, the HVDC cable was not transferring power for the majority of days when the eels were detected by the VPS array (**Figure 3.17**). This power level was unexpected based on the data from the previous years (2015-17) (**Figure 3.12**). To avoid this situation in 2019, where possible, eels moving down the river were caught and subsequently released earlier and with greater numbers of eels released over a longer period of time (**Figure 3.17**). The study was further enhanced with pressure sensor tags to allow three-dimensional positioning and maximise the accuracy in determining the encountered EMF.

There was more variability in the HVDC CSC mean daily power level when the eels were detected in 2019 relative to 2018 (**Figure 3.17**) although the variability was still lower than the non-study years (2015-2017, **Figure 3.12**). As the mean daily power level was not sufficient to determine if eels encountered the HVDC cable when it was powered or not, the encountered EMF was determined from the operational power level at the specific time of detection in the VPS array and the specific 3D proximity to the cable.

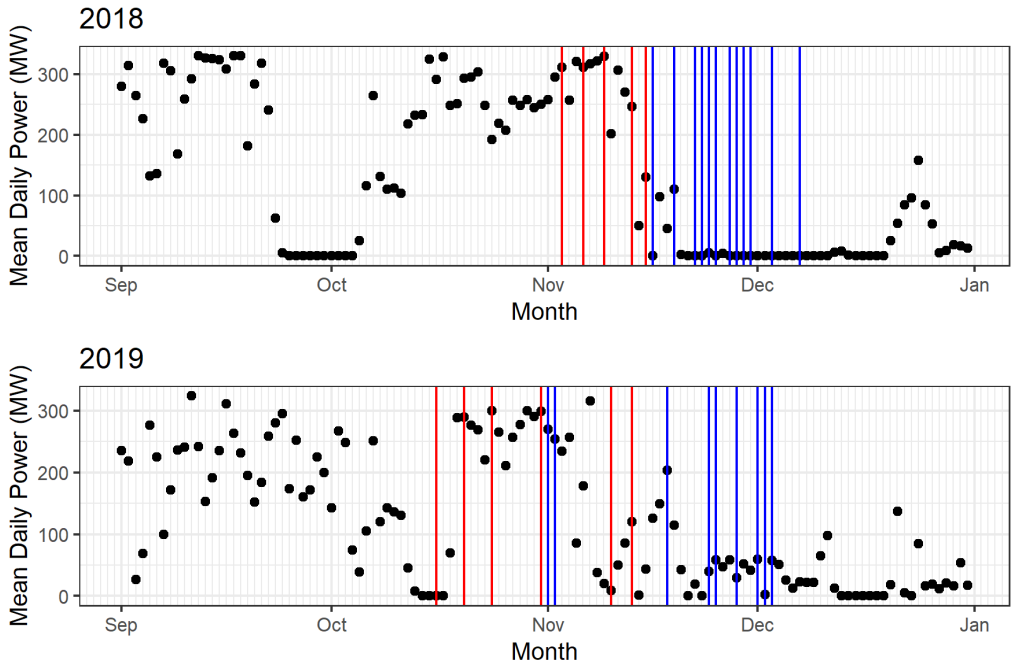

Figure 3.17. The eel release and detection dates relative to the daily mean power in the HVDC Cross Sound Cable. The hourly power level (ISO New England) is shown as the mean daily power during the months of September through to the end of December between 2015 and 2019. Eels were released on 5 and 6 dates in 2018 and 2019, respectively, indicated by the red vertical lines (**Table 3.2**) and the date of VPS detections are shown in blue (**Table 3.3. and 3.4**).

3.5.4.2. The encountered AC and DC EMF when passing the HVDC cable (2019)

The 2018 version of the tags (V9) were not able to record the vertical position in the water column to allow 3D analysis. Furthermore, at the time of all the eel detections, the power transmission level of the HVDC CSC was 0 MW so it was not possible to analyze the movement of the eels in relation to power levels in the cable. Therefore, the analysis focused on the three-dimensional data obtained for eels in 2019.

In 2019, the tags (V9p) were able to determine both the horizontal and the vertical position in the water column. These data were used to determine the EMF encountered by an eel in 3D, by modeling the EMF for the 13 eel tracks and taking into account the power level at the specific time of detection. The DC and AC magnetic fields encountered were modeled for each eel position and are shown in **Figure 3.18** and **Figure 3.19**, respectively. Overall, five of the 12 eels (13 tracks), experienced a magnetic field anomaly greater than 10 nT for both DC and AC fields encountered (**Table 3.5**)**.** The eels encountered the HVDC cable when operational power levels were variable (0-330 MW) and at different distances to the HVDC cable. These two interacting factors mean that eels at a recorded position experienced a unique exposure to the DC and AC magnetic fields and a range of magnetic field intensities were encountered at different distances to the cable. The lowest level considered in this study is 0.1 nT set by the reported background levels that are assumed to be the limiting factor (Constable and Constable, 2004)**.**

Table 3.5. A summary of the DC and AC magnetic field anomalies encountered by eels in year 2 (2019). A total of 12 eels were recorded in 3D in the vicinity of the CSC, providing 13 high resolution tracks around the CSC. The magnetic field anomaly (AC and DC) encountered was modeled and is reported here as the maximal negative to positive range. The anomaly for the DC field was referenced relative to the Earth's magnetic field while the absolute AC anomaly was relative to no AC field present. Eel track numbers with lower case letters are separate tracks of the same eel. The DC magnetic field encountered, for each position was used in the Hidden Markov Modeling to determine the response of eels to the cable EMF.

Eel Track ID	Magnetic Field Anomaly Encountered (nT)			
	Min. DC	Max. DC	Min. AC	Max. AC
14	-10.5	69.3	0.8	33.6
58	-4.6	44.3	0.0	48.1
105	-17.9	86.9	0.0	147.8
107	-7.5	-0.4	0.0	3.6
113	-2.2	23.8	0.0	14.8
129	-13.4	-1.0	0.0	10.5
164	-3.6	-0.3	0.0	0.8
165	-3.5	-0.2	0.0	1.1
179	-0.1	-0.1	0.0	0.0
181a	-0.7	-0.1	0.0	0.1
181b	-1.4	-0.3	0.0	0.0
186	-0.1	-0.1	0.0	0.0
187	-0.1	-0.1	0.0	0.0

In **Figure 3.18**, it is shown that four eels encountered a positive DC magnetic field anomaly (ID' 14, 58, 105 and 113) with a maximum total field of 51.530 µT, which is a maximum positive anomaly of 0.087 µT (87 nT) relative to the background geomagnetic field. The range of positive DC anomalies encountered by eels was between approximately 0.024 and 0.087 µT (23.8 -86.9 nT) (**Table 3.5**). All eels experienced a minor negative DC anomaly (**Figure 3.18, Table 3.5**), with a maximum negative deviation of -0.017 µT (-17.9 nT, **Table 3.5**). The strongest negative anomalies were encountered by eels 14, 105 and 129.

Figure 3.19. shows that the AC magnetic field followed a similar pattern to the encountered DC magnetic field. This similarity is most obvious for Tracks 14 and 105 where the shape of the data is similar but on a smaller magnetic field scale. Only four of the 13 tracks did not experience an AC magnetic field anomaly (**Table 3.5**). Of the eight tracks that experienced an AC magnetic field, five were greater than 10 nT. The full range of absolute AC magnetic field encountered was between 0.0001 and 0.148 µT (0.1 and 147.8 nT), which exceeded the maximum DC field encountered. The AC magnetic fields which were >10 nT correspond to the positive and negative DC anomalies >10 nT (i.e., >10 or <-10 nT, **Table 3.5**).

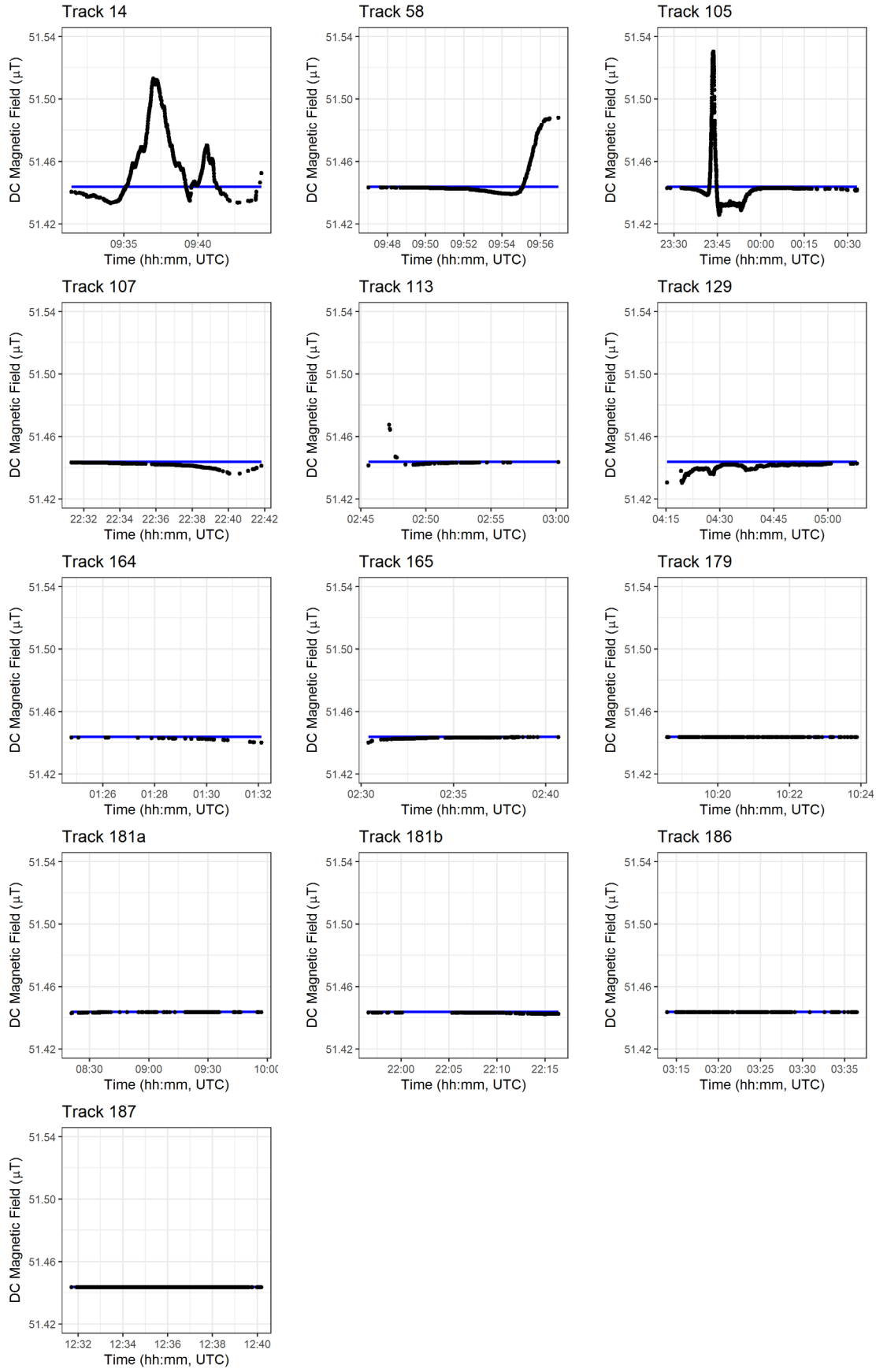

Figure 3.18. The DC magnetic field encountered by American eels in 2019. For each 3D eel position, the emitted DC magnetic field and its interaction with the geomagnetic field was modeled. The encountered DC magnetic field is shown with the geomagnetic field (blue, 54.44 µT) as a reference so that the anomaly is clear.

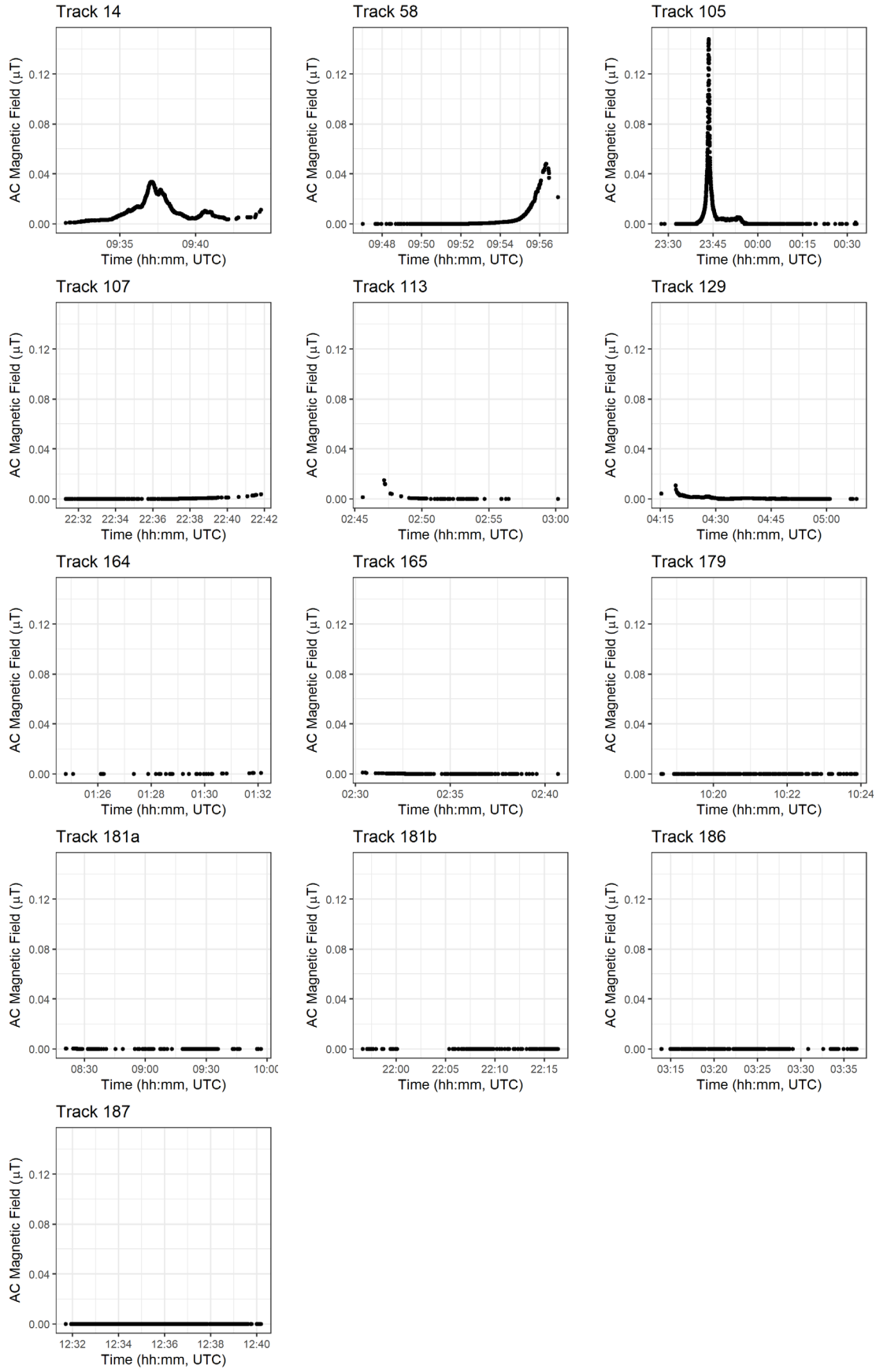

Figure 3.19. The AC magnetic field encountered by American eels in 2019. For each 3D eel position, the emitted AC magnetic field was modeled. The encountered absolute AC magnetic field anomaly is shown.

Key information Box 3.4

- Only eels detected in 2019 were used to determine the EMF encountered (in 3D)
- Eels passed through the VPS array when the HVDC cable was transferring between 0 and 229 MW
- Eels passing the HVDC cable encountered a range of DC and AC magnetic fields
- The operational characteristics at the time of passing and the proximity to the cable resulted in variable intensities of EMF being encountered
- The 'anomaly' in the magnetic field encountered is the difference relative to the background geomagnetic field
- In this study eels encountered a range of DC magnetic fields
    - a maximum positive anomaly of 86.9 nT
    - a maximum negative anomaly of 17.9 nT
- In this study eels encountered a range of AC magnetic fields
    - a maximum positive anomaly of 147.8 nT
    - a minimum anomaly of 0.8 nT

3.5.5. Behavioral Characterization and the Response to the HVDC Cable DC magnetic field (2019 only)

The three-dimensional positional data for eels in 2019, together with the encountered DC magnetic field (only) was used to characterize the eel behavior and the response to the HVDC cable DC magnetic field. Only the DC magnetic field was analyzed because the DC and AC field were highly correlated. The Hidden Markov Model used the observed regularized data to first characterize the three behavioral states based on the step length (i.e., distance moved in 5 s intervals) (**Section 3.5.5.1**), and derived transition probabilities (i.e., transition between behavioral states within a sub-track) enabling eels to be allocated to one of three groups based on behavioral dynamics within sub-tracks (**Section 3.5.5.2**). The response to the DC magnetic field was based on a change in step length at the behavioral state level and is reported in Section 3.5.3.3. The approach is summarized in **Figure 3.11**.

3.5.5.1. Behavioral States identified by the 3D Hidden Markov Model (2019)

The 2019 data used in the 3D HMM analysis comprised 2675 regularized locations split into 19 sub-tracks (from 12 eels and 13 tracks). The majority of eel tracks (ten) were retained as whole tracks, however, 3 eel tracks required splitting on the basis of the 60 s maximum interval, including 181a (five sub-tracks), 181b (two sub-tracks) and 186 (two sub-tracks).

The three behavioral states identified from the 3D HMM are shown in **Figure 3.20**. The behavioral states were based on the step length (i.e., distance moved, m, in a given time) which was regularized to 5 s intervals. Therefore, the three states can be considered small steps (state 1), intermediate steps (state 2) and large steps (state 3) relative to each other. The step length parameters are reported in **Table 3.6**

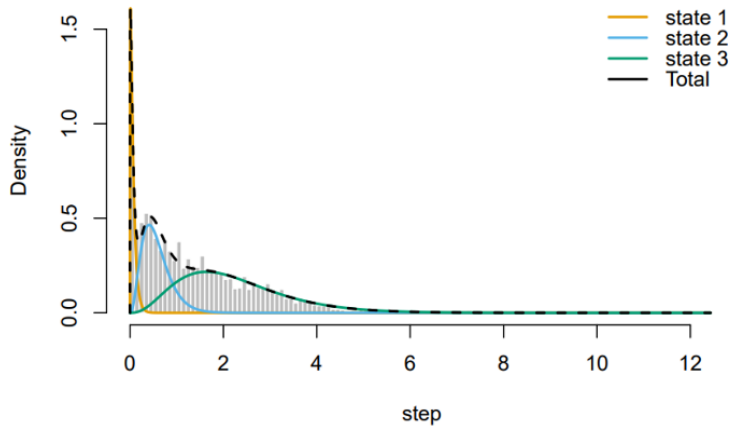

Figure 3.20. The 3D Hidden Markov Models (HMM) identified three behavioral states. The HMM (shows three behavioral states identified from 12 eels, 13 tracks and 19 sub-tracks from 2019.

Table 3.6. Behavioral state step length (m) parameters for the 3D Hidden Markov Model. The mean step length parameter is shown with the standard deviation (SD), the upper and lower confidence intervals (CI). Note that steps were regularized to 5 s intervals.

	3D HMM (2019)		
	State 1	**State 2**	**State 3**
Mean	0.07	0.57	2.26
SD	0.06	0.3	1.15
Upper CI	0.12	0.83	3.36
Lower CI	0.00	0.23	1.05

Key Information Box 3.5

- Three behavioral states were characterized from the Hidden Markov Model
- States are relative to each other and characterized specific to this study because they are based on the observed eel data from the VPS array
- Behavioral states were based on step length which was the distance moved in a 5 s interval
    - State 1 – small step length (mean = 0.07 m) indicative of low or no activity
    - State 2 – medium step length (mean = 0.57 m) indicative of medium activity
    - State 3 – larger step length (mean = 2.26 m) indicative of higher activity

3.5.3.2. Transition probabilities and Groups identified by the 3D Hidden Markov Model (2019)

The likelihood of transition between behavioral states within a sub-track was calculated as the transition probability. Based on the observed sub-track data, the behavioral states identified and the resulting transition probabilities, the eel tracks were assigned to one of three groups. The groups are described and then the transition probabilities are explained. The eel tracks are then presented according to their allocated groups and presented as 2D movements in relation to the VPS array and vertical profiles in the water column.

Of the 19 sub-tracks, seven were categorized as group 1, seven were categorized as group 2 and only two sub-tracks from the same eel were categorized as group 3 (**Table 3.7**). The remaining two tracks were uncertain and could have been considered group 1 or 2 (ID 181 and 186). Eel 181 on its first visit to the VPS area exhibited all three groups and was the only eel to exhibit group 3 behavior. The same eel returned to the VPS array almost 12 hours later and only exhibited group 2 behavior.

Table 3.7. Eel sub-tracks were assigned to groups based on their behavioral states.

Eel Track	Sub-track	Group
14		1
58		1
105		2
107		1
113		2
129		2
164		2
165		1
179		1
181a	1	1 or 2
	2	2
	3	1
	4	3
	5	3
181b	1	2
	2	2
186	1	2
	2	1 or 2
187		1

An eel in group 1, which was in state 2 for step S_t, had an 87% probability that step S_{t+1} would remain in state 2 and a 13% probability that step S_{t+1} would change to state 3 (**Table 3.8**). Similarly, a group 1 eel in state 3 had a 99% probability of staying in state 3. For this reason, group 1 eels were regarded as the fastest moving eels relative to group 2 and 3 because they had the greatest probability of staying in state 3, which had the greatest step length indicating a faster speed of movement. Group 2 eels had an 83% probability of staying in state 1, an 80% probability of staying in state 2 and an 86% probability of staying in state 3. Group 3 was the slowest moving group and had the greatest probability of staying in state 1, the slowest speed. Group 3 eels had a 90% probability of staying in state 3 and a 59% probability of staying in state 2.

Table 3.8. Transition probability matrices for the 3D Hidden Markov Model. The probability of moving from one state to the next was estimated from the HMM. Note that moving from state 1 to 3 or the reverse, must go through the intermediate state 2.

	Group 1			**Group 2**			**Group 3**		
	State 1	State 2	State 3	State 1	State 2	State 3	State 1	State 2	State 3
State 1	1.00*	0.00	0.00	0.83	0.17	0.00	0.95	0.05	0.00
State 2	0.00	0.87	0.13	0.03	0.80	0.18	0.41	0.59	0.00
State 3	0.00	0.01	0.99	0.00	0.14	0.86	0.00	0.10	0.90

* Group 1 state 1 to state 1 was based on one sub-track and should be interpreted with caution.

Key Information Box 3.6

- The Hidden Markov Model provided transition probabilities which are indicative of the probability of moving from one behavioral state to another in the course of one step to the next
- The transition probabilities accommodated the eels being grouped according to their behavioral dynamics based on the observed eel track data from the VPS array
- There were three groups identified
- Group 1 eels
    - Very high probability of staying in same state for both state 3 (high step length) and state 2 (medium step length)
    - 13% probability of transitioning from state 2 to 3 (medium -> high step length)
- Group 2 eels
    - Very high probability of staying in same state for all states 14-18% probability of transitioning from between state 2 to 3 (medium -> high step length) or from state 3 to 2
- Group 3 eels
    - Very high probability of staying in state 1 or 3 and likely to transition to state 1 or 3 if in state 2
- Group 1 and 2 eels were the fastest moving eels
- Group 3 eels were the least active eels

Visualization of HMM outputs on the eel track data

The HMM determined the behavioral states and transition probabilities based on the observed regularized data. The behavioral states of the eels can be visualized within the eel track data by color-coding each step as state 1, 2 and 3. This allows the behavioral dynamics (i.e., transition between states) to be visualized in the observed regularized track data.

To present the horizontal and vertical position of eels recorded within the water column (i.e., the dive profile) in relation to the behavioral state, the eel tracks (including sub-tracks) are shown in panels per eel, according to their assigned group (refer to **Table 3.7**). Eels 181a and 186 were considered mixed group eel tracks because the grouping for their sub-tracks varied (**Table 3.7**).

The horizontal movements for group 1 eel tracks are shown in **Figure 3.21** and group 2 and mixed group eel tracks are shown in **Figure 3.22**. From the horizontal movements shown in 2D with the VPS array as a visual reference, state 2 and 3 were dominant for all tracks and state 1 was barely visible. However, on reviewing the vertical movements against track time, states 1, 2 and 3 were more apparent (**Figure 3.21** and **3.22**). This demonstrates the low activity (i.e., small step lengths) associated with state 1 and greater movement (i.e., larger step lengths) associated with states 2 and 3.

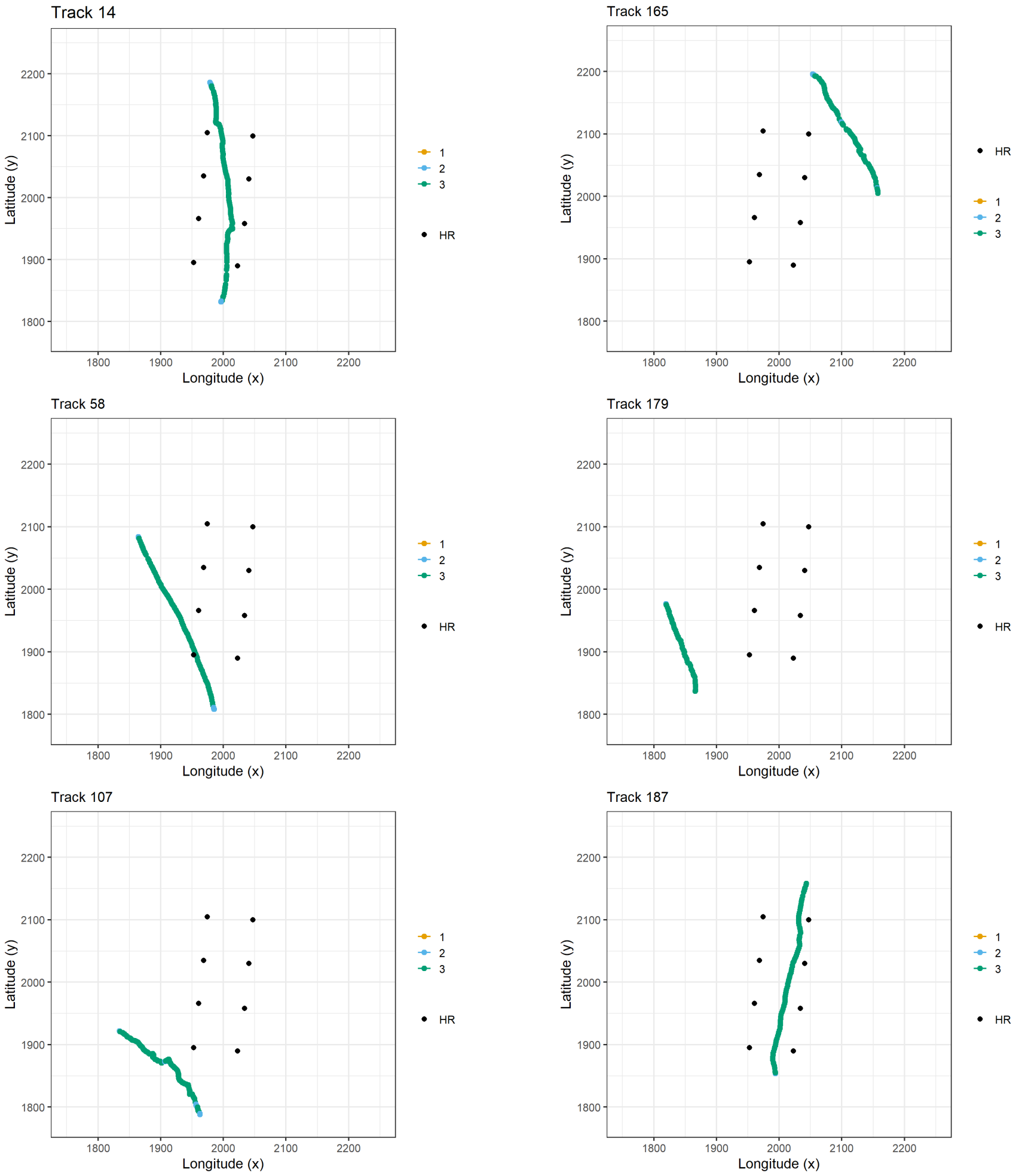

Figure 3.21. The horizontal movements of 2019 group 1 eel tracks and behavioral states as determined by the 3D Hidden Markov Model. The eel tracks shown were categorized as group 1 according to the transition probabilities (**Table 3.7, 3.8**). The high residency receivers (HR) are indicated as a spatial reference.

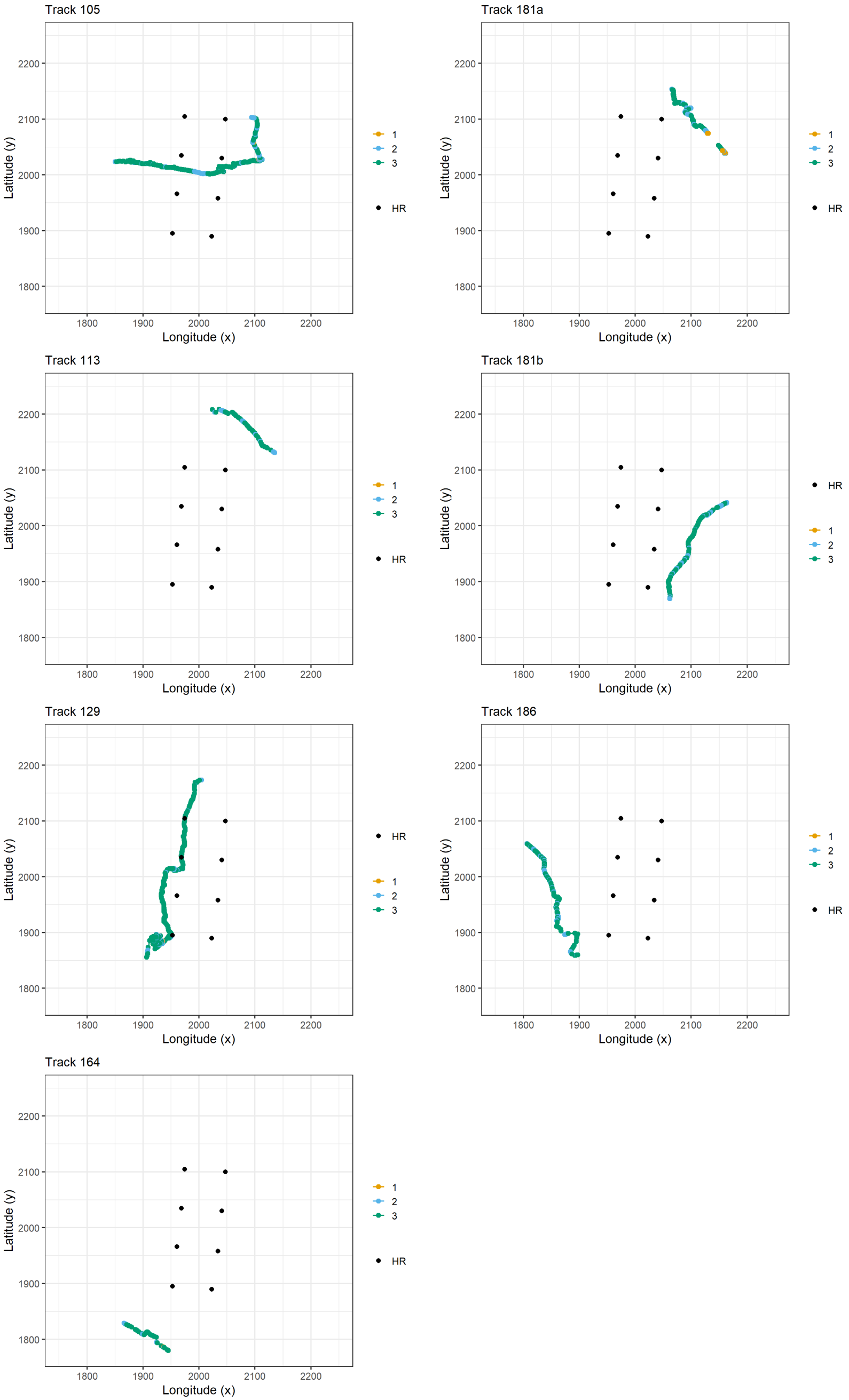

Figure 3.22. The horizontal movements of the 2019 group 2 or mixed group eel tracks and behavioral states as determined by the 3D Hidden Markov Model. The eel tracks shown were categorized predominantly as group 2 according to the transition probabilities (**Table 3.7, 3.8**). The first sub-track of Track 181a was uncertain (either group 1 or 2), followed by 2, 1, 3 and 3. The sub-tracks of Track 181b were both group 2 and the sub-tracks of Track 186 was categorized as group 2, but the second sub-track was uncertain (1 or 2). The high residency receivers (HR) are indicated as a spatial reference.

The vertical movements that were tracked are shown (**Figure 3.23 and 3.24**) on a standardized scale, which allows the eel movements to be compared without the influence of tidal state or whether inside or outside of the shipping channel. As suggested in the transition probabilities (**Table 3.7**), the greater intermittency between state 1, 2, and 3 is visible in group 2 and mixed tracks **Figure 3.23** relative to group 1 tracks in **Figure 3.24** which have an overall greater dominance of state 3. The vertical movements of the eels, in the shallow coastal transitionary waters of New Haven Harbor, can also be observed from **Figure 3.23** and **3.24**. Seven tracks of the 13 showed a predominance of surface swimming (Tracks 58, 165, 179, 187, 107, 113, 164). Track 14 shows an eel swimming in midwater and 181a (sub-track 1 and 2) and 181b could also be classed as surface to mid-water swimming. Comparing the horizontal and vertical tracks with knowledge of the bathymetry (refer to **Figure 3.7** for chart MLLW depths), three eels exhibit bottom associated swimming, including Track 105, 129 and 181a. Seven eels exhibit dives that include V-shaped dives from the surface to variable maximum dive depths, but also dives from midwater starting points as well as dives followed by bottom swimming.

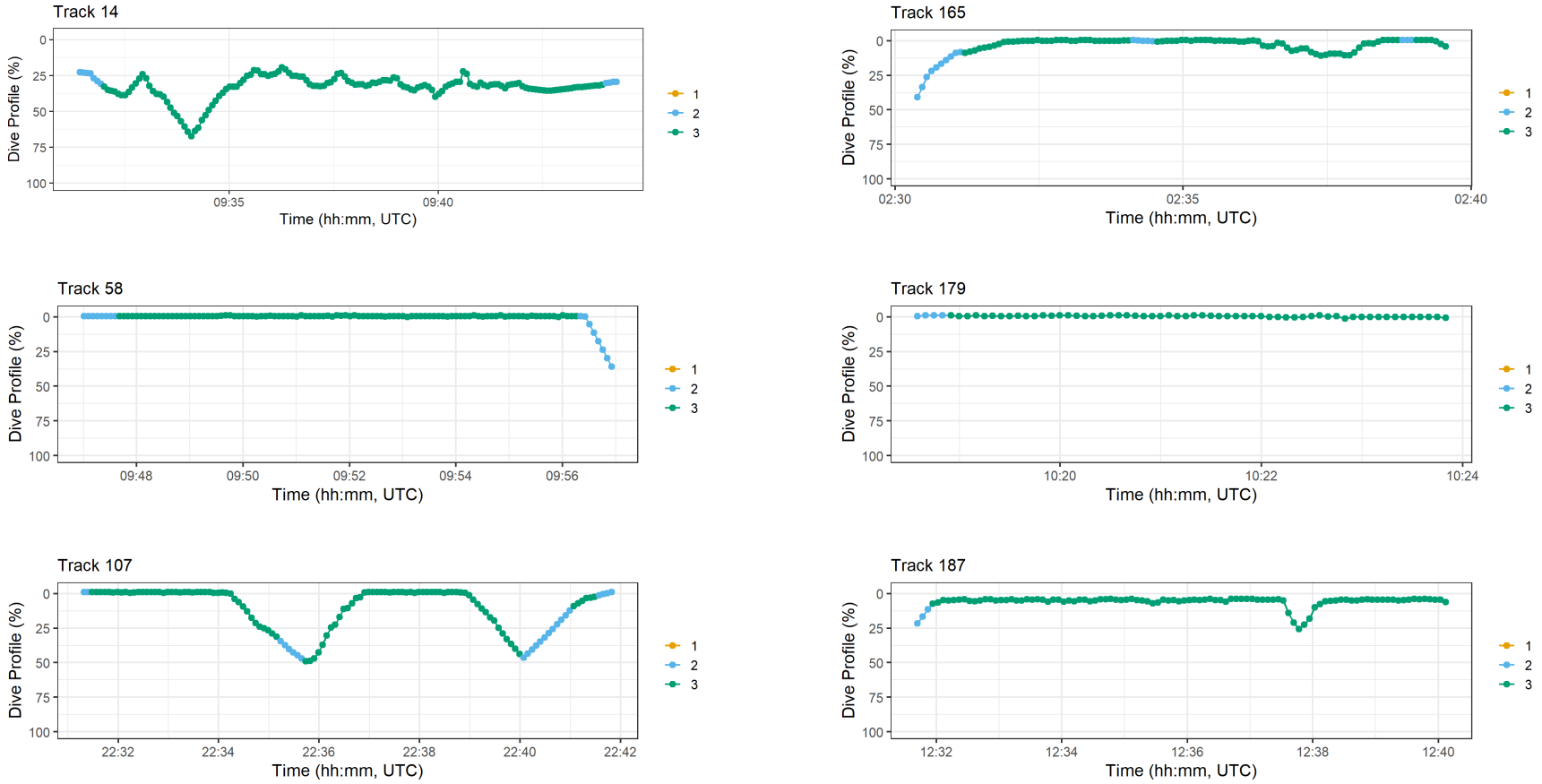

Figure 3.23. The dive profiles of the 2019 eel tracks and behavioral states as determined by the 3D Hidden Markov Model. The eel tracks shown were categorized as group 1 according to the transition probabilities (**Table 3.6, 3.7**). The dive profile is shown on a standardized scale allowing comparability irrespective of the tidal state, to a reference depth (12.9 m) in the shipping channel.

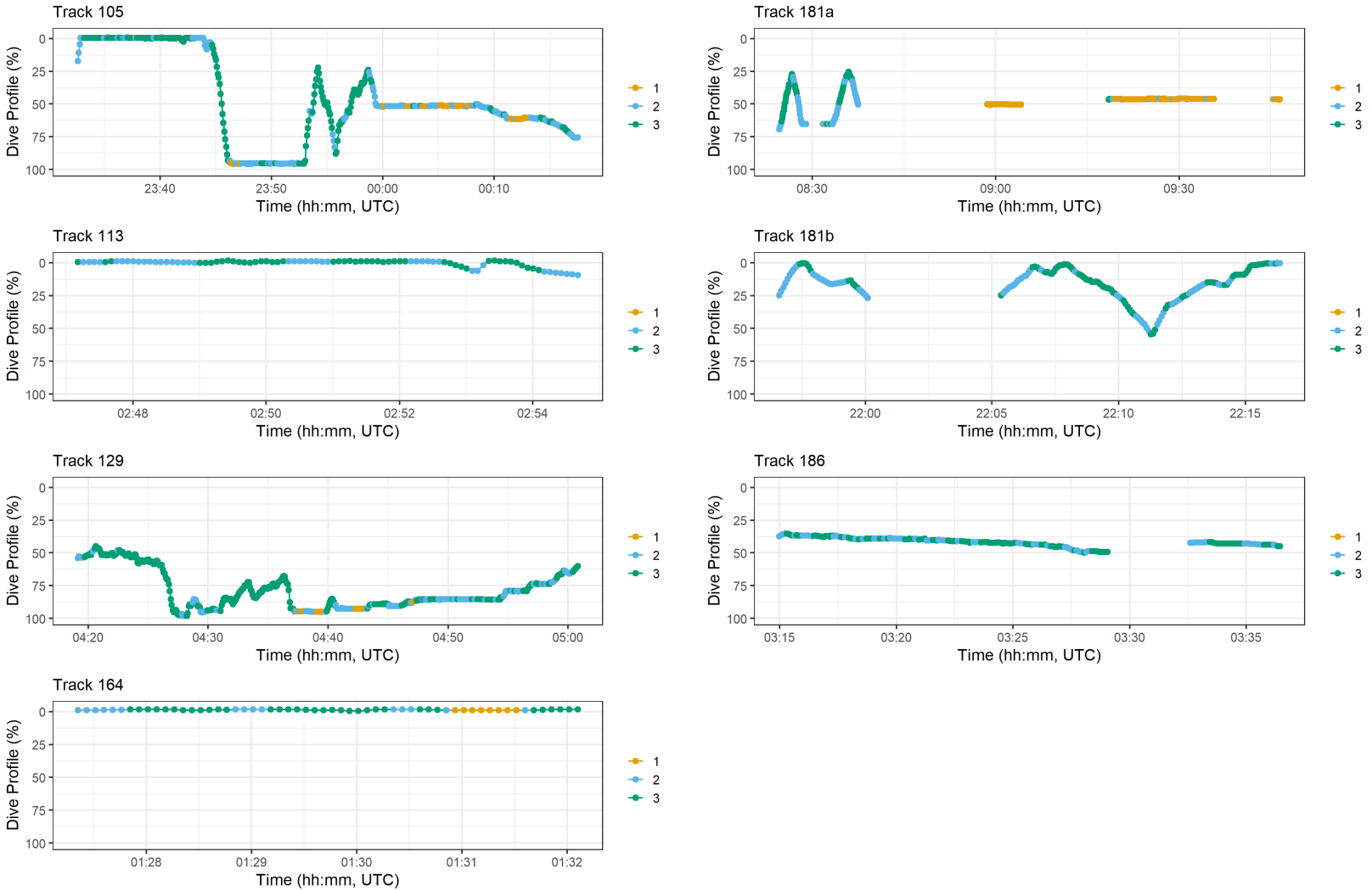

Figure 3.24. The dive profiles of the 2019 eel tracks and behavioral states as determined by the 3D Hidden Markov Model. The eel tracks shown were categorized predominantly as group 2 according to the transition probabilities (**Table 3.6, 3.7**). The first sub-track of Track 181a was uncertain (either Group 1 or 2), followed by 2, 1, 3 and 3. The sub-tracks of Track 181b were both group 2 and the sub-tracks of Track 186 was categorized as group 2, but the second sub-track was uncertain (1 or 2). The dive profile is shown on a standardized scale allowing comparability irrespective of the tidal state, to a reference depth (12.9 m) in the shipping channel.

3.5.3.4. The response to the encountered DC magnetic field anomaly (2019)

The Hidden Markov Model (HMM) characterized the movement behavior of the eels and assessed the response to the encountered DC magnetic field from the HVDC cable (see **Section 3.5.4** for details on encountered EMFs). The response of the eels to the DC magnetic field was assessed in terms of the behavioral state (refer to **Figure 3.11** for an overview). That means the HMM derived changes in the step length parameter in response to the range of DC magnetic fields encountered by the eels. As a free-ranging tracking study was employed, it was not possible to compare between exposed and not-exposed eels (e.g., in the scenario of a control and treatment comparison), however, an assessment across the gradient of exposure intensities for the eels encountering the DC magnetic field as they migrated through the VPS array in the vicinity of the HVDC cable was able to be undertaken.

The 3D HMM included a linear effect of the DC magnetic field encountered by the eels on the parameters of the step length distributions (mean and standard deviation). This model was based on the movements of the 12 eels (captured in 13 tracks and 19 sub-tracks), which experienced a DC magnetic field anomaly ranging from -17.9 nT to 86.9 nT (**Table 3.5**). Within those eel tracks the 3D HMM identified an increase in the step mean parameter with increasing positive DC magnetic field anomaly within state 2 (intermediate step length) and state 3 (large step length) (**Figure 3.25)**. The DC magnetic field anomaly from the CSC was not encountered by many of the eels while in state 1 and therefore the effect could not be modeled. In state 2, the mean step length parameter at 0 nT was estimated as 0.57 m, however, at 80 nT, the step length increases to 1.4 m, which is almost three times the distance (**Figure 3.25**, left). In state 3, the mean step parameter at 0 nT was estimated as 2.26 m, and at 80 nT it was estimated to be 4.1 m, which is nearly a two-fold increase in step distance (**Figure 3.25**, right). In addition to an increase in the mean step parameter in state 3, the step standard deviation decreased with increasing positive magnetic field anomaly encountered (**Figure 3.26**). These data indicate that the mean step length increased, and the step lengths became less variable and more consistent when the eels encountered greater DC magnetic fields in state 3 (**Figure 3.25, 3.26**). The same relationship in step length variability was not observed for state 2 and the very broad confidence intervals indicated the relationship was not well defined (not shown).

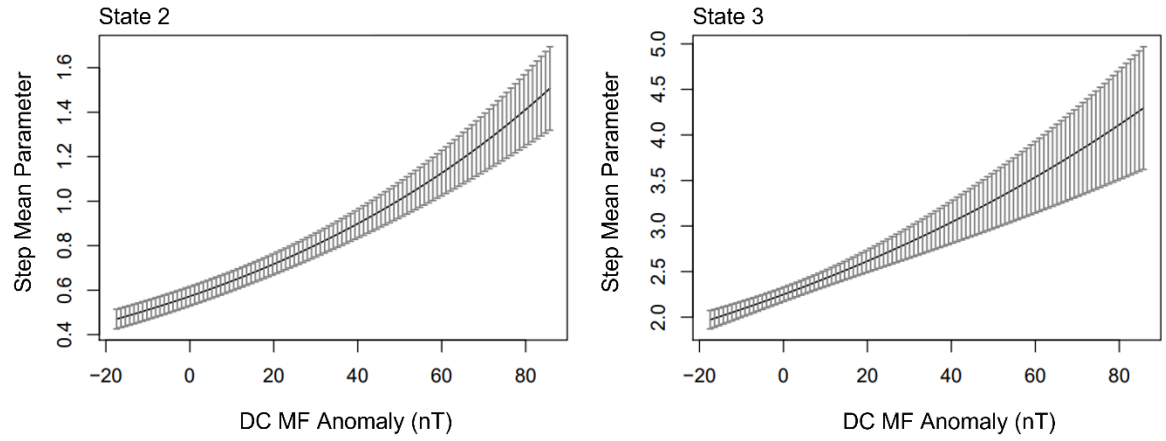

Figure 3.25. The effect of the DC magnetic field anomaly encountered on the step mean parameter within behavioral states in American eels. The 3D HMM based on 2019 eel data, identifies the effect of the DC magnetic field anomaly encountered within behavioral state 2 (left) and state 3 (right). An increase in the mean step parameter is observed for both state 2 and state 3 (with confidence intervals). This analysis is based on the movement and encountered DC magnetic field of 12 eels (captured in 13 tracks and 19 sub-tracks).

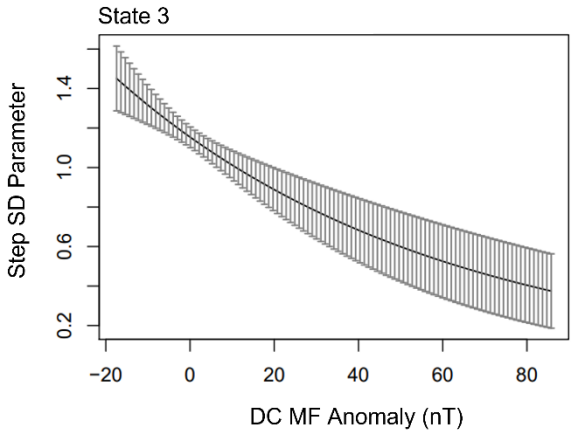

Figure 3.26. The effect of the DC magnetic field anomaly encountered on the step standard deviation parameter within behavioral states in American eels. The 3D HMM based on 2019 eel data, identifies the effect of the DC magnetic field anomaly encountered within behavioral states. A decrease in the step standard deviation (SD) parameter was observed for state 3 (with confidence intervals). This analysis is based on the movement and encountered DC magnetic field of 12 eels (captured in 13 tracks and 19 sub-tracks).

Key information Box 3.7

- A response to the DC magnetic field was assessed by the Hidden Markov Model (HMM) at the level of the behavioral state and was based on the observed regularized track data and encountered DC magnetic fields
- The behavioral states were based on the step length, that is, the distance moved in a 5 s interval and states 1, 2 and 3, corresponded to small, medium and large step lengths
- A change in the step mean parameter and the step standard deviation parameter were observed in response to the DC magnetic fields encountered by eels
- The findings are specific to the range of DC magnetic field encountered by eels (-17.9 to 86.9 nT) in this study
- In state 2, the mean step length became longer in response to greater DC magnetic field anomalies
- In state 3, the mean step length became longer and less variable (i.e., more similar) in response to the greater DC magnetic field anomalies
- The response to the DC magnetic field as derived from the HMM is detailed within behavioral states and not the transition probabilities between states

Visualization of HMM outputs on the eel track data

The effects described above can be observed in the step length and encountered DC magnetic field anomaly data in both group 1 and group 2 and mixed group eels (**Figure 3.27** and **3.28**). In track 14, the eel swam through the VPS array in a north to south direction, diving early in the track but maintaining a mid-water position. The track of eel 14 exhibits two peaks in the encountered DC MF anomaly indicating that the eel crossed the path of the HVDC CSC and then turned back toward it (**Figure 3.27**), which is verified by the horizontal movements in **Figure 3.23**. The increased mean step length and the reduced step length variability in state 3 is observed during the increased DC MF exposure (**Figure 3.27**). It is noteworthy that the peak DC MF encounter was when swimming in mid-water, not during the dive (**Figure 3.24**). Track 58 also demonstrates well, the increased mean and reduced variability in step length at the onset of DC MF exposure toward the end of the track,

and a switch from state 3 into state 2 (**Figure 3.27**). Eel 58 started to dive, during the peak encounter (**Figure 3.23**). Within group 1, the four other eels encountered very low negative anomalies or levels close to background levels and a response to the magnetic field was not observable.

Within group 2 and mixed group eels, Track 105 and 113 encountered the strongest DC magnetic field anomaly, while the others experience either low negative deviations, or close to background values (**Figure 3.28**). Track 105, similar to track 58, switched from state 3 to state 2 during the peak DC MF encounter, however, as the DC magnetic field anomaly reduced it then switched back to state 3. The peak encounter in DC magnetic field was while the eel was still surface swimming, after which it dived down to the seabed (**Figure 3.24**), and the eel then encountered a period of negative deviation in the DC magnetic field (**Figure 3.28**). Track 113 experienced the DC magnetic field at the beginning of the track and also exhibited both state 2 and 3 during that time (**Figure 3.28**). Note that group 2 and 3 eels were characterized by a greater probability of transition between states.

Key information Box 3.8

- The proximity to the cable and the operational characteristics of the cable determined the exposure to the EMF and therefore the encountered EMF (see Section 3.5.4)
    - Whilst it is generally assumed that the closer the eel is to the HVDC cable, the stronger the EMF the eel will encounter this is based on a constant power level and therefore EMF level
- In reality, the proximity of an eel to the cable and the variable operational characteristics of the power transmission must be accounted for, together.
    - This means that an eel passing the cable in midwater while the cable operates at high power level may encounter a stronger magnetic field anomaly than an eel passing a cable swimming close to the seabed when the power level is low
- The DC magnetic field anomalies in this study were both negative and positive deviations from the geomagnetic field
- The response observed (change in step length parameters) was observed to be greater with the greater positive anomalies however the negative anomalies were not as strong; it is important that the observed result is interpreted within context of the range of DC magnetic field encountered (-17.9 to 86.9 nT)

Figure 3.27. The step length and encountered DC magnetic field for the 2019 eel tracks, and behavioral states as determined by the 3D Hidden Markov Model. The eel tracks shown were categorized as group 1 according to the transition probabilities (**Table 3.6, 3.7**). Step length is the distance moved between two positions at a regularized 5 s interval. The encountered DC magnetic field anomaly was calculated based on the 3D proximity to the HVDC cable, the power level at the specific time and the cable properties at that location. The data were also regularized to the 5 s time interval.

Figure 3.28. The step length and encountered DC magnetic field for the 2019 eel tracks, and behavioral states as determined by the 3D Hidden Markov Model. The eel tracks shown were categorized predominantly as group 2 according to the transition probabilities (**Table 3.6, 3.7**). The first sub-track of Track 181a was uncertain (either group 1 or 2), followed by 2, 1, 3 and 3. The sub-tracks of Track 181b were both group 2 and the sub-tracks of Track 186 was categorized as group 2, but the second sub-track was uncertain (1 or 2). Step length is the distance moved between two positions at a regularized 5 s interval. The encountered DC magnetic field anomaly was calculated based on the 3D proximity to the HVDC cable, the power level at the specific time and the cable properties at that location. The data were also regularized to the 5 s time interval.

3.6. Discussion

The use of magnetic cues during their long-distance migration has raised concerns that cable electromagnetic fields (EMFs) may present another pressure to the American eel, *Anguilla rostrata* (Westerberg and Begout-Anras, 2000; Ohman et al., 2007; Westerberg and Lagenfelt, 2008; Jacoby et al., 2015, 2017). This topic has become particularly important due to the upcoming expansion of offshore wind energy along the north-east American coastal and offshore waters and the anticipated proliferation of subsea cables (Hutchison et al., 2020a; BOEM, 2021).

The primary goal of this study was to determine the behavioral response of migratory American eels to the EMF environment created by a high voltage direct current (HVDC) subsea power cable, the Cross Sound Cable (CSC). It is anticipated that eels may encounter the EMF from export cables in coastal transitionary waters. The focus was on HVDC cables since they are more likely to be used as export cables as offshore wind developments increase in capacity and move further offshore. Presently HVDC cables associated with leased OWFs in the USA are rare (e.g., Sunrise Wind, NY) and high voltage alternating current (HVAC) cables are more commonly used because the lower capacity cable is sufficient and shorter cable routes have been planned. Inter-array cables between turbines, are and will likely continue to be lower capacity HVAC cables. The use of HVDC is generally considered optimal to facilitate higher capacity energy transmission over greater distances to onshore grids, comparative to HVAC technology (Soares-Ramos et al., 2020). In general, at maximum operating capacities, HVDC cables will generate greater intensity EMFs than lower capacity HVAC cables. This study focused on an HVDC transmission cable called the Cross Sound Cable, which has similar characteristics to those that are anticipated to be used in future OWF developments.

Prior efforts to assess anguillid eel (European eel, *Anguilla anguilla*) migratory movements and responses to HVDC or HVAC cable EMFs lacked sufficient resolution to reveal interactions *in situ* (Westerberg and Begout-Anras, 2000; Westerberg and Lagenfelt, 2008; Orpwood et al., 2015). Laboratory studies had been completed using Helmholtz coils, which produce magnetic fields but not in a form clearly comparable with the magnetic field component of cable EMFs, and were hampered by inactivity of eels (Westerberg and Begout-Anras, 2000; Westerberg and Lagenfelt, 2008; Orpwood et al., 2015). However, the American eel has never been studied in a similar free-swimming or laboratory context to assess responses to cable EMFs and a free-swimming context offers the best approach to assess changes in migratory behavior. Therefore, we adopted a high-resolution acoustic telemetry approach (VPS, using HR receivers) to observe movements of silver American eels in the vicinity of the HVDC cable, coupled with a presence/absence acoustic array (using VR2W receivers) to provide a total number of tagged eel migrants. To capture potential eel interactions with the HVDC cable EMF, the acoustic array was implemented at the narrowest stretch of the harbor where eels may encounter the HVDC cable EMF on their outward migration to sea. The tagged eels, were released approximately 6.2 km (3.9 miles) upstream of the array in West River, allowing natural behavior to have resumed by the time they reached the acoustic array.

The VPS array located around the subsea buried HVDC cable, enabled the recording of free-ranging tagged eel movements at a fine-scale, high-resolution never previously recorded. The eel movement data were obtained *in situ* in two dimensions (2D) in 2018 and in three dimensions (3D) in 2019. By integrating the EMF modeling reported in **Section 2** with the 3D positioning of the eels, the EMF

environment for each position was determined, providing first evidence of the encountered EMF (DC and AC) throughout the eels tracked movements. Subsequently, the analysis focused on the eel behavioral response to the encountered EMF (DC).

The major finding of this study is that eels did respond to the HVDC Cross Sound Cable EMF. Through the approach taken, information was gained on the movements of American eels in coastal transitionary waters (**Section 3.6.1**) as well as an assessment of the potential for interaction with cable EMFs based on 2D spatial proximity (**Section 3.6.2**). The encountered EMFs (AC and DC) were derived based on 3D proximity to the buried cable and the specific operational characteristics of the cable at the time the eels migrated (**Section 3.6.3**). An analysis of the behavioral response to the encountered DC magnetic field revealed that eels respond to the cable EMFs (**Section 3.6.4**). A brief discussion of the findings in the context of cables associated with offshore wind developments is provided (**Section 3.6.5**).

3.6.1. American Eel Movements in Coastal Transitionary Waters

The seasonal migration of American eels was estimated, from historical knowledge, to occur between late September and December. Eels were collected from the Poquonnock River system (Groton, CT), held only briefly for tagging purposes, and released in West River (New Haven, CT), north of the acoustic array. This approach represented a small translocation and was expected to have had a minimal influence on the eels' behavior. The release site was selected because it was on a similar longitude to the collection point with similar freshwater flow characteristics.

Of 100 eels released in 2018, 25 eels were confirmed to have migrated downstream. In 2019, more tagged eels were released, however, a lower proportion of eels were detected; a total of 31 eels of 200 released were confirmed to have migrated downstream. This data shows that a large proportion of eels released did not migrate during the acoustic array deployment. There was sufficient acoustic coverage (**Figure 3.6**) that eels would have been detected if they migrated during the full deployment in all but exceptionally shallow water. It is possible that some eels were predated, tags were compromised, the eels migrated later after the study ended or that eels changed behavioral mode to non-migrants. The physical appearance of eels on collection, the body coloration and large eyes combined with the fact that they were captured during a downstream migration was strongly suggestive that the eels were mature silver eels on their outward migration to sea (Pankhurst, 1982; Durif et al., 2009). Eels are, however, facultative catadromous fish meaning that they may reside in and transition between freshwater, estuarine and/or marine environments (Lamson et al., 2006; Marohn et al., 2013). Hain (1975), indicated that eels also undergo practice migratory transitions including physiological adaptations, prior to undertaking the full migration to breeding grounds in the Sargasso Sea. Maturation is considered to be a plastic response to environment and opportunity (Svedäng and Wickström, 1997), and regression of some eels cannot be dismissed. However, the data presented were capped to the period for which all receivers were deployed, and detections beyond this time period, confirm that the eel migration was ongoing as the array was recovered. Therefore, a proportion of eels migrated later in December and is the most likely explanation for the proportion not detected.

The movements captured from 56 migratory American eels over two years (2018 and 2019), provide important information on eel behaviors as they transition from a freshwater to coastal marine water environment on their outward migrations (**Section 3.5.2** and **3.5.3**). Eels predominantly exhibit nocturnal behaviors although it is not unusual to have daytime activity (Parker and McCleave, 1997;

Tesch, 2003; Béguer-Pon et al., 2014). Westerberg et al., (2007) tracked European eel movements over a period of days and reported a strict diurnal pattern in activity, where eels became active during crepuscular (twilight) periods with greatest activity through the night, and periods of resting on the seabed during the day. As expected, eels in this study were predominantly detected during the hours of darkness, with few eels detected during daylight hours. Similarly, it has been documented that eel migrations are often aligned with the tidal state, stimulated to move by the flow of water and/or taking advantage of the ebbing tide during estuarine escapement (Béguer-Pon et al., 2014; Verhelst et al., 2018). Eels in this study were predominantly detected during an ebbing tide, with some eels detected during slack tides. There were a few eels which were detected throughout the day and through more variable tidal states, however, these eels were detected by the same receivers and did not move far suggesting that they were in a resting or low-activity behavioral mode. American silver eels migrating downstream are known to have intermittent movements with high individual variability in the distances moved within a migration (Béguer-Pon et al., 2014). Westerberg et al., (2007) also reported some migratory European eels which remained on the bottom for several days before resuming migration.

The greatest number of eels were detected in the center of the transect array (VR2W and VPS), however, all stations within the VR2W array detected eels indicating that eels made full use of the harbor area. If the eels had taken the shortest trajectory of passage to the sea, then there would have been a greater number of eels detected on the west side of the array and a predominant skew in the VR2W data (**Figure 3.13**). Instead, and as anticipated, the passage of eels aligned with the greatest anticipated water flow in the central area of the harbor. However, it is notable that the eels did move from west to east, and east to west, across the harbor area indicating a degree of exploration, also supported by the number of return visits to the array area (VR2W and VPS). The VPS data, showed an overall dominance of eels moving in a southerly direction (**Figure 3.16**), as expected for outward migrating eels making their way to sea. The fine-resolution tracks obtained from the VPS array were relatively short, typically around 20 minutes but variable with time periods ranging from just over one minute to nearly 6 hours (**Table 3.3, 3.4**).

The 3D data obtained for eels in 2019 provided an indication of the vertical movements in coastal waters in addition to their horizontal movements, which was previously lacking. Both vertical and horizontal movements are of great importance in defining how eels may interact with cable EMFs. Yellow eels are considered a benthic life-stage and silver eels in the upper reaches of rivers, migrating downstream, have been tracked exhibiting a predominantly benthic mode of movement with some vertical exploration where obstructions exist (Brown and Castro-Santos, 2009; Haro et al., 2016). However, the movements of silver eels in rivers are not necessarily good predictors of vertical movements in coastal transitionary waters. Recent studies of American silver eels provide evidence of movements including vertical dive profiles for eels moving from the coast to the edge of the Scotian shelf, however the focus was on the diel vertical migrations (up to 700 m) in deep water and only a vague description of erratic dives in shallow waters was provided (Béguer-Pon et al., 2015). Similarly, European eels have been recorded diving to depths between 100 and 400 m or more, in continental waters (bathymetry of 200 to 2500 m) (Tesch, 1978b). More comparable to this study, is the work of Westerberg et al., (2007) who recorded the vertical movements of European eels in bathymetry up to 36 m. Sporadic diving in predominantly surface swimming eels was reported, with eels spending up to >55% of their active time surface swimming (i.e., within 1 m of the surface) but exhibiting dives to variable depths for periods of time proportional to the maximum depth of the dive. The authors

considered a 'deep' exploratory dive to be >4 m. Sporadic dives were observed for all eels, and they were reported to dive between 10 and 25 times per night. The reason for diving is not well defined, however, it was not considered an energy saving mechanism since eels actively swim up and down on a dive with similar ascent and descent rates and it is more likely a way to determine depth (Westerberg et al., 2007 and references therein). Similar to the European eels in coastal waters, the American eels in our study (2019) demonstrated a predominance of surface-swimming activity with intermittent dives. Given they were captured by a benthic air lift, this mode of surface-swimming must become onset during physiological changes in response to environmental cues of transitional waters (e.g., bathymetry, salinity). The dives undertaken were typically from the surface, but eels recorded swimming mid-water also undertook dives to deeper depths (**Figure 3.23, 3.24**). Dives were predominantly V-shaped, however, there was also evidence of diving with bottom swimming prior to ascent, and midwater fluctuations, which may be evidence of different behavioral modes. Silver eels are not expected to be feeding during migratory phases (Tesch, 2003), therefore, bottom swimming was interpreted as exploratory behavior.

Key information Box 3.9

- Tagged silver American eels migrated from West River through New Haven Harbor to sea and passed through the acoustic arrays (high residency VPS and VR2W)
- Eels were predominantly detected at night and during an ebbing or slack tide
- Eels explored the full harbor area and there was evidence of brief periods of residency
- Eels demonstrated directed N-S movement as expected during purposeful migratory movement aligning with the channel area (VPS array)
- Fine-scale movements were captured in 3D (VPS array) and revealed that in coastal waters, eels made full use of the water column
    - There was a predominance of surface swimming with evidence of mid-water and bottom swimming with diving activity

3.6.2. Potential for Interaction with the HVDC Cross Sound Cable EMF

Of 56 eels detected by the acoustic array (VPS and VR2W), 31 were detected by the VPS array in the vicinity of the cable. These data mean approximately 55% of migratory eels in this study had the potential to interact with the HVDC cable EMF (DC or AC) based on their horizontal proximity to the buried HVDC cable within the small study area. The cable area monitored by the VPS array was approximately 400 m, which is 1% of the total HVDC CSC length (40 km, Cross Sound Cable Company, 2020). Assuming that migratory eels exit the harbor area and take the most direct route, transiting east in Long Island Sound into the New York/New Jersey Bight, the eels may encounter approximately 13-20 km of the cable across a range of bathymetry.

In the VPS array, the median track time recorded was 20 minutes (**Table 3.3, 3.4**). Given the water flow characteristics, it is likely that the eels detected by the VPS array retained an approximately central swimming position, particularly the group 1 eels, which showed purposeful transit (**Figure 3.16, Figure 3.21, Section 3.6.4**), meaning they would have likely spent more time in the vicinity of the cable as they

continued their migration through the harbor area. There was also a high likelihood, that eels not detected by the VPS array, would have crossed the cable path later in their transit through the harbor, suggesting that 55% was a low estimate of the potential to encounter the HVDC cable EMF in transitional waters, in this study.

Two-dimensional horizontal proximity to a cable route is not sufficient to derive if a fish or other marine species encounters the cable EMF, however, it provides an estimation of the *potential* to encounter the cable EMF. To determine the EMF encountered, the spatial proximity to the cable must be assessed in three-dimensions in order to account for the animal movement relative to the cable and this must be considered with the specific cable characteristics. As highlighted in **Figure 3.3**, the EMF of a cable will vary along its route owing to the cable characteristics (e.g., burial depth, twist) and also the power level at the time of the encounter (Hutchison et al., 2020b, 2020a, 2021). Here, we consider the characteristics of the HVDC cable and then the movement ecology of the eels.

The surveys conducted on the HVDC CSC to characterize the EMF (DC and AC) indicated that even within the short cable length studied, the twist of the cable varied between 0.53 and 1.1 radians and the burial depth, as derived from the EMF measurements, varied between 1.8 and 3.7 m (**Section 2**). The CSC power level is known to vary between 0 MW (16 A, maintenance current) and 330 MW (1175 A) (Hutchison et al., 2020b), based on the domestic demand of the New England and Long Island power grids. Typically, the power level is at its maximum over the summer period, and the power then becomes more variable in fall and winter as demonstrated in **Figure 3.12** (**Section 3.5.1**). The variability in power also prevented the use of the eel data collected in 2018 since the power level was at 0 MW and no associated trends would have been evident. In 2019, the power level was more typical of previous years (**Section 3.5.1**) and was variable when the eels migrated past the HVDC cables (**Section 3.5.4**). For context, using the mean burial depth (2.7 m) and cable twist (0.8 radians) for the HVDC CSC as measured for the eel study area, the DC magnetic field was calculated at the level of the seabed (i.e., 2.7 m distance) and at 10 m distance from the buried cable, under two different operating scenarios. At a power level of 0 MW with only 16 A maintenance current, the DC magnetic field would be 44 nT at the seabed and 3nT at 10 m from the buried cable. At 330 MW (1175 A), the DC magnetic field would be 3200nT at the level of the seabed and 230nT at 10 m distance from the buried cable. However, note that an AC magnetic and AC electric field were also measured from the CSC and had a greater spatial expanse (**Section 2**, **Figure 2.3**).

Another aspect which influences the encountered EMF in the water column is the movement ecology of the animal which, together with the burial depth of the cable, defines the true proximity from the cable (Hutchison et al., 2021). As demonstrated in this study of eels, but also for other migratory species, this movement includes seasonal as well as local and short-term movements within the water column. While 2D animal movements are typical in telemetry studies, monitoring 3D animal movements are rarer but are absolutely necessary in order to derive the encountered EMF by modeling (**Section 2.2.3**), because the EMF cannot be measured in real-time by tags. The 3D data obtained from the acoustic array employed in this study had an error sensitivity of 0.09 m and the accuracy and precision in depth was in the order of 0.10 m based on the control measures employed (**Appendix A**). Combined with the sub-second temporal resolution of the tag ping frequency, this dataset is a major improvement on the typical resolution of free-ranging tracking studies, particularly those used to determine potential responses to EMF. The high-resolution of the tracking data, provides confidence in the modeled encountered EMF. Since the operational power in the cable is temporally variable and the animal

movement is also temporally variable these factors must be considered together to determine the encountered EMF (**Figure 3.29**).

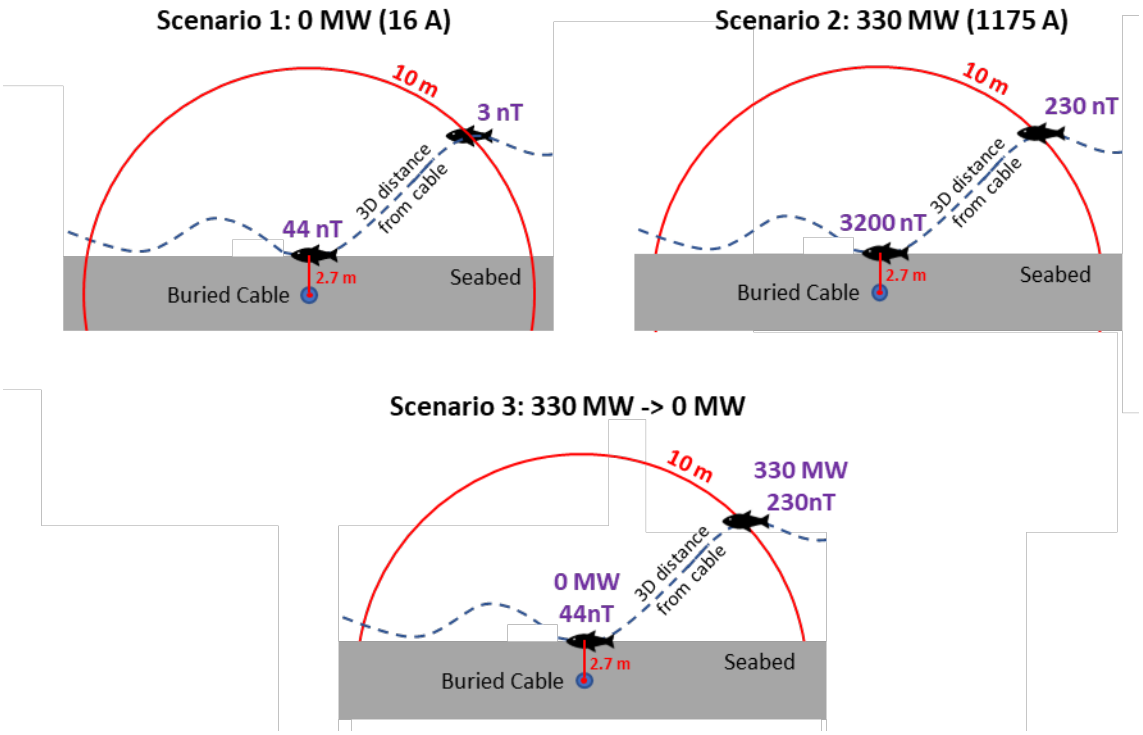

Figure 3.29. The importance of combining the operational characteristics of the cable and animal movement ecology. The three scenarios depict a fish taking the same movement path under three different operational power levels. In Scenario 1, the cable operates at 0 MW with only the maintenance current of 16 A and the fish encounters a DC magnetic field of 3 nT at 10 m distance from the cable and 44 nT at 2.7 m from the cable. In Scenario 2, the cable operates at 330 MW (1175A) and the fish encounters a DC magnetic field of 230 nT at 10 m from the buried cable and 3200 nT at 2.7 m from the cable. In scenario 3, the fish encounters the cable operating at 330 MW and therefore encounters 230 nT at 10 m distance from the cable and as the fish moves closer the operational power level changes to 0 MW (16 A) and the fish encounters a lower DC magnetic field of 44 nT despite being closer to the buried cable (2.7 m). Note that the DC magnetic field is modeled using a mean cable burial depth (2.7 m) and twist (0.8 radians) based on the eel study area and specific HVDC Cross Sound Cable characteristics (the AC EMF is not shown). The image is a hypothetical representation of 3D movements in a 2D vertical plane based on what was found in this study and is not to scale.

Key information Box 3.10

- Based on the data from 2018 and 2019 combined, 56 eels were detected, of which 31 were detected by the VPS array and had the *potential* to encounter the cable EMF
- The 2018 data were 2D and the 2019 data were 3D
    - The EMF encountered could not be determined from 2D data
    - The EMF encountered was determined for 3D data (see **Section 3.6.3**)
- The two-dimensional horizontal proximity to a cable route is not sufficient to derive if a fish or other marine species encounters the cable EMF however it provides an estimation of the *potential* to encounter the cable EMF
- Three-dimensional positional data and knowledge of the operational characteristics of the cable are required to determine the EMF encountered (see **Figure 3.29**)

3.6.3. The encountered DC and AC magnetic fields

For eels in this study, a realistic representation of the encountered EMF was modeled by combining the high-resolution 3D positional data obtained from eels in 2019, with the HVDC cable characteristics and specific power level at the time of eel detection (**Section 2.2.3**). Both the DC and the AC magnetic fields encountered were determined for each position in an individual eel track. The 3D position calculated require each eel's dive profile together with the horizontal movement to define the true distance from the buried cable. This 3D spatial information on the eel movement then had to be combined with the modelled interaction of the time-varying emitted EMF with the geomagnetic field to determine the local magnetic field deviations. Without combined consideration of these spatio-temporally variable factors, one may incorrectly assume that an eel would experience a stronger strength of EMF on the seabed, closer to where a cable is buried (refer to **Figure 3.29**). This assumption is an oversimplification of the 3D interaction of the animals' movements and the 3D emitted field in the context of the geomagnetic field and the variable power level of the cable. For example, eel 105 encountered the greatest positive deviation of DC magnetic field while surface-swimming over the route of the buried cable, after which it dived down to the seabed and experienced a negative deviation (**Figure 3.24, 3.28**). In this recorded scenario, the stronger deviation was experienced by the eel at the surface of the water. Similarly, there was no simple observed relationship between diving activity and the encountered EMF.

The range of the DC magnetic field anomalies encountered by eels were deviations from the geomagnetic field between -17.9 nT and 86.9 nT. The AC magnetic field encountered ranged from 0 to 147.8 nT. The encountered DC and AC magnetic fields were found to be correlated and the greatest AC fields encountered mirrored the greatest DC anomalies experienced by eels. The correlation between DC and AC magnetic fields encountered, makes sense because they were both influenced by the power level in the CSC, however the true relationship between the AC and DC magnetic fields and confirmation that the AC magnetic fields scale with the power level require further empirical measurement. It is noteworthy that there is greater confidence in the modeled DC magnetic fields encountered by eels since the model was based on first principles and has been verified, both in this study and previously (Hutchison et al., 2020b). As discussed in **Section 2.4**, further work is required to develop and verify an AC model for a HVDC cable to the same level of confidence as the DC model. In **Section 3.1.2**, it was highlighted that many studies support the theory that anguillid eels are responsive to magnetic fields

and possess both a magnetic map and magnetic compass sense enabling them to obtain important locational cues from the geomagnetic field (Durif et al., 2013; Cresci et al., 2017a, 2019; Naisbett-Jones et al., 2017; Putman, 2018). While earlier work suggested that anguillids may be responsive to induced electric fields (Rommel Jr and McCleave, 1973; Zimmerman and McCleave, 1975; McCleave and Power, 1978), this hypothesis lacks support and therefore the encountered AC electric fields were not considered (but see **Section 4**, for a discussion of relevance to other species). Due to the correlation between the encountered DC and AC magnetic fields, only the DC magnetic field encountered was analyzed in the HMM.

Key Information Box 3.11

- The range of the DC magnetic field anomalies encountered by eels were deviations from the geomagnetic field between -17.9 nT and 86.9 nT
- The AC magnetic field encountered by eels ranged from 0 to 147.8 nT
- The encountered DC and AC magnetic fields were correlated as a result of being modeled based on the power level; the greatest AC fields encountered by eels mirrored the greatest DC anomalies experienced by eels
- Confirmation that the AC magnetic fields scale with the power level require further empirical measurement
- The eels would encounter the total EMF environment which in the vicinity of the HVDC Cross Sound Cable includes the geomagnetic field, the DC magnetic field and the AC magnetic field
- The AC electric field was not considered for the eels since the focus was on their magnetoreceptive abilities
- The response of eels to the EMF was assessed in the context of the DC magnetic field because the DC and AC fields were highly correlated (see **Section 3.6.4**)

3.6.4. Behavioral Characterization and the Response to the Encountered DC Magnetic Fields from the HVDC cable

3.6.4.1. Behavioral Characterisation of Eel Movements

The Hidden Markov Model (HMM) analysis was applied to provide information on behavioral states which are normally hidden (Patterson et al., 2009; McClintock and Michelot, 2018). The HMM applied analyzed the movement of the eels, which evaluated whether the eel movement tracks exhibited predictable states. These states then translate as identifiable and quantifiable behaviors when encountering the EMF, therefore assisting in inferring behavioral responses to the CSC EMF. Three states described the speed of movement, based on step length and were found to describe the observed data well. State 1 was the smallest step length, indicative of stationary or very low activity, while state 2 and 3 were indicative of transitory activity at intermediate and fast speeds, respectively (i.e., medium and large steps). These dynamic behaviors can be observed in the horizontal movements relative to the VPS array (**Figure 3.21, 3.22**). State 1 is barely visible, because the eel was stationary or not moving very far (**Figure 3.21, 3.22**). In contrast, there was a high frequency of state 3 in horizontal movements when

eels were moving the greatest distances. These states are also visible in the dive profiles shown over time (**Figure 3.23, 3.24**). In these figures, which provide an indication of time, and vertical movements rather than horizontal distance traveled, state 3 is more visible (**Figure 3.24**). However, there does not appear to be an associative pattern of state 1 and 2 with dive profiles. State 1 was less common, and most eels were in state 1 when on the seabed (ID 105, 129, 181a), however one eel exhibited state 1 at the sea surface (ID 164) (**Figure 3.24**).

The HMM also grouped the eels based on the probability of transitioning from one state to another. Recall that group1 eels has the greatest probability of staying in state 3 (the largest step length) and were considered the most active eels (refer to **Section 3.5.5**). The majority of eel tracks in 2019 (6 of 13) were attributed to group 1, which was the faster moving group with a greater probability of staying in state 3 (the largest step length). Given eels were migrating, it is expected that the eels would exhibit this type of behavior, that can be summarized as purposeful transit. Group 1 eels were also observed to move in a southerly direction the most. Group 2 eels and those that exhibited mixed groupings for sub-tracks, showed greater intermittency in the states and could also be summarized as having more south-easterly trajectories, with one eel (ID 105) travelling east and then north. Additionally, group 1 eels were most commonly recorded during an ebbing tide (**Table 3.3, Table 3.4**); five eels tracks were detected during an ebbing tide and only one eel track was recorded during slack tide. Similarly, three of four group 2 eels were recorded during an ebbing tide and only one during a slack tide while both mixed group eels were detected during a slack tide. Eel 181 showed the greatest variation in state and also in grouping; the eel was detected first in states 1 and 2 and then later switched to state 3, exhibiting resting (also detected by the VR2W array). However, the eel returned 12 hours later and was in group 2 (state 1 and 2), showing more purposeful transit. Interestingly, eel 187 showed purposeful transit (group 1, state 3) in full daylight. These behaviors, align with the individual variation, pauses in migration and differences in migratory distances traveled, identified in other studies (Westerberg et al., 2007; Béguer-Pon et al., 2014).

Key information Box 3.12

- The HMM analysis identified three behavioral states
  - State 1 – small steps indicative of low or no activity
  - State 2 – medium steps indicative of medium speeds of movement
  - State 3 – large steps indicative of higher speeds of movement
- Based on the probability of transitioning between states, eels were grouped
- Group 1 eels were most likely to stay in state 3 and exhibited movement with the greatest purpose

3.6.4.2. The Response to the Encountered DC Magnetic Field

The HMM analysis (based on 12 eels) revealed that eels in state 2 and 3 (exhibiting medium and large steps), which were most commonly observed, responded to the DC magnetic fields encountered. In both state 2 and 3, an increase in the mean step length occurred indicating that eels moved faster within each state, when they encountered greater positive deviations in the total magnetic field (**Figure 3.25**). Additionally, the step lengths became more consistent and less variable in state 3, as indicated by

the standard deviation parameter, which is indicative of a more consistent and purposeful movement (**Figure 3.26**). This increase in speed in response to the encountered DC magnetic field, is in contrast to the response based on the work of Westerberg and Lagenfelt (2008), who found from 2D tracking that European eels slowed down in the zone nearest to an operating AC cable in the Kalmar Strait of the Baltic Sea (**Figure 3.2a**). The slowing down in the region of the AC Kalmar Strait cable was partially explained by some eels that paused for several hours or a full day in alignment with normal eel behavior (Westerberg et al., 2007; Béguer-Pon et al., 2014) but the slower speeds were still evident in the region of the cable when those eels were removed from the analysis. The study does not report the specific intensity of the AC magnetic field. The authors reported a potential weak relationship between the slower swimming speeds and increasing power in the AC Kalmar Strait cable (140-280 A) but noted that there was a 30% probability that the correlation coefficient was zero. The weak relationship observed by Westerberg and Lagenfelt (2008) between swimming speed and the power level may be an artefact of the range of Amps and lack of data at the lower spectrum (<180 A) and greater density at the higher range (200 – 280 A). The power range in the HVDC CSC cable when the EMF was encountered by American eels in this study, was broad (16 – 1175 A) and the approach taken was a much finer-resolution 3D tracking which provided greater confidence in the position of the eels relative to the HVDC cable and therefore the encountered DC magnetic field. Ultimately, the CSC is a DC cable, and the Kalmar Strait cable is AC, therefore differences in the response may be expected. However, the resolution of the tracking in each study are vastly different and may be the most valid explanation for the differences observed. It is noteworthy that an AC magnetic field was emitted from the HVDC CSC and as modeled, the eels encountered both an DC and AC magnetic field. While we report on the results of the DC magnetic field encounter it is plausible that the American eels may be responding to the AC magnetic field, or both.

The earlier 2D tracking study of European eels was in relation to the Baltic Cable, a monopolar DC cable that was reported to emit 5 µT at 60 m from the cable when operating at 1300 A (Westerberg and Begout-Anras, 2000). The study first predicted the deviation in the eels' trajectory based on the anomaly expected from the cable, for both the polar compass and inclination compass, however, note that the predictions were based on the scenario of eels using only the magnetic field for navigation. In the first year of releases, the European eels appeared to deviate strongly from the anticipated trajectory and instead follow the route of the Baltic cable south instead of passing over it. This behavior was not observed in the second year when the eels travelled in a predominant east to west direction with minor changes in trajectory and it was proposed that the routes observed were either minor perturbations due to the Baltic cable or may have simply been initial disorientation following the release. Owing to the resolution of the 2D tracks, it is not possible to relate the movements to the encountered EMF of the DC Baltic cable. In contrast, in this study of the HVDC CSC, a small portion of the cable was studied in detail with fine-scale high resolution 3D tracking, which does not provide a good comparison for the overall larger scale trajectories of the eels. However, the data did show variable degrees of meandering movements within the short tracks obtained in 2018 and 2019 (**Figure 3.16**) and there was potentially evidence that eels explored the HVDC cable EMF. For example, Track 14, experienced two peaks in the encountered DC magnetic field indicating that the eel turned back toward the cable (**Figure 3.21, 3.27**) and in Track 105, the eel dived to the seabed after encountering the peak DC magnetic field (**Figure 3.22, 3.28**). Interestingly, the models from the earlier study suggested that the angle of an eels approach to the cable may be an important factor in the influence of the EMF (Westerberg and Begout-Anras, 2000). The study of Westerberg and Lagenfelt (2008) reported eels slowing down when in the

vicinity of the AC Kalmar Strait cable which presented as being perpendicular to the trajectory of eel travel. In the study of the HVDC CSC, the majority of eels were transiting in a similar direction as the path of the CSC. Wyman et al., (2018) reported salmon smolts transiting faster in the region of an active DC cable in a parallel orientation to trajectories of travel. Future studies may want to explore this phenomenon with eels on a larger section of the CSC or with multiple cables in differing orientations.

Magnetoreception in eels is most plausibly explained by magnetite-based reception and is expected to have a sensitivity in the region of 10 nT (Formicki et al., 2019; **Section 3.1.2**). That level of sensitivity is sufficient to allow eels to respond to gradient of change in the geomagnetic field and facilitate the magnetic compass sense and magnetic map sense that has been experimentally derived (Durif et al., 2013; Cresci et al., 2017a, 2019; Naisbett-Jones et al., 2017). This study of American eels and the HVDC CSC has demonstrated that eels also respond to cable EMFs. As highlighted in previous studies, there is a high degree of individual variability when studying the magnetoreception of eels and the movements of eels will be driven by internal states (Nathan et al., 2008; Cresci et al., 2019). Evidently, there is also a high degree of plasticity in the maturation of eels (Hain, 1975; Svedäng and Wickström, 1997) which may also transfer into the use of, or activation of the magnetic sense. Additionally, Cresci et al., (2017) proposed that the magnetic compass sense may be endogenously regulated by circa-tidal cues in glass eels and later demonstrated the ability to orientate to the magnetic field in relation to the memorized water flows, which may provide important migratory cues in adult outward migrations (Cresci et al., 2019). However, the ability to memorize a cable EMF, which is a temporally variable entity due to fluctuating power levels, is not known. The focus of research on the topic of magnetoreceptive abilities in eels has been on the migratory life-stages (i.e., glass eels and silver eels; **Section 3.1.2**). Naturally, research on the effects of anthropogenic cable EMFs has also focused on migratory life-stages in eels (Westerberg and Begout-Anras, 2000; Westerberg and Lagenfelt, 2008; Orpwood et al., 2015) and in other teleost fish such as salmon smolts (Wyman et al., 2018). However, since eels are facultative catadromous fish and may move between freshwater and marine environments during their life (Lamson et al., 2006; Marohn et al., 2013), it is plausible that magnetic fields may provide orientational cues throughout their life cycles and the potential for anthropogenic cable EMFs may also be encountered.

Key Information Box 3.13

- The HMM revealed that eels in this study responded to the DC magnetic field by increasing their mean step length as the positive anomalies increased (up to 86.9 nT)
- A greater mean step length was observed in state 2 (intermediate steps, medium activity) and state 3 (large step length, higher activity)
- In state 3, the step length also became less variable and more consistent
- The assessment was made in relation to the DC magnetic field however due to the correlation between the DC and AC magnetic fields, it is plausible that eels responded to either the DC or AC magnetic field
- The resolution of the tracking in this study is far greater than previous studies of eels in the context of cables and EMFs
- The levels of magnetic field encountered by eels in this study and the observed response, aligns with the anticipated sensitivity levels based on the magnetite-based reception
- The major finding of this study is that the eels responded to the HVDC cable DC magnetic field
    - This did not constitute an acute barrier to migration
    - The importance of the cable EMF in the context of deriving locational cues from the geomagnetic field requires further work

3.6.5. Conclusion

This study has built on prior 2D free-ranging tracking studies looking at the potential for eels to respond to cable EMFs. Through this study, high-resolution 2D data in 2018 and 3D data in 2019 were collected. The 3D movement tracks for 12 eels (13 tracks, 19 sub-tracks) were used to assess the encountered DC and AC magnetic field from the HVDC cable and facilitate the assessment of whether eels responded to the DC magnetic field. Adopting 3D telemetry and recalling that the time between each position fix was of the order of seconds we can be confident that the resolution in this study was suitable to model the EMF encountered by the eels. Through modeling, the movement behavior of eels was characterized in terms of the speed and described by three behavioral states with the probability of transition between states enabling eels to be grouped based on behavioral dynamics. Assessing the behavioral state of the eels which encountered the DC magnetic field (-18 to 87 nT DC) showed that the eels in this study responded to the DC magnetic field anomaly caused by the HVDC CSC within the intermediate and faster states (state 2 and 3). Eels encountering the HVDC cable DC magnetic field moved faster and more purposefully in relation to greater positive anomalies. While there was an effect on behavioral state, the cable was not a barrier to eel movement and therefore did not impact their ability to migrate past the cable. The interpretation of the results should be restricted to the range of EMF encountered (-18 to 87 nT DC magnetic fields) and further work would be required to define responses outside of this range. Due to the correlation between the encountered DC and AC magnetic fields, the possibility that eels were responding to AC fields cannot be discounted. Of the 56 eels that were confirmed to migrate over the two year study, 55% were found to be in the vicinity of the cable however only 12 eels were tracked in 3D with high resolution along the small stretch of the HVDC CSC enabling the encountered

EMF to be determined. Nevertheless, there is potential for eels to encounter a single cable multiple times or multiple cables on their outward or inward migration, depending on the number and location of cables along the migration route. With the expansion of offshore wind development and subsea transmission cable deployment there are questions about the potential for cumulative encounter of subsea cable EMFs. Along the US east coast, current plans are for the installation of multiple cables primarily HVAC to transmit the offshore wind power. HVAC cables have lower levels of EMF emissions compared to HVDC cables due to lower operational power levels. However, as shown through the present study eels can still respond to low levels of EMF. Therefore, the potential for multiple encounters with cable EMF leading to cumulative impacts remains a question for future work which needs to be set in the context of other pressures to the local eel population. Cable routes, their orientation, the specific cable characteristics and the interaction of the cable EMF with the local geomagnetic field will need to be considered. Further work to validate the eel response for a higher number of eels in different cable locations and consideration of variable cable EMF intensities and interaction scenarios, including a broader range of EMF anomalies is advised.

4. General Discussion

The primary aim of the research project was to understand the potential for electromagnetic field (EMF) impacts on American eel migratory movement when encountering high voltage direct current (HVDC) electricity transmission cables, one of the types of cable anticipated to be used for offshore renewable electricity transmission in USA coastal and offshore waters.

Previous research on the European eel used 2D acoustic tracking to assess whether there was any change detectable in the migratory movements of individual eels associated with a power cable (Westerberg and Begout-Anras, 2000; Westerberg and Lagenfelt, 2008). However, the tracking technology at the time was only able to position fix at a relatively coarse scale (of the order of metres) and the 2D nature of the method meant that only the horizontal components of the movement were tracked. Yet European eels are known to conduct regular dives during their movement (Westerberg et al., 2007) and these will give rise to a 3D movement track which is unaccounted for by 2D based methods. As EMFs are present in the environment in 3D (whether natural or anthropogenic), eels will encounter and experience EMFs in 3D. Furthermore, the HVDC cable EMF interacts with the local geomagnetic field resulting in EMF variability in the water column and both positive and negative deviations from the background (Hutchison et al., 2020b). Therefore, the actual EMF experienced by an eel will vary at fine spatial scales in 3D and so the individual movement must be determined in 3D in order to define the encounter interaction.

Taking account of the limited background knowledge and the need to understand how an eel would encounter the cable EMF in space and time, the project aim was met by completing each of the following integrated objectives:

1. Build on previous work on the HVDC CSC, to further characterize the emitted EMF using custom equipment enabling three-dimensional measurements of the magnetic and electric fields.
    a. To characterize EMFs in the selected area for the eel study, in conjunction with Objective 2.
    b. Conduct measurements along the length of the HVDC cable to better define the DC and AC fields emitted by the cable.
2. To develop a free-ranging tracking study employing novel tagging technology to determine individual eel proximity to the HVDC cable and enable fine-scale (2D and 3D) movement behaviors and responses to the EMF be assessed.
    a. Development of the tagging study including a testing and refinement phase.
    b. In conjunction with Objective 1a, define the EMF encountered by individual eels based on their proximity to the buried HVDC cable and the operational characteristics.
    c. Based on the encountered EMF (Objective 2b) determine if the eels respond to the HVDC cable EMF in an ecologically meaningful way.

The innovative and integrated methodological approach and analysis was first broken down into specific project activities to align with the objectives and then the outputs of each objective were analyzed with regards to the overarching aim (see **Figure 1.7** for overview). Each of the objectives and how they were met, including the methodological approach and specific findings are discussed (**Section 4.1**) and set in the broader context (**Section 4.2**) and summarized at the end, including key findings, knowledge gaps and recommendations (**Section 4.3**).

4.1. Adopting the position of the American eel in the experimental approach

Hutchison et al., (2020a) set out the context of taking the vantage point of an EM-receptive species to understand the potential responses and resultant consequences, to link to the determination of whether impacts occur or not. This perspective relies on addressing the critical physical and biological/ecological components of the system being fully considered. Here, that included the American eel migratory behavior in relation to EMF emitted by an HVDC power cable over spatio-temporal scales relevant to the eels.

In a previous experimental enclosure study of the HVDC CSC EMF, fine scale 3D movement of seabed associated animals showed behavioral responses in relation to the HVDC CSC EMF, which was characterized in 3D and monitored throughout the experiment period (Hutchison et al., 2020b). The vertical movement of American eels in coastal waters has not been well defined, however, it was predicted from other anguillid eel studies that the American eels would migrate within surface waters exhibiting dives down through the water column (Westerberg et al., 2007). Whilst the enclosure approach would have provided an opportunity to closely quantify some movement *in situ,* it would have prevented natural surface-swimming behavior, therefore a free-ranging tracking approach was most suitable. Furthermore, technological advancements during the project have facilitated understanding 3D behavior of an animal within a free-ranging telemetry approach.

4.1.1. The three-dimensional context of HVDC cable EMFs encountered by eels

To understand the EMF environment that was encountered by free-ranging eels required that the EMF emitted by the HVDC CSC was characterized in the context of its interaction with the local geomagnetic field in 3D. The previous HVDC CSC EMF study showed that the measured EMF emitted could be modeled in relation to the gradients of the EMF that may be encountered by a receptive organism (Hutchison et al., 2020b).

The essential components to model cable emitted EMF are the cable characteristics, including the materials they are made of, any twisting of the cable, the position in the environment, such as whether the cable is buried and if so the depth of burial, and the power being transmitted at a given time (which varies through time). These aforementioned factors determine the emitted EMF at a given location (i.e., proximity to source). Therefore, the EMF can be determined for a species (and relevant life stages) whether they are positioned within the sediment, at the seabed surface and/or within the water column, with specific reference to their proximity to the cable as the source of the EMF.

Organisms that detect EMF, either magnetic fields, electric fields or both, do so in 3D (Hutchison et al., 2020a, 2021). In past studies, when modeling has been undertaken, the cable emitted EMF is usually represented in 2D at or near to the seabed and typically as a snapshot in time (Normandeau Exponent et al., 2011; Gill et al., 2012; Dhanak et al., 2015). In the present project a major advancement was using the characterization of the EMF in 3D, combined with the fine-scale positioning of the eel individuals in 3D, as a basis to model the EMF level encountered by an eel at fine-scale resolution throughout the duration of the tracked movements. Furthermore, to reflect the true nature of the encountered EMF, the 3D modeling included the interaction with the local geomagnetic field to provide a measure of the deviation of the EMF compared to background. The deviation was expressed as a positive or negative anomaly in the DC magnetic field encountered and the total AC magnetic field encountered at each position of the eel's tracked movement.

In the area of the eel study, the HVDC CSC is considered to be buried deeply (in study area, average of 2.7 m, sd = 0.7) as it runs through a shipping channel, yet, there was a measurable deviation in the EMF at the seabed and in the water column, and the eels that encountered the EMF anomaly responded. Other cable routes, such as OWF cables are likely to have the cable buried at shallower targeted depths, between 1 and 2 m and in some areas may not be buried (BERR, 2008; Det Norske Veritas AS, 2016). Therefore, the expectation is that for cables with similar properties, the EMF would be detectable in the water over greater distances for shallower burial depths and when considering unburied scenarios (including seabed mounted and dynamic cables used for floating energy devices), the EMF deviation from background in the water column would be greater. However, the specific variable properties of different cables must be accounted for and will not necessarily be the same as the HVDC Cross Sound Cable.

4.1.2. Response of the eels to the EMF anomalies of the HVDC CSC

The eels tracked within the fine-scale acoustic array encountered variable EMF anomalies which were both DC and AC in nature. The encountered negative DC anomalies (i.e., below the background magnetic field level) were very small, between -17.9 and -0.1 nT whereas the encountered positive anomalies were larger in the range of +0.1 to +86.9 nT. The encountered AC anomaly was defined as the total deviation regardless of being positive or negative, and ranged between +0.8 to +147.8 nT. Importantly, during movement through the study area, an eel could encounter the peak intensity of the field whilst at the surface of the water owing to its direction of movement with regard to the HVDC cable route and the local geomagnetic field orientation. Therefore, it cannot be assumed that when travelling close to the seabed or diving that the vertical position alone is a good indicator of higher 3D EMF exposure by an individual animal. The 3D interaction of both the animal and cable EMF in space and time must be accounted for, including the specific operational power level of the cable.

Based on the HMM, the eels had three identifiable states of movement, which play a role in defining the behavioral response to encounter with the DC magnetic field anomaly. Within the intermediate and fast states (state 2 and 3), the eels demonstrated a faster and more purposeful movement. This finding is evidence of a change in behavior in response to a HVDC cable EMF. Whilst the analysis showed a change in eel behavior the number of eels that were tracked and therefore which experienced an anomaly was small. Further work is required to improve the predictability of the response across multiple eels and different eel populations at comparable and broader EMF anomaly levels. Faster movement has been recorded in some migratory Salmonid smolts, which had shorter transit times (i.e., they swam faster) through regions where an HVDC cable was active, although other environmental factors were influential too (Wyman et al., 2018).

The linearity of the relationship between the step length parameters and the DC magnetic field anomalies modeled by the HMM was based on encounter data in the range of -18 nT to +87 nT approximately. These values appear small yet they were evidently detectable by the eels and led to a behavioral response. Experimental studies making small alterations to magnetic field intensity and direction have been shown to result in swimming behavioral responses in eels (Tesch et al., 1992). In other species, nT anomalies were implied as having some influence on migrating salmonid smolts (Wyman et al., 2018). A number of marine migrants use magnetic compass and magnetic map sensory cues (Putman, 2018) and it is generally assumed they use biogenic magnetite based magnetoreception to perceive the direction, intensity and inclination of the magnetic field (Walker et al., 2002). The sensitivity threshold of the magnetite system to changes in the field intensity has been estimated to be

around 10 nT (Kirschvink and Gould, 1981; Kirschvink and Walker, 1985), which aligns with the findings of a response to deviations in the range of tens of nT in this study.

4.1.3. The potential for impact to American eels from HVDC EMF

The tracked eels that encountered the magnetic field anomaly created by the HVDC CSC during power transmission exhibited a behavioral response. This response requires interpretation in the context of whether the American eels passing in the area of the HVDC CSC will incur an impact during their migration. (Boehlert and Gill, 2010). The effect found in the present study, is biologically relevant as the migratory movement of the subset of eels that encountered the HVDC CSC cable EMF altered their behavior in relation to anomalies in the local magnetic field; the same field that is presumed to be used for local orientation and direction finding in migratory species (Klimley et al., 2021). While the eels did alter their behavior, they were found on either side of the cable route, therefore, the effect did not suggest that the HVDC CSC was an absolute barrier to migratory movement. It should be noted that the study was only able to track eels over a very small section of the cable and also the short durations of recorded tracks represented a relatively brief encounter with the EMF anomalies from a small proportion of the cable route.

An important consideration in the future is whether the eels will respond in a similar way each time they encounter an anomaly as this would suggest the potential for cumulative effects, particularly when encounters with cables will occur over larger spatial scales with multiple cables as part of future offshore wind and cabling plans. If eels respond in the same way to a cable EMF encounter, then the cumulative effect over greater spatial and temporal scales should be determined in order to deem whether the impacts are significant enough to be interpreted as biologically or ecological meaningful. This will require consideration of the biological consequences (such as altered energy budgets), the ecological effects (such as timing to reach spawning grounds) and the conservation status of the American eel population (Jacoby et al., 2015, 2017).

4.2. Broader context

4.2.1. Other taxa and cable EMFs

The anomalies created by the interaction between the subsea cable EMF and the local geomagnetic field are defined as DC and AC components and magnetic or electric field components of the EMF. There is a broad range of taxa that are known to respond to magnetic and electric field cues in the environment and should also be considered (Putman, 2018; Newton et al., 2019; Klimley et al., 2021). EM-receptive organisms that are primarily magnetoreceptive are generally categorized into migrators and non-migrators, the latter may use cues for local orientation. Organisms that are electroreceptive (mainly the elasmobranchs and taxonomic relatives) use electric field cues for obtaining food, avoiding predation or detecting conspecifics (Newton et al., 2019).

Several taxa undertake migratory movements in relation to the direction, intensity and inclination of the magnetic fields encountered (Putman, 2018; Klimley et al., 2021), therefore, they too could respond to the EMF anomalies associated with power cables. Whether these migratory taxa (e.g., teleosts, elasmobranchs, crustacea, turtles, cetaceans) respond and what the specific consequences would be, need to be set within the appropriate context for each taxon before any determination of impact can be made. The path of migration in relation to the location of cable routes will determine the likelihood of encounter, whilst the sensitivity of the specific taxon to EMF and the characteristics of the power cables

defining the EMF will determine likelihood of response. The approach developed in the present project could serve as a template for taking the vantage point of other migratory, magnetoreceptive taxa.

Non-migratory magnetoreceptive taxa (and in some cases life stages) are known to respond to localised magnetic fields, for orientation within a habitat or regular movement between local areas (e.g., crustacea, fish larvae (Boles and Lohmann, 2003; Putman et al., 2018)). Crustacea and mollusks, several of which are commercially important, are known to associate with hard surface scour or cable protection or may bury in sediments where cables are also buried (Albert et al., 2020; Gill et al., 2020; Taormina et al., 2020). The EMF that will be present in the sediment or extending into the hard protection can be estimated in 3D at appropriate spatio-temporal scales, taking the *in situ* measurement and subsequent 3D modeling approach applied in the present project. Again, the key aspect with regard to any impacts of the EMF on the organisms, is when and how they may experience the EMF in relation to the time they spend associated with the hard substrate or buried, and the extent of their movement.

For taxa that primarily use electroreception, the interaction scenario also depends on the likelihood of EMF encounter and their sensitivity to electric fields (Newton et al., 2019; Hutchison et al., 2020a). While AC electric fields are typically considered for AC cables, this study and earlier evidence has demonstrated that AC fields are associated with DC cables and the spatial extent of AC electric fields is greater than both AC and DC magnetic fields (Hutchison et al., 2020b). Benthic associated electroreceptive species are expected to be more likely to encounter the EMF from a buried cable, however, the movement ecology of bentho-pelagic and pelagic species and potential EMF interactions should also be a consideration (Hutchison et al., 2020a). In an earlier project (Hutchison et al., 2018, 2020b) which studied the same HVDC CSC, it was demonstrated that there was a strong behavioral response of a benthic elasmobranch species, the little skate (*Leucoraja erinacea*) to the HVDC cable EMF, whereby the skates traveled much further but at a slower speed and had increased frequency of large turns in movement compared to a reference site. This study also showed that the benthic lobster (*Homarus americanus*), regarded as potentially magnetoreceptive, also exhibited changes in their movement response but to a lesser extent than the little skate. Therefore, the EMF from the same HVDC power cable was detected by different taxa (reported here and in Hutchison et al., 2018, 2020b), which have different sensory modes of detection, and the response was exhibited as a behavioral change in movement.

When interpreting the response of organisms to EMF it should be recognized that the primary sensory mode is assumed, and as the magnetic field and electric field interact, the organism may actually be responding to one or both fields. For subsea HVDC cable EMF, the fact that DC and AC magnetic and AC electric fields are present and measurable should be taken into account when determining the potential for impacts on receptor species.

4.2.2. Understanding EMFs from HVDC power cables and other subsea power cables

In previous studies, *in situ* measurements and modeling of DC cables have been shown to be appropriate to determine the EMF environment emitted close to the seabed (Dhanak et al., 2015; Kavet et al., 2016; Hutchison et al., 2020b). The method of EMF measurement and modeling developed here for the HVDC CSC extends these approaches by using the measured EMF to determine the cable burial depth and from this determine the 3D EMF encountered by a receptor through time; this approach can be applied to other cables. The *in situ* measurements are key to modeling realistic EMFs.

While HVDC cables such as the CSC transmit DC power, an AC-DC transformer station at each end converts the electricity to the domestic supply of 60 Hz AC (Railing et al., 2004). In the case of the HVDC CSC and a second HVDC cable (the Neptune cable), the DC EMF was measured and modeled and in addition an associated AC EMF was measured (Hutchison et al., 2018, 2020b). The present study used the same transect approach and equipment to measure the EMF and extended this to assess the extent of the AC fields along the length of the cable. Contrary to the prediction of a decay in the AC EMF with distance from the transformer station (at either end), the EMF was present along the cable, which while based on a limited number of transects, indicates that the AC fields in the marine environment may be more complex than first expected based on power transformation knowledge.

During the development of the encountered EMF model there were several key characteristics of the cable that influenced the EMF environment and the anomaly encountered by the animals. It is known that the mechanical and electrical properties of the material used in the construction of the cable influence the EMF (Gill et al., 2012). Deployed cables can also have angular rotation (i.e., twisting), which is either employed directly in the manufacturing (e.g., AC 3-phase cables) or simply as a result of the cable being laid and the conductors lying twisted over a length of the cable (e.g., bipolar cable, such as the CSC). Furthermore, the depth at which a section of cable lies or the amount of protective material (i.e., sediment, concrete mattress) will determine the physical proximity of the animal to the EMF encountered as will the habitat association of the organisms (i.e., in or on the seabed, or in the water column (Hutchison et al., 2020a, 2021)). However, the operational characteristics must also be considered (refer to **Figure 3.29**).

Data on whether the cable is twisted and the actual burial depths of cables, are typically not available and may be estimated, which introduces potential errors into the models. Where EMF measurements are undertaken, these aspects can be derived, such as in this study, with sufficient knowledge of the cable and sensitivity of the measurement apparatus. There are usually data of the 'as-laid' burial depths, which relate to the time when the cable was installed, however as shown through the EMF model derived burial depths here, the 'as laid' depths are not accurate enough. This may be a consequence of sediment movement since the time of the installation or could be related to equipment inaccuracies when obtaining the 'as-laid' depths, or both. For determining the EMF at a 3D position in the water column it is important to ensure that the burial depths are realistic in present time and accurate because the measured deviations of relevance are of the order of tens of nT and an inaccurate burial depth may have a strong influence. Verification of EMF models should be a component of future work and based on determination of the actual burial depth (or hard protection cover depth). This also requires data on the power being transmitted at the time of measurement of the EMF to derive the true position of the cable.

In the context of OSW, while the cables may differ in terms of the transmission type (AC or DC) and purpose, (e.g., export cables, inter-array cables), their routes will cross migratory paths and more generally the regular movement pathways of animals. With the high number and spatial extent of the planned cable networks there should be an estimation of the likely encounter rate, i.e., the likelihood of animals coming into the vicinity of these cables and the potential to interact with the cable EMFs. The methods applied in the present study can be used to determine the 3D EMF environment that will be created by DC cables and with some additional developments the same can be achieved for AC fields. It is important to note that offshore wind is a variable resource and the power production and subsequent energy transfer through cables will vary too. Therefore, to properly determine the EMF environment encountered by receptive species there needs to be data on the power transmitted over short time

intervals that ideally match the time intervals of the data collected by the tracking method used to realistically determine the EMF intensity encountered by a receptor (Hutchison et al., 2021).

4.3. Conclusions and Recommendations

The study reported here highlights that taking the vantage point of an animal in terms of their exposure and response to EMF requires 3D knowledge on the EMF anomaly and the movements of the animal on spatio-temporal scales relevant to the receptor animals. For the modeling of EMF encountered by the eels it was essential to have information on cable characteristics, the power level in the cable, the interaction of the cable EMF with the geomagnetic field, and the horizontal and vertical proximity of the eel to the buried cable, to determine exposure. These aforementioned parameters allowed the speed of movement of migratory eels to be assessed in the response to the EMF and indicated that eels increased their speed and were more directed in their movement.

The approach taken in the study was comprehensive, however, as with all research, there were limitations and knowledge gaps remain. The intermittency of the power in the cable meant that the EMF was variable and some of the tracking was undertaken when there was little, or no power being transmitted. The range of EMF exposures as a result of variable power (and animal movement) was useful in the analysis but the small range was also a limiting factor in the interpretation and transferability of knowledge gained. It is important to understand the temporal nature of the power transmission to ensure that models used reflect the EMF that may be encountered by a receptive organism on relevant spatio-temporal scales. The low number of tracks obtained highlights that these types of free-ranging studies should try to maximise the number of released animals and consider repeat studies over subsequent years. Furthermore, ensuring a comprehensive look at the potential sources of variation in the likelihood of encounter is essential. Further data would be obtained by tracking tagged animals over longer periods in the vicinity of subsea cables and may be practically achieved by combining efforts of EMF focused and non-EMF focused research in the vicinity of subsea cables; this then will provide understanding towards cumulative effects.

The key recommendations to advance the knowledge of organism response to EMF are:

- Consideration of the biological and ecological consequences in terms of the conservation status of the American eel population is required in the context of cumulative effects of multiple encounters (see below).

- 2D data can provide detail on whether an animal may be in the vicinity of a cable but 3D positioning of free-ranging animals is required to properly understand the encounter likelihood for the species of interest.

- There is a need for more EM-sensitive taxa to be studied and for studies conducted in different locations and with different levels of power in the subsea cables as this would increase the confidence in and expand on the outputs from the study reported here.

- The larger EMF anomalies expected for OSW cables, particularly the dynamic floating OSW cables, are expected to be beyond the range encountered in this study, therefore further knowledge is required on responses to a broader range of anomalies.

- Whether the animals respond to DC and/or AC fields has to be determined and this will require experimental approaches with variable exposure treatments.

- The behavioral response to multiple encounters should be interpreted in the context of cumulative exposure and cumulative effects; this requires determination of the encounter rate with EMF which will assist the assessment of whether there may be an impact.

The key recommendations to advance the knowledge of subsea power cable EMFs are:

- Better availability of information regarding OWF cables and networks, sources of variability, and anticipated EMF emissions would better enable realistic experimental studies on species effects.

- Power systems, including those of OWFs, should make recordings with short temporal resolutions to capture fluctuations in the power which will influence the EMF emitted and access to these data would be valuable when considering environmental effect studies.

- The generation of side harmonics of AC-DC conversion adds to the complexity EMFs being emitted and should be investigated and interpreted by power engineering experts in collaboration with ecologists.

- Understanding of AC fields associated with HVDC cables needs to feed into the development of an AC EMF model applicable for HVDC cables in future projects.

References

Albert, L., F. Deschamps, A. Jolivet, F. Olivier, L. Chauvaud, and S. Chauvaud. 2020. A current synthesis on the effects of electric and magnetic fields emitted by submarine power cables on invertebrates. *Marine Environmental Research*, 159(November 2019) https://doi.org/10.1016/j.marenvres.2020.104958.

ASMFC. 2017. *2017 American Eel Stock Assessment Update*. 110 pp.

Bedore, C. N., and S. M. Kajiura. 2013. Bioelectric fields of marine organisms: voltage and frequency contributions to detectability by electroreceptive predators. *Physiological and Biochemical Zoology*, 86(3):298–311, https://doi.org/10.1086/669973.

Béguer-Pon, M., M. Castonguay, J. Benchetrit, D. Hatin, G. Verreault, Y. Mailhot, V. Tremblay, D. Lefaivre, M. Legault, D. Stanley, and J. J. Dodson. 2014. Large-scale migration patterns of silver American eels from the St. Lawrence River to the Gulf of St. Lawrence using acoustic telemetry. *Canadian Journal of Fisheries and Aquatic Sciences*, 71(10):1579–1592, https://doi.org/10.1139/cjfas-2013-0217.

Béguer-Pon, M., M. Castonguay, S. Shan, J. Benchetrit, and J. J. Dodson. 2015. Direct observations of American eels migrating across the continental shelf to the Sargasso Sea. *Nature Communications*, 6:8705, https://doi.org/10.1038/ncomms9705https://www.nature.com/articles/ncomms9705#supplementary-information.

Béguer-Pon, M., J. J. Dodson, M. Castonguay, D. Jellyman, K. Aarestrup, and K. Tsukamoto. 2018. Tracking anguillid eels: five decades of telemetry-based research. *Marine and Freshwater Research*, 69(2):199–219,.

Béguer-Pon, M., J. Benchetrit, M. Castonguay, K. Aarestrup, S. E. Campana, M. J. W. Stokesbury, and J. J. Dodson. 2012. Shark Predation on Migrating Adult American Eels (Anguilla rostrata) in the Gulf of St. Lawrence. *PLoS ONE*, 7(10) https://doi.org/10.1371/journal.pone.0046830.

Bergström L., Kautsky L., T. Malm, R. Rosenberg, M. Wahlberg, N. Å. A. Å. Capetillo, D. Wilhelmsson, L. Bergström, L. Kautsky, Malm T., R. Rosenberg, Wahlberg M., N. Å. A. Å. Capetillo, D. Wilhelmsson, Bergström L., Kautsky L., T. Malm, R. Rosenberg, M. Wahlberg, N. Å. A. Å. Capetillo, and D. Wilhelmsson. 2014. Effects of offshore wind farms on marine wildlife—a generalized impact assessment. *Environmental Research Letters*, 9(3):034012 (12pp),.

Boehlert, G. W., and A. B. Gill. 2010. Environmental and ecological effects of ocean renewable energy development: a current synthesis. *Oceanography*, 23(2):68–81, https://doi.org/10.5670/oceanog.2010.46.

BOEM. 2021. *Outer Continental Shelf Renewable Energy Leases Map Book*. pp.

Boles, L. C., and K. J. Lohmann. 2003. True navigation and magnetic maps in spiny lobsters. *Nature*, 421(6918):60–63, https://doi.org/10.1038/nature01226.

Brown, L., and T. Castro-Santos. 2009. Three-dimensional movement of silver-phase American eels in the forebay of a small hydroelectric facility. *Eels at the Edge: Science, Status, and Conservation Concerns*, (March 2016):277–291,.

Busch, W.-D. N., S. J. Lary, C. M. Castiglione, and R. McDonald. 1998. *Distribution and Availability of Atlantic Coast Freshwater Habitsts for American Eel (Anguilla Rostrata). Administrative Report #98-2*. Amherst, New York, 27 pp.

Byer, J. D., M. Lebeuf, S. Trottier, M. Raach, M. Alaee, R. Stephen Brown, S. Backus, J. M. Casselman, and P. V. Hodson. 2015. Trends of persistent organic pollutants in American eel (Anguilla rostrata) from eastern Lake Ontario, Canada, and their potential effects on recruitment. *Science of the Total Environment*, 529:231–242, https://doi.org/10.1016/j.scitotenv.2015.05.054.

Chaput, G., D. K. Cairns, S. Bastien-Daigle, C. LeBlanc, L. Robichaud, J. Turple, and C. Girard. 2014. Recovery Potential Assessment for the American Eel (Anguilla rostrata) for eastern Canada: mitigation options. *Canadian Science Advisory Secretariat Research Document*, 133(February 2014):i--iv, 1--30,.

Clarke, D., H. Whitney, G. Sutton, and D. Robert. 2013. Detection and Learning of Floral Electric Fields by Bumblebees. *Science*, 340(6128):66 LP – 69, https://doi.org/10.1126/science.1230883.

Constable, C. G., and S. C. Constable. 2004. Satellite Magnetic Field Measurements: Applications in Studying the Deep Earth. *The State of the Planet: Frontiers and Challenges in Geophysics*, 147–159, https://doi.org/https://doi.org/10.1029/150GM13.

Côté, C. L., M. Castonguay, M. S. Kalujnaia, G. Cramb, and L. Bernatchez. 2014. In absence of local adaptation, plasticity and spatially varying selection rule: A view from genomic reaction norms in a panmictic species (Anguilla rostrata). *BMC Genomics*, 15(1):1–15, https://doi.org/10.1186/1471-2164-15-403.

Cresci, A., C. M. Durif, C. B. Paris, S. D. Shema, A. B. Skiftesvik, and H. I. Browman. 2019. Glass eels (Anguilla anguilla) imprint the magnetic direction of tidal currents from their juvenile estuaries. *Communications Biology*, 2(1):1–8, https://doi.org/10.1038/s42003-019-0619-8.

Cresci, A., C. B. Paris, C. M. F. Durif, S. Shema, R. M. Bjelland, A. B. Skiftesvik, and H. I. Browman. 2017a. Glass eels (Anguilla anguilla) have a magnetic compass linked to the tidal cycle. *Science Advances*, 3(6):1–9, https://doi.org/10.1126/sciadv.1602007.

Cresci, A., C. B. Paris, C. M. F. Durif, S. Shema, R. M. Bjelland, A. B. Skiftesvik, and H. I. Browman. 2017b. Glass eels Anguilla anguilla have a magnetic compass linked to the tidal cycle. *Science Advances*, 3(6):9, https://doi.org/10.1126/sciadv.1602007.

Cross Sound Cable Company. 2002. *Survey Date May 2002, Internal Document Issued by Thales. Project Referene 707317.* 1 pp.

Cross Sound Cable Company, L. 2020. Converter Stations. Retrieved August 28, 2021. http://www.crosssoundcable.com/hvdc-technology/converter-stations/.

Dannheim, J., L. Bergström, S. N. R. Birchenough, R. Brzana, A. R. Boon, J. W. P. Coolen, J.-C. Dauvin, I. De Mesel, J. Derweduwen, A. B. Gill, Z. L. Hutchison, A. C. Jackson, U. Janas, G. Martin, A. Raoux, J. Reubens, L. Rostin, J. Vanaverbeke, T. A. Wilding, D. Wilhelmsson, and S. Degraer. 2020. Benthic effects of offshore renewables: identification of knowledge gaps and urgently needed research. *ICES Journal of Marine Science*, 77(3):1092–1108, https://doi.org/10.1093/icesjms/fsz018.

Degraer, S., Z. L. Hutchison, C. LoBue, K. A. Williams, J. Gulka, and E. Jenkins. 2021. *Benthos Workgroup Report State of the Science Workshop on Wildlife and Offshore Wind Energy 2020: Cumulative Impacts*. Albany, NY, 1–45 pp.

Department for Business Enterprise & Regulatroy Reform (BERR). 2008. *Review of Cabling Techniques and Environmental Effects Applicable to the Offshore Wind Farm Industry: Technical Report*. 2–3 pp.

Det Norske Veritas AS. 2016. *Subsea Power Cables in Shallow Water Renewable Energy Applications; Recommended Practice DNV-RP-J301*. 145 pp.

Dhanak, M., E. An, R. Coulson, J. Frankenfield, S. Ravenna, D. Pugsley, G. Valdes, and W. Venezia. 2015. AUV-based characterization of EMF emissions from submerged power cables. *MTS/IEEE OCEANS 2015: Discovering Sustainable Ocean Energy for a New World*, 1–6, https://doi.org/10.1109/OCEANS-Genova.2015.7271719.

Diebel, C. E., R. Proksch, C. R. Green, P. Neilson, and M. M. Walker. 2000. Magnetite defines a vertebrate magnetoreceptor. *Nature*, 406(6793):299–302, https://doi.org/10.1038/35018561.

Dinmohammadi, F., D. Flynn, C. Bailey, M. Pecht, C. Yin, P. Rajaguru, and V. Robu. 2019. Predicting Damage and Life Expectancy of Subsea Power Cables in Offshore Renewable Energy Applications. *IEEE Access*, 7:54658–54669, https://doi.org/10.1109/access.2019.2911260.

Drouineau, H., C. Durif, M. Castonguay, M. Mateo, E. Rochard, G. Verreault, K. Yokouchi, and P. Lambert. 2018. Freshwater eels: A symbol of the effects of global change. *Fish and Fisheries*, 19(5):903–930, https://doi.org/10.1111/faf.12300.

Durif, C., S. Dufour, and P. Elie. 2005. The silvering process of Anguilla anguilla: a new classification from the yellow resident to the silver migrating stage. *Journal of Fish Biology*, 66(4):1025–1043, https://doi.org/10.1111/j.0022-1112.2005.00662.x.

Durif, C., A. Guibert, and P. Elie. 2009. Morphological discrimination of the silvering stages of the European eel; Pp. In Eels at The Edge: Science, Status, and Conservation Concerns. Volume 58 of American Fisheries Association. J. M. Casselman, and D. K. Cairns, eds, American Fisheries Association, Bethesda, MD.

Durif, C. M. F., S. Bonhommeau, C. Briand, H. I. Browman, M. Castonguay, F. Daverat, W. Dekker, E. Diaz, R. Hanel, M. J. Miller, A. Moore, C. B. Paris, A. B. Skiftesvik, H. Westerberg, and H. Wickström. 2017. Whether European eel leptocephali use the Earth's magnetic field to guide their migration remains an open question. *Current Biology*, 27(18):R998–R1000, https://doi.org/10.1016/j.cub.2017.08.045.

Durif, C. M. F., H. I. Browman, J. B. Phillips, A. B. Skiftesvik, L. A. Vøllestad, and H. H. Stockhausen. 2013. Magnetic compass orientation in the European eel. *PLoS One*, 8(3):e59212, https://doi.org/10.1371/journal.pone.0059212.

Enbody, E. D., M. E. Pettersson, C. G. Sprehn, S. Palm, H. Wickström, and L. Andersson. 2021. Ecological adaptation in European eels is based on phenotypic plasticity. *Proceedings of the National Academy of Sciences*, 118(4):e2022620118, https://doi.org/10.1073/pnas.2022620118.

Finlay, C. C., S. Maus, C. D. Beggan, T. N. Bondar, A. Chambodut, T. A. Chernova, A. Chulliat, V. P. Golovkov, B. Hamilton, M. Hamoudi, R. Holme, G. Hulot, W. Kuang, B. Langlais, V. Lesur, F. J. Lowes, H. Lühr, S. Macmillan, M. Mandea, S. McLean, C. Manoj, M. Menvielle, I. Michaelis, N. Olsen, J. Rauberg, M. Rother, T. J. Sabaka, A. Tangborn, L. Tøffner-Clausen, E. Thébault, A. W. P. Thomson, I. Wardinski, Z. Wei, and T. I. Zvereva. 2010. International Geomagnetic Reference Field: The eleventh generation. *Geophysical Journal International*, 183(3):1216–1230,

https://doi.org/10.1111/j.1365-246X.2010.04804.x.

Fish and Wildlife Service. 2015. *Endangered and Threatened Wildlife and Plants; 12-Month Findings on Petitions To List 19 Species as Endangered or Threatened Species*. USA, 17 pp.

Formicki, K., A. Korzelecka-Orkisz, and A. Tański. 2019. Magnetoreception in fish. *Journal of Fish Biology*, (Special Issue) https://doi.org/10.1111/jfb.13998.

Gill, A. B., and M. Desender. 2020. Risk to Animals from Electromagnetic Fields Emitted by Electric Cables and Marine Renewable Energy Devices; Pp. 86–103. In OES-Environmental 2020 State of the Science Report: Environmental Effects of Marine Renewable Energy Development Around the World. A. E. Copping, and L. G. Hemery, eds, Report for Ocean Energy Systems (OES) https://doi.org/10.2172/1633088.

Gill, A. B., Y. Huang, J. Spencer, and I. Gloyne-Philips. 2012. *Electromagnetic Fields Emitted by High Voltage Alternating Current Offshore Wind Power Cables and Interactions with Marine Organisms*. Institute of Engineering and Technology, London, 5 pp.

Gill, A. B., I. Gloyne-Philips, J. Kimber, and P. Sigray. 2014. Marine renewable energy, electromagnetic (EM) fields and EM-sensitive animals; Pp. 61–79. In Marine Renewable Energy Technology and Environmental Interactions. M. A. Shields, and A. I. L. Payne, eds, Springer Netherlands, Dordrecht https://doi.org/10.1007/978-94-017-8002-5_6.

Gill, A. B., S. Degraer, A. Lipsky, N. Mavraki, E. Methratta, and R. Brabant. 2020. Setting the context for offshore wind development effects on fish and fisheries. *Oceanography*, 33(4):118–127, https://doi.org/10.5670/oceanog.2020.411.

GWEC. 2021. Global Wind Report | Gwec. *Global Wind Energy Council*, 75,.

Hain, J. H. W. 1975. The behaviour of migratory eels,Anguilla rostrata, in response to current, salinity and lunar period. *Helgoländer Wissenschaftliche Meeresuntersuchungen*, 27(2):211–233, https://doi.org/10.1007/BF01611808.

Hanson, M., and H. Westerberg. 1987. Occurrence of magnetic material in teleosts. *Comparative Biochemistry and Physiology Part A: Physiology*, 86(1):169–172, https://doi.org/https://doi.org/10.1016/0300-9629(87)90296-9.

Haro, A. 2013. *Proceedings of a Workshop on American Eel Passage Technologies*. pp.

Haro, A. 2014. Anguillidae: Freshwater eels; Pp. 9781421412016. In Freshwater Fishes of North America: Volume 1: Petromyzontidae to Catisomidae. and B. M. B. Melvin L. Warren, Jr., ed, Johns Hopkins University Press.

Haro, A., B. Watten, and J. Noreika. 2016. Passage of downstream migrant American eels through an airlift-assisted deep bypass. *Ecological Engineering*, 91:545–552, https://doi.org/https://doi.org/10.1016/j.ecoleng.2016.02.028.

Haro, A. J., and W. H. Krueger. 1988. Pigmentation, size, and migration of elvers (Anguilla rostrata (Lesueur)) in a coastal Rhode Island stream. *Canadian Journal of Zoology*, 66(11):2528–2533, https://doi.org/10.1139/z88-375.

Harriman, J. A. E., and B. F. Noble. 2008. CHARACTERIZING PROJECT AND STRATEGIC APPROACHES TO REGIONAL CUMULATIVE EFFECTS ASSESSMENT IN CANADA. *Journal of Environmental Assessment*

Policy and Management, 10(01):25–50, https://doi.org/10.1142/S1464333208002944.

Harris, M. P. 2021. Bioelectric signaling as a unique regulator of development and regeneration. *Development (Cambridge)*, 148(10) https://doi.org/10.1242/DEV.180794.

HDR. 2020a. *Benthic and Epifaunal Monitoring During Wind Turbine Installation and Operation at the Block Island Wind Farm, Rhode Island – Project Report.* Final Report to the U.S. Department of the Interior, Bureau of Ocean Energy Management, Office of Renewable Energy Programs. OCS Study BOEM 2020-044, Volume 1: 263 pp; Volume 2:380 pp.

HDR. 2020b. *Seafloor Disturbance and Recovery Monitoring at the Block Island Wind Farm, Rhode Island – Summary Report. Final Report to the U.S. Department of the Interior, Bureau of Ocean Energy Management, Office of Renewable Energy Programs. OCS Study BOEM 2020-019*. 65 pp.

Hein, J. L., I. de Buron, W. A. Roumillat, W. C. Post, A. P. Hazel, and S. A. Arnott. 2016. Infection of newly recruited American eels (Anguilla rostrata) by the invasive swimbladder parasite Anguillicoloides crassus in a US Atlantic tidal creek. *ICES Journal of Marine Science*, 73(1):14–21, https://doi.org/10.1093/icesjms/fsv097.

Hutchison, Z. L., D. H. Secor, and A. B. Gill. 2020a. The interaction between resource species and electromagnetic fields associated with electricity production by offshore wind farms. *Oceanography*, 33(4):96–107, https://doi.org/10.5670/oceanog.2020.409.

Hutchison, Z. L., A. B. Gill, P. Sigray, H. He, and J. W. King. 2020b. Anthropogenic electromagnetic fields (EMF) influence the behaviour of bottom-dwelling marine species. *Scientific Reports*, 10(1):4219, https://doi.org/10.1038/s41598-020-60793-x.

Hutchison, Z. L., A. B. Gill, P. Sigray, H. He, and J. W. King. 2021. A modelling evaluation of electromagnetic fields emitted by buried subsea power cables and encountered by marine animals: considerations for marine renewable energy development. *Renewable Energy*, https://doi.org/10.1016/j.renene.2021.05.041.

Hutchison, Z. L., P. Sigray, H. He, A. B. Gill, J. King, and C. Gibson. 2018. *Electromagnetic Field (EMF) Impacts on Elasmobranch (Shark, Rays, and Skates) and American Lobster Movement and Migration from Direct Current Cables*. OCS Study BOEM 2018-003 pp.

Innovasea. 2020. *Fine-Scale Positioning Datasheet*. 2 pp.

Jacoby, D., J. Casselman, M. DeLucia, and M. Gollock. 2017. *Anguilla rostrata*. *The IUCN Red List of Threatened Species 2017*, 8235:32,.

Jacoby, D. M. P., J. M. Casselman, V. Crook, M. B. DeLucia, H. Ahn, K. Kaifu, T. Kurwie, P. Sasal, A. M. C. Silfvergrip, K. G. Smith, K. Uchida, A. M. Walker, and M. J. Gollock. 2015. Synergistic patterns of threat and the challenges facing global anguillid eel conservation. *Global Ecology and Conservation*, 4:321–333, https://doi.org/10.1016/j.gecco.2015.07.009.

Jessop, B. M. 1987. Migrating American Eels in Nova Scotia. *Transactions of the American Fisheries Society*, 116:161–170,.

Jessop, B. M., J. C. Shiao, Y. Iizuka, and W. N. Tzeng. 2004. Variation in the annual growth, by sex and migration history, of silver American eels Anguilla rostrata. *Marine Ecology Progress Series*, 272:231–244, https://doi.org/10.3354/meps272231.

Johnson, D. S., J. M. London, M.-A. Lea, and J. W. Durban. 2008. Continuous-Time Correlated Random Walk Model For Animal Telemetry Data. *Ecology*, 89(5):1208–1215, https://doi.org/https://doi.org/10.1890/07-1032.1.

Kalair, A., N. Abas, and N. Khan. 2016. Comparative study of HVAC and HVDC transmission systems. *Renewable and Sustainable Energy Reviews*, 59:1653–1675, https://doi.org/10.1016/j.rser.2015.12.288.

Karlsson, L. 1985. Behavioural responses of European silver eels (Anguilla anguilla) to the geomagnetic field. 81:71–81,.

Kavet, R., M. T. Wyman, and A. P. Klimley. 2016. Modeling magnetic fields from a DC power cable buried beneath San Francisco Bay based on empirical measurements. *PLoS One*, 11(2):e0148543, https://doi.org/10.1371/journal.pone.0148543.

Kimber, J. A., D. W. Sims, P. H. Bellamy, and A. B. Gill. 2014. Elasmobranch cognitive ability: using electroreceptive foraging behaviour to demonstrate learning, habituation and memory in a benthic shark. *Animal Cognition*, 17(1):55–65, https://doi.org/10.1007/s10071-013-0637-8.

Kirschvink, J. L., and J. L. Gould. 1981. Biogenetic magnetite as a basis for magnetic field sensitivity in animals. *BioSystems*, 13:181–201,.

Kirschvink, J. L., and M. M. Walker. 1985. Particle-Size Considerations for Magnetite-Based Magnetoreceptors BT - Magnetite Biomineralization and Magnetoreception in Organisms: A New Biomagnetism; Pp. 243–254. In J. L. Kirschvink,, D. S. Jones, and B. J. MacFadden, eds, Springer US, Boston, MA https://doi.org/10.1007/978-1-4613-0313-8_11.

Klimley, A. P., M. T. Wyman, and R. Kavet. 2017. Chinook salmon and green sturgeon migrate through San Francisco Estuary despite large distortions in the local magnetic field produced by bridges. *PLoS One*, 12(6):e0169031, https://doi.org/10.1371/journal.pone.0169031.

Klimley, A. P., N. F. Putman, B. A. Keller, and D. Noakes. 2021. A call to assess the impacts of electromagnetic fields from subsea cables on the movement ecology of marine migrants . *Conservation Science and Practice*, (April):1–8, https://doi.org/10.1111/csp2.436.

Krueger, W. H., and K. Oliveira. 1999. Evidence for Environmental Sex Determination in the American eel, Anguilla rostrata. *Environmental Biology of Fishes*, 55(4):381–389, https://doi.org/10.1023/A:1007575600789.

Lamson, H. M., J. C. Shiao, Y. Iizuka, W. N. Tzeng, and D. K. Cairns. 2006. Movement patterns of American eels (Anguilla rostrata) between salt- and freshwater in a coastal watershed, based on otolith microchemistry. *Marine Biology*, 149(6):1567–1576, https://doi.org/10.1007/s00227-006-0308-2.

Lohmann, K. J., C. M. F. Lohmann, and C. S. Endres. 2008. The sensory ecology of ocean navigation. *Journal of Experimental Biology*, 211(11):1719–1728, https://doi.org/10.1242/jeb.015792.

Marohn, L., E. Jakob, and R. Hanel. 2013. Implications of facultative catadromy in Anguilla anguilla. Does individual migratory behaviour influence eel spawner quality? *Journal of Sea Research*, 77:100–106, https://doi.org/10.1016/j.seares.2012.10.006.

McCleave, J. D., and J. H. Power. 1978. Influence of weak electric and magnetic fields on turning behavior in elvers of the American eel Anguilla rostrata. *Marine Biology*, 46(1):29–34,

https://doi.org/10.1007/BF00393817.

McClintock, B. T., and T. Michelot. 2018. momentuHMM: R package for generalized hidden Markov models of animal movement. *Methods in Ecology and Evolution*, 9(6):1518–1530, https://doi.org/10.1111/2041-210X.12995.

McKellar, A. E., R. Langrock, J. R. Walters, and D. C. Kesler. 2015. Using mixed hidden Markov models to examine behavioral states in a cooperatively breeding bird. *Behavioral Ecology*, 26(1):148–157, https://doi.org/10.1093/beheco/aru171.

Meckley, T. D., C. M. Holbrook, C. M. Wagner, and T. R. Binder. 2014. An approach for filtering hyperbolically positioned underwater acoustic telemetry data with position precision estimates. *Animal Biotelemetry*, 2 https://doi.org/10.1186/2050-3385-2-7.

Michelot, T., R. Langrock, and T. A. Patterson. 2016. moveHMM: an R package for the statistical modelling of animal movement data using hidden Markov models. *Methods in Ecology and Evolution*, 7(11):1308–1315, https://doi.org/10.1111/2041-210X.12578.

Miller, M. 2009. Ecology of Anguilliform Leptocephali: Remarkable Transparent Fish Larvae of the Ocean Surface Layer. *Aqua-BioScience Monographs*, 2(4) https://doi.org/10.5047/absm.2009.00204.0001.

Monticini, P. 2014. *Eel, Anguilla Spp. Production and Trade According to Washington Convention Legislation*. pp.

Moore, A., and W. D. Riley. 2009. Magnetic particles associated with the lateral line of the European eel anguilla anguilla. *Journal of Fish Biology*, 74(7):1629–1634, https://doi.org/10.1111/j.1095-8649.2009.02197.x.

Naisbett-Jones, L. C., N. F. Putman, J. F. Stephenson, S. Ladak, and K. A. Young. 2017. A Magnetic Map Leads Juvenile European Eels to the Gulf Stream. *Current Biology*, 27(8):1236–1240, https://doi.org/10.1016/j.cub.2017.03.015.

Nathan, R., W. M. Getz, E. Revilla, M. Holyoak, R. Kadmon, D. Saltz, and P. E. Smouse. 2008. A movement ecology paradigm for unifying organismal movement research. *Proceedings of the National Academy of Sciences*, 105(49):19052–19059,.

Newton, K. C., A. B. Gill, and S. M. Kajiura. 2019. Electroreception in marine fishes: chondrichthyans. *Journal of Fish Biology*, 95:135–154, https://doi.org/10.1111/jfb.14068.

Nishi, T., G. Kawamura, and S. Sannomiya. 2005. Anosmic Japanese eel Anguilla japonica can no longer detect magnetic fields. *Fisheries Science*, 71(1):101–106, https://doi.org/https://doi.org/10.1111/j.1444-2906.2005.00936.x.

NOAA. 2012. Navigational Chart 12371, New Haven Harbour. .

Nordmann, G. C., T. Hochstoeger, and D. A. Keays. 2017. Magnetoreception—a sense without a receptor. *PLOS Biology*, 15(10):e2003234, https://doi.org/10.1371/journal.pbio.2003234.

Normandeau Exponent, T. Tricas, A. Gill, E. Normandeau, T. Tricas, A. Gill, Normandeau Exponent, T. Tricas, and A. Gill. 2011. *Effects of EMFs from Undersea Power Cables on Elasmobranchs and Other Marine Species*. U.S. Dept. of the Interior, Bureau of Ocean Energy Management, Regulation, and Enforcement, Pacific OCS Region, Camarillo, CA. OCS Study, 426 pp.

Nyqvist, D., C. Durif, M. G. Johnsen, K. De Jong, T. N. Forland, and L. D. Sivle. 2020. Electric and magnetic

senses in marine animals, and potential behavioral effects of electromagnetic surveys. *Marine Environmental Research*, 155:104888, https://doi.org/https://doi.org/10.1016/j.marenvres.2020.104888.

Ohman, M. C., P. Sigray, and H. Westerberg. 2007. Offshore windmills and the effects of electromagnetic fields on fish. *Ambio*, 36(8):630–633,.

Oliveira, K., and J. D. McCleave. 2002. Sexually Different Growth Histories of the American Eel in Four Rivers in Maine. *Transactions of the American Fisheries Society*, 131(2):203–211, https://doi.org/10.1577/1548-8659(2002)131<0203:sdghot>2.0.co;2.

Orpwood, J. E., R. J. Fryer, P. Rycroft, J. D. Armstrong, and S. M. and F. Science. 2015. *Effects of AC Magnetic Fields (MFs) on Swimming Activity in European Eels Anguilla Anguilla*. Marine Scotland, 22 pp. https://doi.org/10.7489/1618-1.

Pankhurst, N. W. 1982. Relation of visual changes to the onset of sexual maturation in the European eel Anguilla anguilla (L.). *Journal of Fish Biology*, 21(2):127–140, https://doi.org/10.1111/j.1095-8649.1982.tb03994.x.

Panofsky, W., and M. Phillips. 2005. *Classical Electricity and Magnetism*, Dover Edit. Dover Publications Inc. New York, pp.

Parker, S. J., and J. D. McCleave. 1997. Selective Tidal Stream Transport by American Eels During Homing Movements and Estuarine Migration. *Journal of the Marine Biological Association of the United Kingdom*, 77(3):871–889, https://doi.org/DOI: 10.1017/S0025315400036237.

Patterson, T. A., M. Basson, M. V. Bravington, and J. S. Gunn. 2009. Classifying movement behaviour in relation to environmental conditions using hidden Markov models. *Journal of Animal Ecology*, 78(6):1113–1123, https://doi.org/10.1111/j.1365-2656.2009.01583.x.

Pettersson, P., and N. Schönborg. 1997. Reduction of Power System Magnetic Fields by Configuration Twist. *IEEE Trans. Power Delivery*, 12(4):1678–1683, https://doi.org/10.1109/61.634190.

Pohle, J., R. Langrock, F. M. van Beest, and N. M. Schmidt. 2017. Selecting the Number of States in Hidden Markov Models: Pragmatic Solutions Illustrated Using Animal Movement. *Journal of Agricultural, Biological, and Environmental Statistics*, 22(3):270–293, https://doi.org/10.1007/s13253-017-0283-8.

Pratt, T. C., D. R. Stanley, S. Schlueter, J. K. L. La Rose, A. Weinstock, and P. T. Jacobson. 2021. Towards a downstream passage solution for out-migrating American eel (Anguilla rostrata) on the St. Lawrence River. *Aquaculture and Fisheries*, 6(2):151–168, https://doi.org/10.1016/j.aaf.2021.01.003.

Putman, N. 2018. Marine migrations. *Current Biology*, 28(17):R972–R976, https://doi.org/10.1016/j.cub.2018.07.036.

Putman, N. F. 2021. Animal navigation: What is truth? *Current Biology*, 31(7):R330–R332, https://doi.org/10.1016/j.cub.2021.02.054.

Putman, N. F., L. C. Naisbett-Jones, J. F. Stephenson, S. Ladak, and K. A. Young. 2017. Response to Durif et al. *Current Biology*, 27(18):R1000–R1001, https://doi.org/10.1016/j.cub.2017.08.046.

Putman, N. F., M. M. Scanlan, A. M. Pollock, J. P. O'Neil, R. B. Couture, J. S. Stoner, T. P. Quinn, K. J.

Lohmann, and D. L. G. Noakes. 2018. Geomagnetic field influences upward movement of young Chinook salmon emerging from nests. *Biology Letters*, 14(2) https://doi.org/10.1098/rsbl.2017.0752.

R Core Team. 2020. R: A language and environment for statistical computing. .

Railing, B. D., G. Ronström, L. Moreau, J. J. Lindberg, P. Miller, J. Bard, and P. Steckley. 2004. Cross Sound Cable Project Second Generation VSC Technology for HVDC. *CIGRE Conference*, Contribution B4-102, 8pp,.

Redmann, E., A. Sheikh, A. Alqahtani, M. McCarty-Glenn, S. Syed, R. S. Mehta, and A. B. Ward. 2020. Terrestrial Locomotion in American Eels (Anguilla rostrata): How Substrate and Incline Affect Movement Patterns. *Integrative and Comparative Biology*, 60(1):180–189, https://doi.org/10.1093/icb/icaa016.

Rommel Jr, S. A., and J. D. McCleave. 1973. Sensitivity of American Eels (Anguilla rostrata) and Atlantic Salmon (Salmo salar) to Weak Electric and Magnetic Fields. *Journal of the Fisheries Research Board of Canada*, 30(5):657–663, https://doi.org/10.1139/f73-114.

Sanford, T. B. 1971. Motionally induced electric and magnetic fields in the sea. *Journal of Geophysical Research (1896-1977)*, 76(15):3476–3492, https://doi.org/https://doi.org/10.1029/JC076i015p03476.

Schmidt, J. 1923. IV.—The breeding places of the eel. *Phil. Trans. R. Soc. Lond. B*, 211(179–208).

Shearer, C., D. Tong, R. Fofrich, and S. J. Davis. 2020. Committed Emissions of the U.S. Power Sector, 2000–2018. *AGU Advances*, 1(3) https://doi.org/10.1029/2020av000162.

Sheehan, E. V, A. Y. Cartwright, M. J. Witt, M. J. Attrill, M. Vural, and L. A. Holmes. 2020. Development of epibenthic assemblages on artificial habitat associated with marine renewable infrastructure. *ICES Journal of Marine Science*, 77(3):1178–1189, https://doi.org/10.1093/icesjms/fsy151.

Sherwood, J., S. Chidgey, P. Crockett, D. Gwyther, P. Ho, S. Stewart, D. Strong, B. Whitely, and A. Williams. 2016. Installation and operational effects of a HVDC submarine cable in a continental shelf setting: Bass Strait, Australia. *Journal of Ocean Engineering and Science*, 1(4):337–353, https://doi.org/https://doi.org/10.1016/j.joes.2016.10.001.

Skiles, D. D. 1985. The Geomagnetic Field Its Nature, History, and Biological Relevance; Pp. 43–102. In Magnetite Biomineralization and Magnetoreception in Organisms: A New Biomagnetism. J. L. Kirschvink,, D. S. Jones, and B. J. MacFadden, eds, Springer US, Boston, MA https://doi.org/10.1007/978-1-4613-0313-8_3.

Smith, F. 2013. *Understanding HPE in the VEMCO Positioning System (VPS)*. VEMCO, 33 pp.

Soares-Ramos, E. P. P., L. de Oliveira-Assis, R. Sarrias-Mena, and L. M. Fernández-Ramírez. 2020. Current status and future trends of offshore wind power in Europe. *Energy*, 202:117787, https://doi.org/10.1016/j.energy.2020.117787.

Souza, J. J., J. J. Poluhowich, and R. J. Guerra. 1988. Orientation responses of american eels, Anguilla rostrata, to varying magnetic fields. *Comparative Biochemistry and Physiology Part A: Physiology*, 90(1):57–61, https://doi.org/https://doi.org/10.1016/0300-9629(88)91005-5.

Stranko, S. A., M. J. Ashton, R. H. Hilderbrand, S. L. Weglein, D. C. Kazyak, and J. V Kilian. 2014. Fish and

Benthic Macroinvertebrate Densities in Small Streams with and without American Eels. *Transactions of the American Fisheries Society*, 143(3):700–708, https://doi.org/10.1080/00028487.2014.889750.

Svedäng, H., and H. Wickström. 1997. Low fat contents in female silver eels: Indications of insufficient energetic stores for migration and gonadal development. *Journal of Fish Biology*, 50(3):475–486, https://doi.org/10.1006/jfbi.1996.0313.

Taormina, B., J. Bald, A. Want, G. Thouzeau, M. Lejart, N. Desroy, and A. Carlier. 2018. A review of potential impacts of submarine power cables on the marine environment: knowledge gaps, recommendations and future directions. *Renewable and Sustainable Energy Reviews*, 96(July):380–391, https://doi.org/https://doi.org/10.1016/j.rser.2018.07.026.

Taormina, B., M. Laurans, M. P. Marzloff, N. Dufournaud, M. Lejart, N. Desroy, D. Leroy, S. Martin, and A. Carlier. 2020. Renewable energy homes for marine life: Habitat potential of a tidal energy project for benthic megafauna. *Marine Environmental Research*, 161:105131, https://doi.org/10.1016/j.marenvres.2020.105131.

Teng, H. Y., Y. S. Lin, and C. S. Tzeng. 2009. A new Anguilla species and a reanalysis of the phylogeny of freshwater eels. *Zoological Studies*, 48(6):808–822,.

Tesch, F.-W. 1974. Influence of geomagnetism and salinity on the directional choice of eels. *Helgoländer Wissenschaftliche Meeresuntersuchungen*, 26(3):382–395, https://doi.org/10.1007/BF01627623.

Tesch, F.-W. 1978a. Horizontal and Vertical Swimming of Eels During the Spawning Migration at the Edge of the Continental Shelf BT - Animal Migration, Navigation, and Homing. 378–391,.

Tesch, F. -W, T. Wendt, and L. Karlsson. 1992. Influence of geomagnetism on the activity and orientation of the eel, Anguilla anguilla (L.), as evident from laboratory experiments. *Ecology of Freshwater Fish*, 1(1):52–60, https://doi.org/10.1111/j.1600-0633.1992.tb00007.x.

Tesch, F. W. 1978b. Telemetric observations on the spawning migration of the eel (Anguilla anguilla) west of the European continental shelf. *Environmental Biology of Fishes*, 3(2):203–209, https://doi.org/10.1007/BF00691944.

Tesch, F. W. 2003. *The Eel*. Blackwell Science, Oxford, pp. https://doi.org/10.1002/9780470995389.

Tetra Tech. 2012. Block Island Wind Farm Block Island Transmission System; Environmental Report / Construction and Operations Plan. (September):373,.

Thomsen, F., A. B. Gill, M. Kosecka, M. Andersson, M. Andre, S. Degraer, T. Felegot, and B. Wilson. 2015. *MaRVEN – Environmental Impacts of Noise, Vibrations and Electromagnetic Emissions from Marine Renewable Energy. Final Study Report*. European Commission RTD-KI-NA-27-738-EN-N, pp.

Tricas, T. C., and J. G. New. 1997. Sensitivity and response dynamics of elasmobranch electrosensory primary afferent neurons to near threshold fields. *Journal of Comparative Physiology A*, 182(1):89–101, https://doi.org/10.1007/s003590050161.

Twigg, E., S. Roberts, and E. Hofmann. 2020. Introduction to the special issue on: Understanding the effects of offshore wind development on fisheries. *Oceanography*, 33(4):13–15, https://doi.org/10.5670/oceanog.2020.401.

U.S. FWS. 2015. *American Eel Anguilla Rostrata*. pp.

Van Ginneken, V., B. Muusze, J. K. Breteler, D. Jansma, and G. Van Den Thillart. 2005. Microelectronic detection of activity level and magnetic orientation of yellow European eel, Anguilla anguilla L., in a pond. *Environmental Biology of Fishes*, 72(3):313–320, https://doi.org/10.1007/s10641-004-2585-2.

van Ginneken, V. J. T., and G. E. Maes. 2005. The European eel (Anguilla anguilla, Linnaeus), its lifecycle, evolution and reproduction: A literature review. *Reviews in Fish Biology and Fisheries*, 15(4):367–398, https://doi.org/10.1007/s11160-006-0005-8.

Verhelst, P., S. Bruneel, J. Reubens, J. Coeck, P. Goethals, D. Oldoni, T. Moens, and A. Mouton. 2018. Selective tidal stream transport in silver European eel (Anguilla anguilla L.) – Migration behaviour in a dynamic estuary. *Estuarine, Coastal and Shelf Science*, 213:260–268, https://doi.org/https://doi.org/10.1016/j.ecss.2018.08.025.

Wahlberg, M., H. Westerberg, K. Aarestrup, E. Feunteun, P. Gargan, and D. Righton. 2014. Evidence of marine mammal predation of the European eel (Anguilla anguilla L.) on its marine migration. *Deep-Sea Research Part I: Oceanographic Research Papers*, 86:32–38, https://doi.org/10.1016/j.dsr.2014.01.003.

Walker, M. M., T. E. Dennis, and J. L. Kirschvink. 2002. The magnetic sense and its use in long-distance navigation by animals. *Current Opinion in Neurobiology*, 12(6):735–744, https://doi.org/https://doi.org/10.1016/S0959-4388(02)00389-6.

Walker, M. M., C. E. Diebel, C. V. Haugh, P. M. Pankhurst, J. C. Montgomery, and C. R. Green. 1997. Structure and function of the vertebrate magnetic sense. *Nature*, 390(6658):371–376, https://doi.org/10.1038/37057.

Westerberg, H., and M.-L. Begout-Anras. 2000. Orientation of silver eel (Anguilla anguilla) in a disturbed geomagnetic field. *Advances in Fish Telemetry*, 149–158,.

Westerberg, H., and I. Lagenfelt. 2008. Sub-sea power cables and the migration behaviour of the European eel. *Fisheries Management and Ecology*, 15(5–6):369–375, https://doi.org/10.1111/j.1365-2400.2008.00630.x.

Westerberg, H., I. Lagenfelt, and H. Svedäng. 2007. Silver eel migration behaviour in the Baltic. *ICES Journal of Marine Science: Journal Du Conseil*, 64(7):1457–1462, https://doi.org/10.1093/icesjms/fsm079.

Willsteed, E., A. B. Gill, S. N. R. Birchenough, and S. Jude. 2017. Assessing the cumulative environmental effects of marine renewable energy developments: Establishing common ground. *Science of the Total Environment*, 577:19–32, https://doi.org/10.1016/j.scitotenv.2016.10.152.

Willsteed, E. A., S. Jude, A. B. Gill, and S. N. R. Birchenough. 2018. Obligations and aspirations: A critical evaluation of offshore wind farm cumulative impact assessments. *Renewable and Sustainable Energy Reviews*, 82(June 2017):2332–2345, https://doi.org/10.1016/j.rser.2017.08.079.

Wyman, M. T., A. Peter Klimley, R. D. Battleson, T. V Agosta, E. D. Chapman, P. J. Haverkamp, M. D. Pagel, and R. Kavet. 2018. Behavioral responses by migrating juvenile salmonids to a subsea high-voltage DC power cable. *Marine Biology*, 165(8):134, https://doi.org/10.1007/s00227-018-3385-0.

Zimmerman, M. A., and J. D. McCleave. 1975. Orientation of elvers of American eels (Anguilla rostrata) in weak magnetic and electric fields. *Helgoländer Wissenschaftliche Meeresuntersuchungen*, 27(2):175–189, https://doi.org/10.1007/BF01611805.

Zucchini, W., I. L. MacDonald, and R. Langrock. 2016. *Hidden Markov Models for Time Series: An Introduction Using R*, 2nd ed. (C. and Hall, ed). CRC Press, pp. https://doi.org/10.1201/b20790.

Appendix A

A1.1 Introduction

The horizontal position error (HPE) is a relative, unitless metric provided by Vemco for the analyzed data and is unique to each study, providing an estimate of error sensitivity for the hyperbolic positioning (Smith, 2013). The HPEm is the horizontal distance in meters between a VPS generated position and a known location of a transmitter. Stationary reference tags (Ref 1, 3, 4 and 5) were deployed throughout the study period and allowed the relationship between the HPE and HPEm to be explored accommodating HPE filtering of the eel data. This was further supported by exploration of the HPE of 'tag drags' through the array for both the reference tags and control V9p tags.

Following the recommendations of Meckley et al., (2014), our objectives for the HPE filtering, criteria, and rationale are provided. The objectives of the HPE filtering were to balance (i) maximizing the volume of data retained and the number of eel tracks, (ii) minimizing the error sensitivity and (iii) retaining the depth profiles of the tracks. The assumed criteria, based on the 2D error sensitivity, was that the majority of data should have an error sensitivity in the low centimeter range (e.g., <25 cm) based on the rationale that the proximity of the eel to the cable was the highest priority in determining the exposure of eels to EMFs and resultant effect on eel behavior. Depth profiles were an important factor in determining the distance from the cable and had to be considered in addition to the 2D error sensitivity. Although HPE filtering was applied to the data to minimize the error sensitivity for the 3D analysis, the unfiltered data were used for a qualitative assessment of eel movements.

Since the 3D analysis was the primary focus, the HPE filter determination focused on the 2019 data. For each reference tag, the total yield of positions and consistency over time were assessed for the full deployment period. The median position for each reference tag, was considered the known position, and was compared to the deployed and recovered GPS positions for confirmation. For each 2D position, the HPEm was calculated as the Euclidean distance from the median.

For the full duration of the study, the reference tag positions were visually inspected and enumerated at a range of HPE filters (HPE's of less than 20, 15, 10-5, 2, 0.75 and 0.5). For those HPE filter levels, the percentage of eel data retained, and number of eel tracks was visually inspected and enumerated. For each HPE level, the reference tag data were used to determine the median and maximum HPEm as well as the proportion of data which were within the <0.15m, <0.25m, <0.5m range. In addition, the HPE of the tag drag data from both the reference tags and the control V9p tags were visually inspected to provide a comparison to the stationary tags and also assess the accuracy of the depth profiles.

A1.2. HPE filter determination

The HPE filter determination was based on the 2019 eel data obtained from the VPS array. Throughout the full HD-array deployment period, there was good detection of the stationary reference tags (1, 3, 4 and 5) with an average yield of 232,939 positions. There was a period of intermittency in Ref 5 detections resulting in a lower yield of positions (190,908). The median positions for each reference tag were in good agreement for the GPS positions recorded during field deployment and recovery. Visual inspection of the reference tag and eel tag positions at different filtering levels, indicated that HPE levels under 10 would be most appropriate to explore in more detail. Due to the large volume of positions, the

HPE filtering levels explored had little effect on the percentage of data retained, with all HPE's >2 retaining 99.9% of all data. Subsequent steps focused on the V9p tags (Ref 4 and 5 combined) which provided 3D data.

Due to the high data retention, HPE filtering had a negligible effect on the depth data for Refs 4 and 5 combined. Similarly, there was little effect on the proportion of data within the desired error sensitivity range. This was due to the majority of Ref data being within HPE <1 however filtering too strongly resulted in major loss of eel data and the number of eel tracks without comparable improvements in the error sensitivity based on the reference tag data (**Figure A1, Table A1**). Although filtering had little effect on the depth profiles of stationary reference tags, a loss of depth profiles was observed for control tag drags at HPE <2 yet dive profiles were appropriately retained at HPE <5. Additionally, filtering at the lowest HPEs considered (<0.5 and <0.75, 1, 2), did not remove all obvious outliers and was accompanied with an unjustified loss of eel data (**Table A1, Figure A1**).

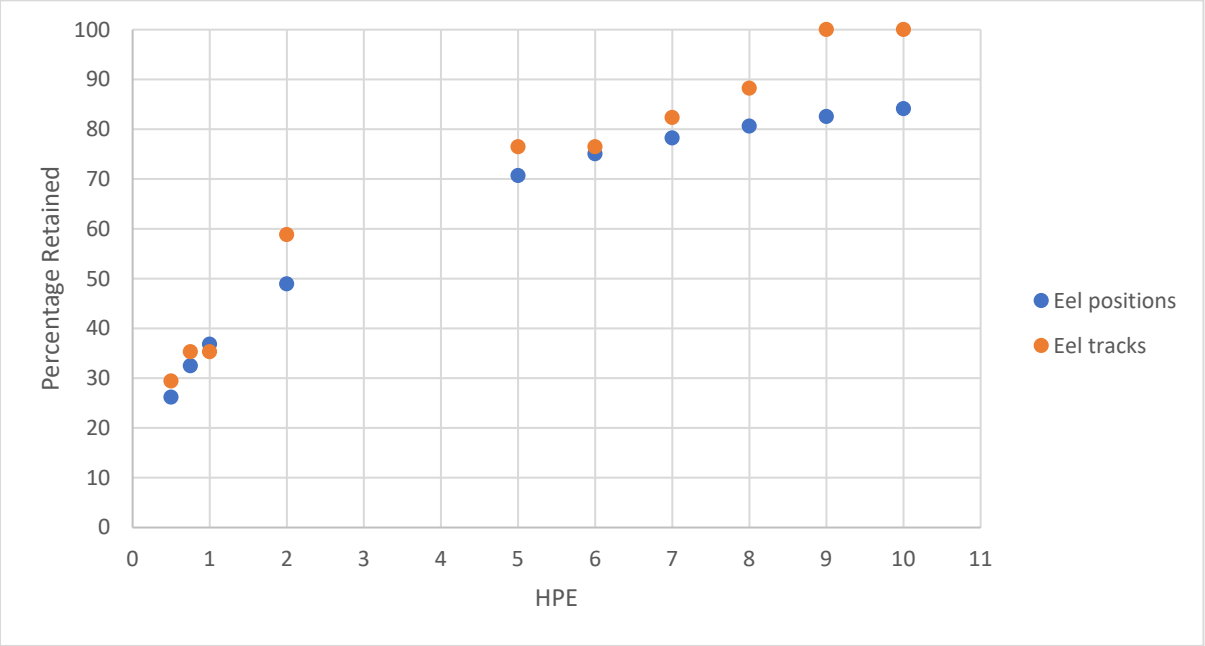

Figure A1.1. The percentage of eel position data and number of eel tracks retained at different HPE filter levels. The full unfiltered eel data set obtained in 2019 contained 8,290 positions and a total of 17 eel tracks in 3D.

Table A1.1. Error sensitivity estimates based on Ref 4 and Ref 5 Vp9 tags combined.

HPE	Positions (n)	Retained Data (%)	Error sensitivity estimates				Proportion (%) of data	
			Median	Max	Mean	St. dev.	<0.15 m	<0.25m
<10	448459	99.99	0.09	72.41	0.72	1.37	62.94	66.91
<9	448435	99.99	0.09	72.41	0.72	1.37	62.94	66.91
<8	448420	99.98	0.09	72.41	0.72	1.37	62.94	66.92
<7	448385	99.97	0.09	72.41	0.72	1.36	62.95	66.92
<6	448344	99.97	0.09	72.41	0.72	1.36	62.95	66.93

<5	**448321**	**99.96**	**0.09**	**72.41**	**0.72**	**1.35**	**62.96**	**66.93**
<2	448023	99.89	0.09	68.60	0.72	1.32	63.00	66.98
<1	447151	99.70	0.09	33.71	0.69	1.30	63.12	67.10
<0.75	445601	99.35	0.09	27.57	0.69	1.21	63.33	67.32
<0.5	443487	98.88	0.09	27.57	0.69	1.20	63.58	67.54

Balancing these factors, an HPE of 5 was selected. Based on the reference tag data (Ref 4 and 5 combined), an HPE of 5 retained 99.96% of data and provided a median error sensitivity of 0.09m (**Table A1.1**). At this HPE < 5 level, 66.93% of all data had an error sensitivity less than 0.25 m and 62.96% of all data had an error sensitivity range less than 0.15 m. Applying the filter of HPE <5 to the eel data retained 70.7% of the data and 76.5% of the eel tracks.

The full dataset and the filtered dataset at HPE <5, for the reference tags can be visualized in **Figure A1.2** together with the color coded HPE level for each position demonstrating majority of data had an HPE of <1.

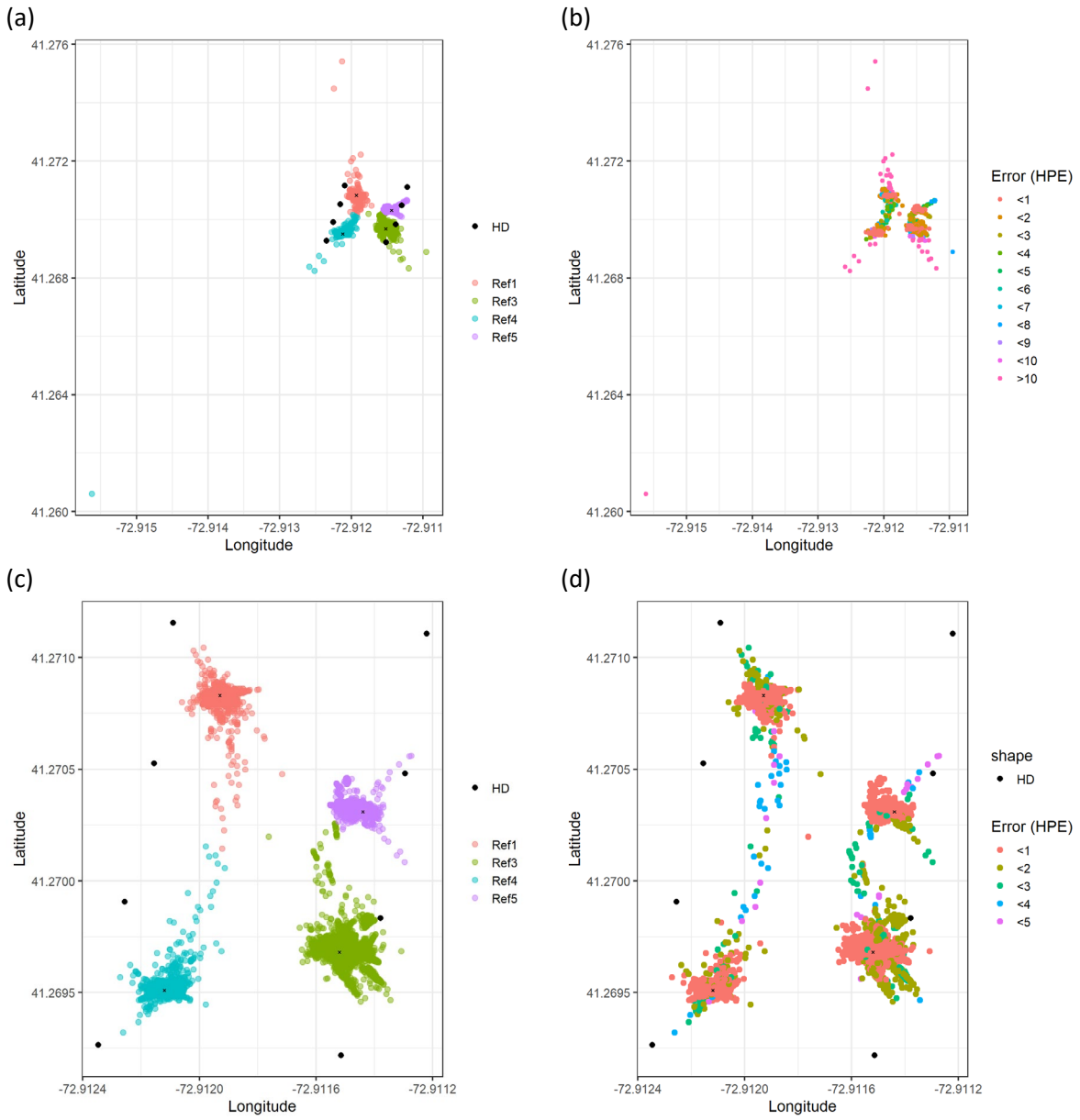

Figure A1.2. All reference tag positions for the full and filtered datasets (HPE <5). The full dataset is shown in figure a color coded for the four reference tags (a) and then color coded for HPE level (b) which the hydrophones (HD) indicated as a reference. The filtered dataset at HPE <5 is shown color coded for the four reference tags (c) and for the HPE level (d) indicating the majority of data has an HPE <1. It is not possible to visualize the proportion of data that overlaps with the known position.

While the HPE filtering was based on the known positions of stationary tags where an HPEm could be calculated, the tag drags provide further information with regard to how the array performed with moving tags. The reference tag drags were in good agreement with each other and offer further support of the filtering level selected (**Figure A3**). Ref 4 and 5 depths also showed good agreement for the depth profiles. For the three tag drags Ref 4 was positioned at an average depth of 2.06m (s = 0.00) and Ref 5 was positioned at an average depth of 7.46m (s = 0.01) from the surface. This was within 0.10

m of the expected distance between tags based on land measurements which was likely due to rope tension in the water. The control V9p tag drag with four tags suspended on one line drifting through the middle quadrant of the array also offered good agreement of 2D position and depth profiles (**Figure A4**).

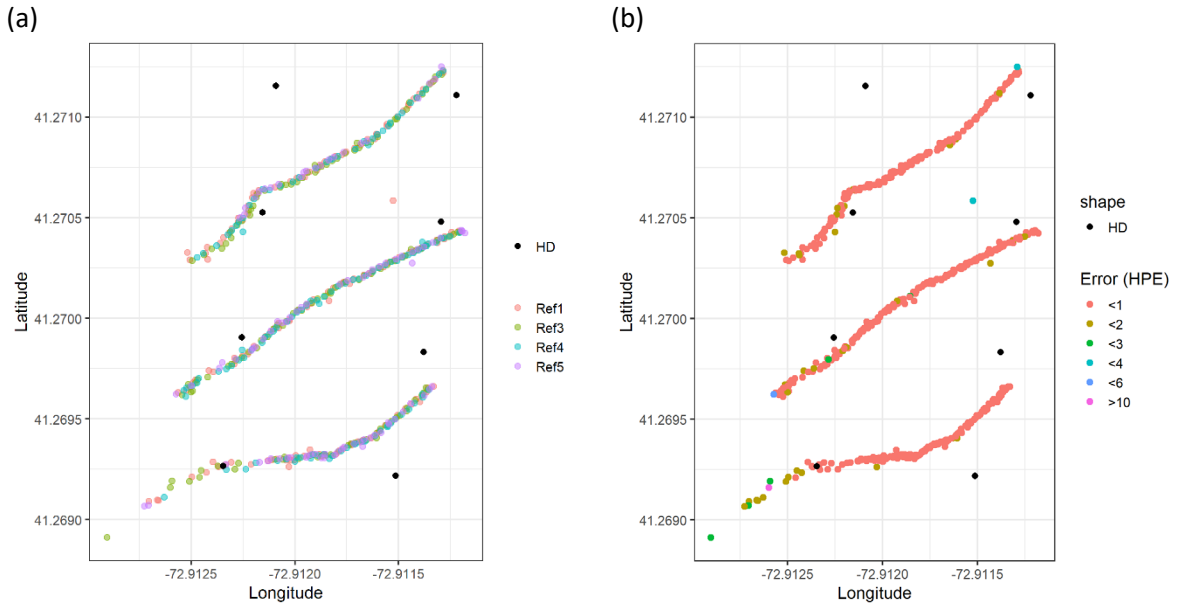

Figure A1.3. The reference tag drags indicate good agreement in positions. Reference tag drags were completed in the upper, middle and lower quadrants of the array, with tags attached at four different depths on a line suspended from a drifting vessel. Each reference tag shows good track agreement (a) and demonstrates a low HPE.

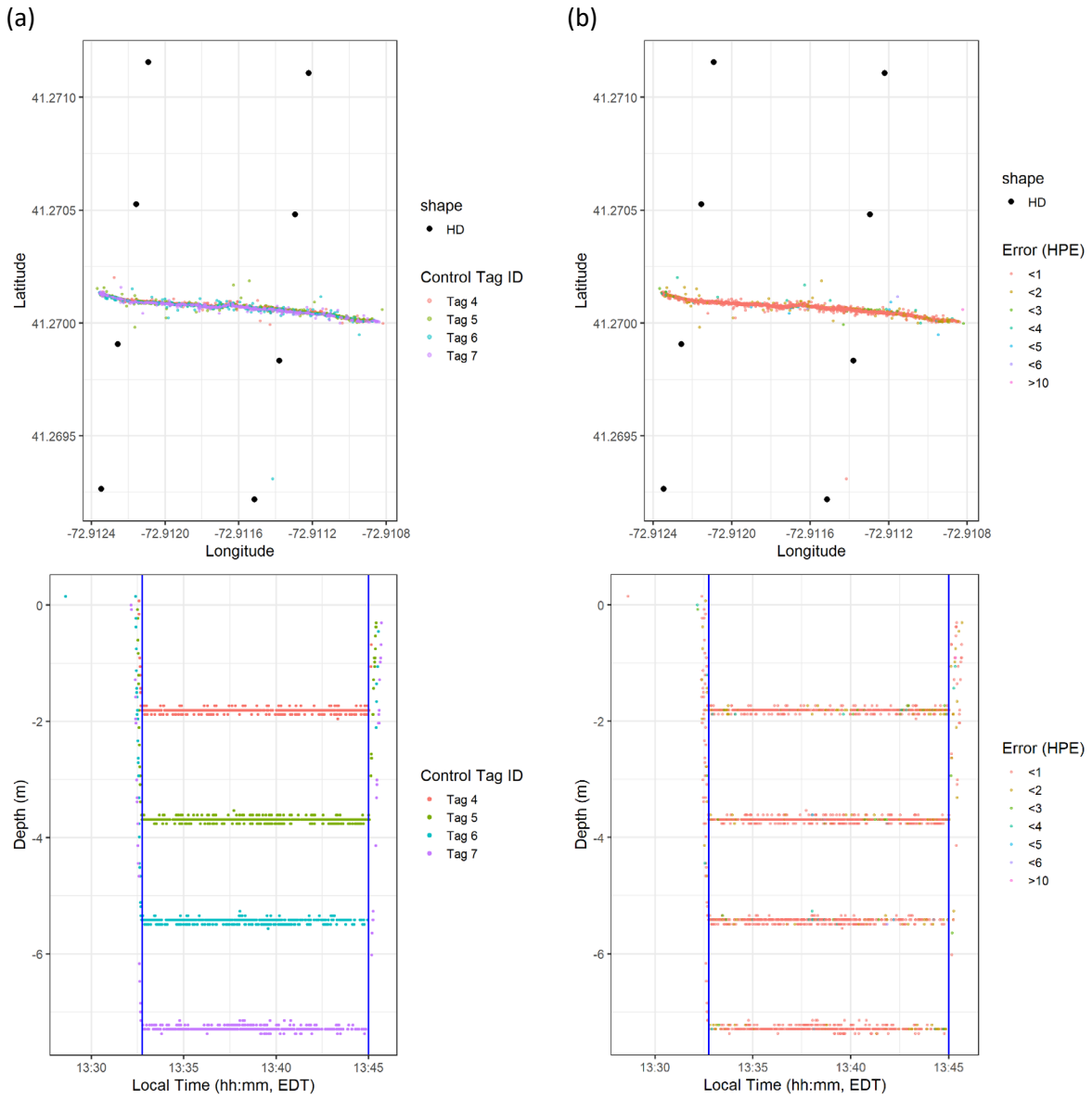

Figure A1.4. The control V9p tag drags indicate good agreement in positions and depths. Control V9p tag drags were completed in middle quadrant of the array, with tags attached at four different depths on a line suspended from a drifting vessel. Each reference tag shows good track agreement (a) and good depth profiles (c) with predominant low HPE. The start and end times of the tag drags are marked as blue vertical lines.

The eel tracks obtained in 2019 are visualized in **Figure A1.5** together with an indication of data retained and lost when filtered for an HPE <5. The filtered tracks were the high-resolution tracks used in the analysis applied in this report. Based on the HPE level selected the 2D positions had an error sensitivity of approximately 0.09 m and a vertical profiled accuracy and precision within 0.10 m. This is a major advancement on telemetry studies of fish due to the application of modern technology.

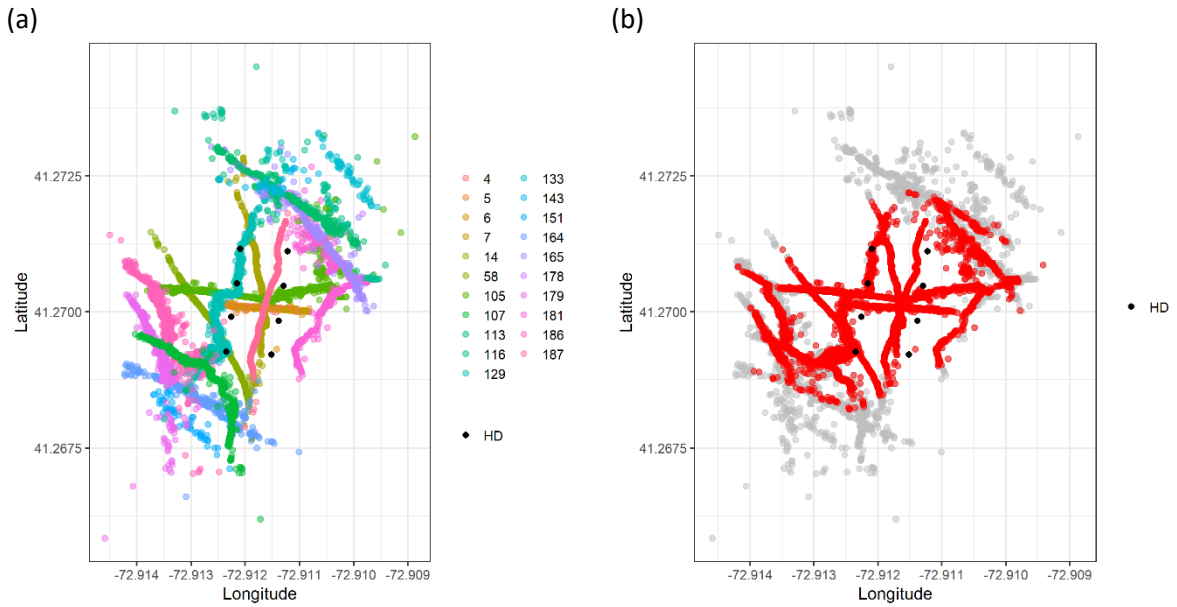

Figure A1.5. The unfiltered and filtered V9p data (HPE <5) for the 2019 study period. All V9p tracks and positions are shown in (a) color coded for individual tags (note that tags 4, 5, 6, and 7 were the control tag drags) which HD hydrophone positions indicated as a reference (black). The retained data (red) verses the lost data (grey) is shown in (b) for an HPE <5.

Department of the Interior (DOI)

The Department of the Interior protects and manages the Nation's natural resources and cultural heritage; provides scientific and other information about those resources; and honors the Nation’s trust responsibilities or special commitments to American Indians, Alaska Natives, and affiliated island communities.

Bureau of Ocean Energy Management (BOEM)

The mission of the Bureau of Ocean Energy Management is to manage development of U.S. Outer Continental Shelf energy and mineral resources in an environmentally and economically responsible way.

BOEM Environmental Studies Program

The mission of the Environmental Studies Program is to provide the information needed to predict, assess, and manage impacts from offshore energy and marine mineral exploration, development, and production activities on human, marine, and coastal environments. The proposal, selection, research, review, collaboration, production, and dissemination of each of BOEM’s Environmental Studies follows the DOI Code of Scientific and Scholarly Conduct, in support of a culture of scientific and professional integrity, as set out in the DOI Departmental Manual (305 DM 3).